A study on Measurement of Human Brain Activity in Steering Operation Using Functional Magnetic Resonance Imaging

（機能的核磁気共鳴画像法を用いた
ステアリング操作中の人間の脳活動計測に関する研究）

2021年 3月

広島大学大学院工学研究科
システムサイバネティクス専攻
D161008　岡本　宜久

Contents

Contents……...i

List of Figures iv

List of Tables ix

Chapter 1 Introduction 1

1.1. Background and purpose 1

1.2. Related works 3

1.3. Outline 8

Chapter 2 Development of fMRI-compatible steering reaction force generation unit ……11

2.1. Introduction 11

2.2. Expected performance of the unit 12

2.2.1. Steering reaction force generation performance 13

2.2.2. MRI acquisition performance 13

2.3. System implementation 15

2.3.1. Steering reaction force generation unit 15

2.3.2. Reaction force transmission unit 16

2.4. Verification of steering reaction force generation performance 20

2.4.1. Methods 20

2.4.2. Results 21

2.4.3. Discussion 26

2.5. Conclusion remarks 26

Chapter 3 Verification of fMRI acquisition performance of fMRI-compatible steering reaction force generation unit 28
3.1. Introduction 28
3.2. Noise assessment caused by motor operation 29
3.2.1. Methods 29
3.2.2. Results and discussion 31
3.3. Verification of fMRI acquisition performance during steering 32
3.3.1. Methods 32
3.3.2. Results 39
3.3.3. Discussion 44
3.4. Conclusion remarks 48
Chapter 4 Brain activity while waiting for the upcoming steering task 50
4.1. Introduction 50
4.2. Methods 51
4.2.1. fMRI-compatible steering reaction force generation unit 51
4.2.2. Measuring brain activities while waiting for the upcoming steering task 51
4.3. Results 59
4.4. Discussion 66
4.5. Conclusion remarks 68
Chapter 5 Brain activity during driving operations modulated by the viscoelastic characteristics of a steering wheel 69
5.1. Introduction 69
5.2. Methods 71

5.2.1. Apparatus 71
5.2.2. Experiment 73
5.3. Results 90
5.3.1. Steering behaviors 90
5.3.2. Common brain activity in the stiffness and viscosity conditions 90
5.3.3. Subjective ratings and performance scores 91
5.3.4. Brain activity correlated with physical parameters 94
5.4. Discussion 103
5.4.1. Validity of fMRI data 103
5.4.2. Brain activity correlated with viscoelastic conditions 104
5.4.3. Subjective perceptions 107
5.4.4. Limitations 108
5.5. Conclusion remarks 109
5.6. Appendix 111
Chapter 6 Conclusions 115
Bibliography 120
Acknowledgments 132

List of Figures

2.1 Experimental system consisting of fMRI-compatible steering reaction force generation unit.

2.2 Configuration of fMRI-compatible steering reaction force generation unit.

2.3 Steering posture.

2.4 Changes in reaction force with time at motor and steering wheel for (a) low and (b) high reaction force stiffnesses.

2.5 Characteristics of the frequency domain with steering torque as the input and motor rotation torque as the output.

2.6 Correlation of reaction force at motor output and steering wheel for (a) low and (b) high reaction force stiffnesses.

2.7 Changes in steering angle and reaction force with time at steering wheel for (a) low and (b) high reaction force stiffnesses.

2.8 Correlation of steering rotation angle and reaction force at steering wheel for (a) low and (b) high reaction force stiffnesses

3.1 Experimental protocol.

3.2 Timeline of experiment. Ten repetitions of the rest (10 s) and task (20 s) blocks. A fixation cross was displayed at the center of the screen throughout the experimental run. Ten seconds after the beginning of the experiment, bars tilted by ±π/4 rad were presented alternately for 1 s each. The participants were instructed to look at the fixation cross and hold the steering wheel. The colors of the bars indicate rest or task

block. The participants were instructed to steer in the direction in which the bar was tilted when white bars were presented, and to not steer when red bars were shown. The relationship between the colors and the task/rest block was counterbalanced across participants.

3.3 Displacement and rotation of head position for (a) analyzed and (b) excluded volumes. The *X, Y,* and *Z* axes are coordinate axes in the MNI (Montreal Neurological Institute) coordinate system [31], and $\theta\,yaw$, $\theta\,pitch$, and $\theta\,roll$ indicate rotation about the *X, Y*, and *Z* axes, respectively.

3.4 Detected brain activated area.

3.5 BOLD signal change rate in primary motor cortex for subjects screened with LQ > 0.7.

4.1 Experimental system consisting of fMRI-compatible steering.

4.2 fMRI-compatible steering reaction force generation unit.

4.3 Experimental protocol.

4.4 Timeline of experiment. Ten repetitions of the rest (10 s) and task (20 s) blocks were performed. A fixation cross was displayed at the center of the screen throughout the experimental run. Ten seconds after the beginning of the experiment, bars tilted by $\pm\,\pi$ /4 rad were presented alternately for 1 s each. The participants were instructed to look at the fixation cross and hold the steering wheel. The colors of the bars indicate rest or task block. The participants were instructed to steer in the direction in which the bar was tilted when white bars were presented, and to not steer when red bars were shown. The relationship between the colors and the task/rest block was counterbalanced across participants.

4.5 Activation in the anterior cingulate cortex and insula (uncorrected for multiple comparisons $p < 0.001$ with cluster-level corrected FDR $p < 0.05$).

4.6 Activation in the amygdala under Low_L condition (LQ > 0.7) (uncorrected for multiple comparisons $p < 0.001$ with cluster-level corrected FDR $p < 0.05$).

4.7 Activation in the supplementary motor area under Low_L condition for participants (LQ > 0.7) (uncorrected for multiple comparisons $p < 0.001$ with cluster-level corrected FDR $p < 0.05$).

4.8 Bold signal change rate in anterior cingulate cortex.

5.1 Experimental system for presenting steering reaction forces during simulated driving in a magnetic resonance imaging (MRI) scanner.

5.2 Steering posture with the participant in a supine position inside the gantry.

5.3 Schematic of the experimental protocol showing the timing and duration of each phase. VAS = visual analog scale.

5.4 Example of the screen of the input interface shown to the participants during the subjective evaluation of performance based on certain descriptive words using a visual analog scale (VAS).

5.5 Measured steering torques for each stiffness (top row) and viscosity (bottom row) experimental conditions. Prior to the experiment, steering reaction force characteristics were measured by an experimenter outside the magnetic resonance imaging (MRI) scan-room for one run comprised of six trials. The linear regression equation for each condition is shown by a red line.

5.6 Design matrix showing each phase of one run (a), all runs each subject participated in (b), and group analysis.

5.7 Time-series examples of steering angle during the driving task. (a) to (d) are examples of one trial under one viscosity condition (V2). These examples correspond to four patterns of combinations of two gates that appear randomly on the left or right during a single trial. (a) An example of a trial in which both gates appeared on the left. (b) An example of a trial in which the first gate appeared on the left, the second on the right. (c) An example of a trial in which the first gate appeared on the right, the second on the left. (d) An example of a trial in which both gates appeared on the right. (e) and (f) show the average and standard deviation of the absolute values of steering angles over all trials of all subjects for each stiffness and viscosity condition. (e) shows the time series under the stiffness condition, and (f) under the viscosity condition. These measurements were performed with the steering angle meter built in the reaction force generation motor. The measured values showed good agreement with those measured at the steering position under the measurement conditions shown in Fig. 5.5. CD = Countdown.

5.8 Brain regions significantly activated at the thresholds of family-wise error (FWE) with a corrected $p < 0.05$ at the voxel level in the stiffness (top row) and viscosity (bottom row) conditions during the “countdown” (a), “straight” (b), and “gate” (c) periods. BA: Brodmann area, IPL: Inferior parietal lobule, IPS: Intraparietal sulcus, V1: Primary visual, cortex, V2: Secondary visual cortex, V3: Tertiary visual cortex, V4: Quaternary visual cortex, V5/MT: Middle temporal visual area, Hem: Hemisphere, Verm: Vermis

5.9 Performance scores for each of the three stiffness (a) and viscosity (b) condition parameters. **: $p < 0.01$. Error bar: SEM.

5.10 VAS4 subjective evaluation scores for trials based on a visual analog scale (VAS)

for each descriptive word for stiffness (a) and viscosity (b) conditions. The factor loading and contribution ratios for each principle component based on descriptive words are shown in (c). **: $p < 0.01$, *: $p < 0.05$, +: $p < 0.1$, Error bar: SEM. CR: Contribution ratio.

5.11 VAS7 subjective evaluation scores at the end of the run based on a visual analog scale (VAS) for each descriptive word for the stiffness (a) and viscosity (b) conditions. The factor loadings and contribution ratios for each principal component based on the descriptive words are shown in (c). **: $p < 0.01$, *: $p < 0.05$, Error bar: SEM. CR: Contribution ratio.

5.12. (a) Significant brain activation in the contrast of S3 > S1 in the stiffness condition during the gate period at the threshold of family-wise error (FWE) with a corrected $p < 0.05$ at the voxel level. The blue rectangles indicate a left motor cortex cluster containing the Montreal Neurological Institute (MNI) coordinates -48, -24, 62. (b) Percent signal change in the activated cluster in the contrast of S3 > S1. (c) Spatial relationship between activation peaks observed at MNI coordinates: -48, -24, 62 and the central sulcus. **: $p < 0.01$, *: $p < 0.05$, Error bar: SEM.

5.13 (a) Significant brain activation in the contrast of V3 > V1 in the viscosity condition during the gate period at the threshold of family-wise error (FWE) with a corrected $p < 0.05$ at the peak level. (b) Percent signal change in the activated cluster in the contrast of V3 > V1. (c) Spatial relationship between significant activation in the contrast of V3 > V1 with the peak activation in the left premotor cluster including the Montreal Neurological Institute (MNI) coordinates -22, -30, 62 and the significant activation in the contrast of S3 > S1. **: $p < 0.01$, *: $p < 0.05$, Error bar: SEM.

List of Tables

3.1 Experimental conditions for steering arm and reaction torque stiffness.

3.2 Location and volume of activation clusters.

4.1 Experimental conditions for steering arm and reaction torque stiffness.

4.2 Activated cluster location and volume under Low_L and Low_R condition.

4.3 Activated cluster location and volume under Low_B and High_B condition.

5.1 Experimental condition: Motor control for reaction force generation.

5.2 Words for subjective evaluation.

S1 Location and volume of active clusters in the stiffness condition.

S2 Location and volume of active clusters in the viscosity condition.

S3 Location and volume of active clusters. Stiffness condition S3 > S1 at Cluster 1.

S4 Location and volume of active clusters. Viscosity condition V3 > V1.

Chapter 1
Introduction

1.1. Background and purpose

Driving a car is indispensable in modern society. Nowadays, automobiles are required to serve many functions, such as ensuring safety, while being environmentally friendly and economically efficient. The author focused attention to the features of automobiles that drivers can control and move by themselves in developing these technologies. The author considers that enhancing the driving pleasure by self-manipulation is an important technological development target. One of the most important aspects in this regard is steering performance.

Recently, electrically powered steering systems have become common, and steering reaction forces can now be configured with high degrees of freedom as a result of advancements in the research and development of electronic control technology. Therefore, it is desirable to quantitatively optimize the characteristics of the steering reaction forces. In order to efficiently configure mechanical steering characteristics, a force perception model has been proposed in humans when performing steering operations; this model can be applied to configure the mechanical characteristics of steering so that the subjective sensations of the steering reaction force change linearly in relation to the steering operation, facilitating better prediction of vehicle responses to steering.

Previous studies, however, have adopted an ergonomics-based approach to measuring behavioral and psychophysiological indices of the vehicle and driver, such as a subjective evaluation of feelings experienced while driving, musculoskeletal activities related to steering behavior, and resultant emotional responses induced by the autonomic nervous system. These measurements may further the understanding of how the characteristics of steering reaction force affect the predictability of vehicular behavior, the operability of a vehicle, and the driving pleasure elicited by these factors. To date, unfortunately, the underlying mechanisms can only be indirectly estimated using these behavioral and psychophysiological indices.

In view of this, researchers have recently proposed the use of "neuroergonomic"-based approaches, combining neuroscientific findings and ergonomics. Such approaches could reveal the neural basis of driving behavior, providing novel findings that could in turn improve previous ergonomic theories and models that evaluated the relationships between a car and a driver.

On the other hand, the Center of Innovation Program (COI), in which the author participates, aims to create new values in various fields of life such as food, clothing, lifestyle, mobility, education, and medical care through research studies on emotional information based on neuroscience [1].

Against such a background, the author attempts to convince people that it is possible to apply neuroscience in order to better reveal the underlying mechanisms associated with the ways by which the characteristics of steering reaction force affect the vehicle's operability and the driver's perception, which is expected to provide a stronger neuroscientific basis for the design of novel steering systems, especially model-based

development (MBD).

The purpose of this study is, thus, to elucidate the neural basis of automobile steering operation in situations in which a steering reaction force is applied.

To achieve this aim, it is suitable to measure brain activity using functional magnetic resonance imaging (fMRI), which can measure activity in the entire brain at a high spatial resolution. Therefore, a new device was developed to measure fMRI during steering. This study seeks to determine the characteristics of the steering reaction force that are focused on the influence of viscoelasticity, which is the most basic mechanical element. In addition, the standby state of steering, which has no behavioral output and is difficult to handle by conventional ergonomic methods, is also examined.

1.2. **Related works**

In recent years, electric power-assisted steering has become common in automobile steering systems. As research and development on electronic control technology progresses, the degrees of freedom in setting the characteristics of the steering force continue to increase (e.g., [2]). Conventionally, these characteristics are developed by repeating a feeling test involving test drivers. Therefore, as the number of degrees of freedom in setting the characteristics of the steering force increases, a large number of feeling tests are required. In light of this situation, Takemura *et al*. proposed a mathematical model to convert mechanical properties into spaces of subjective force perception using a force perception model for the steering operation [3]. Such a model allows for the design of the steering system in an early stage of development. They controlled the characteristics of the steering force such that the driver felt that the steering

reaction force changed linearly with the steering operation. Such characteristics of the steering force make it easy to predict the response of the vehicle to the steering operation, thereby leading to automobiles that are easy and pleasurable to drive.

Research and development engineers generally measure vehicle behavior as well as the driver's behavioral and psychophysiological indices, such as subjective evaluation, musculoskeletal activity, and responses generated by the autonomic nervous system. These measurements allow them to understand how well the driver can predict future vehicle behavior as well as his/her experience relating to how easy and pleasurable driving the vehicle is depending on the characteristics of the steering force. These indices have been applied to automobile development (e.g., [4]-[7]) However, it is not clear which brain mechanism directly relates to the characteristics of the steering force that can help determine ease of driving and the pleasure derived from driving.

Understanding brain mechanisms pertaining to the influence of the characteristics of the steering force on the driver can provide a neuroscientific basis for the design of a steering system through the simulation of a mechanical system that considers subjective perception. For this purpose, it is necessary to identify neural substrates that govern not only the planning and control of the voluntary movements directly involved in the steering operation, but also the emotions related to the pleasure extracted from driving. Although various methods have been proposed to measure activity in the brain, to approach the problems considered in the context mentioned above, the author selected magnetic resonance imaging (MRI), which can measure activity in the entire brain at a high spatial resolution.

On the other hand, researchers have recently proposed the use of "neuroergonomic"-

based approaches, combining neuroscientific findings and ergonomics [8]. It is possible that such approaches could reveal the neural basis of driving behavior, providing novel findings that could improve previous ergonomic theories and models that have evaluated the relationships between a car and a driver [9], [10]. In particular, neuroimaging studies of car-driving using functional magnetic resonance imaging (fMRI) and driving simulators have been conducted since around the early 21st century. These previous studies revealed the neural substrates of driving under normal and disturbed conditions, including driving under the influence of alcohol (e.g., [8], [11]). It is possible that fMRI studies could better reveal the brain mechanisms associated with the ways that steering reaction force characteristics affect the vehicle's operability and the driver's perception, and may provide a stronger neuroscientific basis for the design of novel steering systems.

Many MRI studies related to simulated driving have been conducted. For example, the neural substrates of driving behavior when making a right or a left turn with or without distracting tasks were examined using a driving simulator equipped with a steering wheel and an accelerator pedal on an MRI scanner (e.g., [12], [13]). A functional MRI (fMRI) study used a joystick to control a virtual vehicle in a driving simulator to show the relationship between maintaining a constant distance between vehicles and the activity of the anterior cingulate cortex [14]. Although these studies aimed to explain fundamental brain activities involved in driving by fMRI, they did not examine the relationship between these activities and the characteristics of the force feedback from the automobile to the steering operation. In other MRI studies on simulated driving (e.g., [15], [16]), the characteristics of the force feedback to the steering operation have not been considered.

Many studies have been conducted on the function of the musculoskeletal system and

brain activities using MRI. For example, several MRI studies have examined the relationship between the force of the arm and brain activity during gripping tasks using the right hand [17], [18]. Another fMRI study reported functional interaction between the cerebellum and the premotor cortex in error correction when slowly exercising fingertip force [19]. Developmental research has been conducted on a robot system to provide force feedback to the wrist by employing MRI [20]. An MR-compatible actuation system was developed for a parallel force-feedback exoskeleton to measure and/or assist wrist-pointing movements [21]. Brain activity for the motions involved in pedaling a bicycle, accompanied by multijointed movement of the lower limbs, were studied by employing MRI [22]. However, to the best of the author's knowledge, no study has examined the cooperative operation of two hands using the proximal muscles, such as the steering operation of an automobile.

Although the author aimed to obtain brain activity during steering operation, it is also important to examine the brain mechanisms related to affective states of drivers, such as anxiety. A previous study reported that many drivers feel anxious during their daily drive [23]. Drivers' anxiety is caused not only by the performance of the car but also by various factors including environmental factors, for instance, narrow roads, frozen roads, heavy rain, and thick fog. Therefore, it may be difficult to control anxiety only by changing the characteristics of the steering force needed. However, at a minimum, if the brain activation related to anxiety during driving is clarified, it would be helpful to design the steering force characteristics to reduce drivers' anxiety.

Recent neuroimaging studies on the intrinsic brain network showed that there exist three typical networks called the default mode network (DMN), salience network (SN),

and central executive network (CEN) (e.g., Menon *et al*. [24]). Menon *et al*. proposed a hypothesis that the SN, which consists of the insula and the anterior cingulate cortex (ACC), plays a role in switching the DMN, which is dominantly active when participants are at rest, to the CEN, which is active when participants engage in a task. In this study, the author hypothesized that the brain regions comprising the SN, such as the insula and the ACC, are active when participants are on standby for steering, that is, when the SN switches the DMN to the CEN in order to perform the steering operation immediately after the participants receive a cue to start steering. Furthermore, the author hypothesized that activation in the SN will be enhanced in the condition in which anxiety is elicited, for instance, when participants are waiting for steering operation with a large reaction force.

As described above, conventional experiments that simulate driving represented using MRI have emphasized visual information, and have used a simple steering wheel, pedal, computer mouse, or dial as the input device. The intrinsic value of driving pleasure is rooted in the driver's self-efficacy provided by good feedback from the automobile, which can activate the brain's reward system by providing the driver with a way to emotionally and cognitively evaluate motor control. As the first step to investigate feedback from the automobile, the author focuses on the steering reaction force because it is the most primitive and direct feedback. In addition to its importance in industrial applications of the automobile, evaluating the mechanical feedback accompanying manual operations is a highly universal research subject. Numerous previous studies revealed important insights into the reward system of the brain, including the psychological aspects of monetary, artistic, and musical rewards (e.g., [25]), and medical effects such as depression

and dependence (e.g., [26]). However, to the best of the author's knowledge, no study has dealt with the functions of the reward system related to mechanical feedback given by human operation and machine interaction. To study this relationship, the brain functions related to emotional and cognitive evaluation must be measured simultaneously with the motor control of the human body. The author thus employed fMRI that can measure the activity of the whole brain, including deep parts with a high spatial resolution to reveal brain functions. This study is the first attempt to manufacture a device that applies a controlled reaction force to both arms (proximal muscles) of the participant in the MRI gantry with a high magnetic field, which potentially enables the brain-function-based mechanical design that provides the driver with both self-efficacy and driving pleasure. Even though a force feedback is performed in a general driving simulator, similar experiments have not been conducted in an MRI environment because a device capable of measuring brain activity under the action of steering reaction forces that simulate automobile steering using MRI has not yet been developed.

1.3. **Outline**

The thesis is organized as follows:

In chapter 2, the author describes a newly developed fMRI-compatible steering reaction force generation unit. To avoid disturbance in the electromagnetic field of the MRI, the proposed apparatus was configured as follows: A motor installed outside a scan room generated a reaction force that was transmitted to a steering wheel placed in the hands of a subject using a nonmagnetic transmission unit. By verifying its performance

for steering reaction force generation, the author confirms that the steering reaction force of different magnitudes can be presented at the position of the hand using an MRI scanner.

In chapter 3, the author describes the verification of fMRI measurement performance using the proposed device. To verify the performance of the unit, the author measures the brain activity of participants of an experiment by using fMRI while they performed steering operations using their arm/arms under various steering forces. The results are consistent with those for motor-related brain activity obtained in past neuroimaging studies. The author conclude that the proposed unit can measure brain activity through fMRI in the presence of a steering reaction force.

In chapter 4, the author focuses on the brain activity while waiting to steer about the experimental data of chapter3, assuming that it reflects participants' affective state in preparation of the upcoming steering task. The author observes activations in the anterior cingulate and insular cortices comprising the salience network, which is one of the intrinsic brain networks and involved in preparation for an upcoming task. Intriguingly, when waiting for the steering task having larger reaction force, the anterior cingulate cortex, known to be related to anxiety, was more active.

In chapter 5, the author describes changes in human brain activity induced by varying the viscoelastic characteristics associated with manipulating a car steering wheel. Participants performed a simulated driving task with three levels of stiffness and viscosity. An amplitude effect of reaction forces on the measured brain activity varying stiffness was found in the primary motor cortex (M1) associated with hand representation. Conversely, the changes in the brain activity induced by varying viscosity were found more dorsally in the premotor cortex and the M1 than in regions associated with hand

representation. These results are the first to demonstrate that various viscoelastic characteristics activate different motor regions; more specifically, stiffness and viscosity of the steering wheel mainly affected the motor control of the distal and proximal muscles, respectively.

Finally, Chapter 6 concludes the dissertation and outlines related challenges and future work.

Chapter 2
Development of fMRI-compatible steering reaction force generation unit

2.1. Introduction

This chapter describes a newly developed fMRI-compatible steering reaction force generation unit. To the best of my knowledge, the proposed experimental apparatus is the first effort to enable a simulator of driving operation with reaction force feedback in an MRI with exposure to a strong magnetic field. To avoid disturbance in the electromagnetic field of the MRI, the proposed apparatus is configured as follows: A motor installed outside a scan room generated a reaction force that is transmitted to a steering wheel placed in the hands of a subject using a nonmagnetic transmission unit. Therefore, in this chapter, it is further explained that an appropriate reaction force transmission characteristic was obtained as a mechanical characteristic in such a unique device layout.

The structure of this chapter is as follows. Section 2.2 describes the performance required for this device. Section 2.3 describes the implementation of the device. Section 2.4 describes the measured mechanical properties. Section 2.5 describes the conclusion remarks.

2.2. **Expected performance of the unit**

The proposed fMRI-compatible simulated steering reaction force generation unit was used in conjunction with a driving simulator (a device that presented various sensory stimuli according to vehicle behavior, such as a simulated visual scene corresponding to a driving operation) in an MRI scan room. Fig. 2.1 shows the experimental environment containing the proposed unit (hereinafter referred to as “the unit”). The unit consisted of a steering reaction force generation part and a reaction force transmission part. The rotation angle of the steering wheel obtained from this unit was sent to the driving simulator and used as the steering rotation angle input to the vehicle model of the driving simulator. The unit simultaneously generated a steering reaction force corresponding to the steering rotation angle, which was fed back to a participant lying in the MRI scanner. Using this unit, we constructed an experimental system that could acquire the functional image of the brain in an experimental situation where the participant virtually drove according to the steering operation in a driving scene generated by the driving simulator and received the steering reaction forces as somatosensory stimuli in addition to visual and auditory stimuli. This subsection describes the expected performance of this system and its implementation.

The proposed unit used in the MRI scan room was expected to fulfill the following two performance criteria: (1) The steering reaction force intended by an experimenter should be reproduced on the steering wheel in the hands of the participant lying in the MRI scanner. (2) The unit should not adversely affect magnetic resonance images, e.g., by the introduction of measurement noise.

2.2.1. Steering reaction force generation performance

Steering characteristics during the steering operation of the automobile were quantified by the steering force generated corresponding to the steering rotation angle. Therefore, the technical problems in reproducing the steering reaction force using the characteristics of the steering force intended by the experimenter on the steering wheel in the hands of the participant should be solved.

2.2.2. MRI acquisition performance

The technical problems involved in ensuring that the measurement magnetic field of the MRI is not disturbed by the operation of the reaction force generation motor should be solved. Moreover, the rotational movement of the members constituting the unit according to the steering movement can disturb the magnetic field used for MRI measurement. Preventing imaging noise generated by these members might also be a technical problem that needs to be solved.

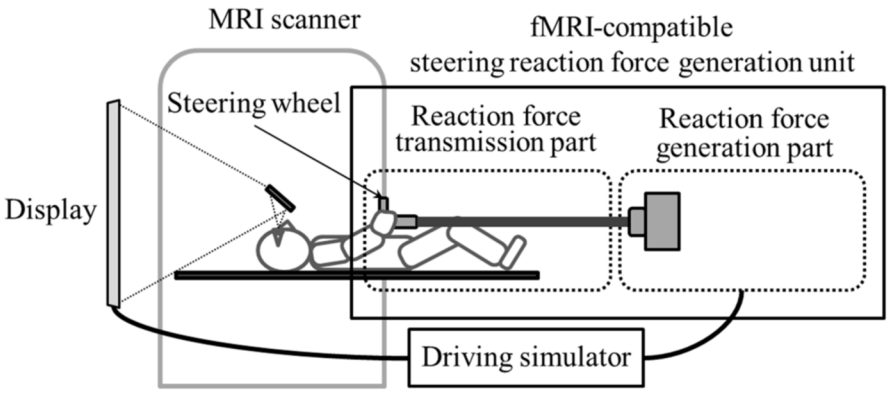

Fig. 2.1. Experimental system consisting of fMRI-compatible steering reaction force generation unit.

2.3. System implementation

To solve the abovementioned problems, the fMRI-compatible steering reaction force generation unit (Fig. 2.1) was designed to consist of a reaction force generation unit specification. To realize the steering reaction force generation unit in the fMRI environment with a high magnetic field limitation because of heat, adsorption, and abnormal movements affected by magnetism had to be placed outside of the MRI scan room (the control room). This strictly limited the arrangement of the equipment. We examined several layouts and equipment configurations to maximize the performance of the steering torque presentation (maximum steering torque of 6 Nm) and constructed a variable mechanism for the body interface to adjust to the subject's height (155 cm to 185 cm). We also considered the simplicity of installation and withdrawal of the unit, so the equipment could be installed and withdrawn within 10 minutes.

2.3.1. Steering reaction force generation unit

The steering reaction force generation unit was built based on the configuration of the steering reaction force generation unit of the driving simulator developed in a previous study [3]. The reaction force was generated by using a direct drive-type rotary motor (M-YSB, NSK Ltd., Tokyo, Japan; maximum torque: 20 Nm). The axis of the motor was connected to the rotating shaft of the reaction force transmission unit via a steering force meter (TR60, SOHGOH KEISO Co., Ltd., Tokyo Japan; rated torque: 50 Nm). A DSP board (DS1103, dSPACE GmbH, Paderborn, Germany) was used to control the motor. The rotation angle of the rotating shaft used in the reaction force transmission unit was

measured using an encoder (resolution: 51200 pulse/rad) built into the motor.

With this configuration, the steering wheel was operated by the participant of the experiment, and the torque and rotation angle transmitted by the rotating shaft were detected and digitized by the steering force meter and encoder. This signal was entered into the DSP board, and the motor was controlled so that a predetermined reaction force was generated. The reaction force generation unit was installed outside the MRI scan room with magnetic shielding so that electromagnetic noise from the motor did not affect the MRI images.

2.3.2. Reaction force transmission unit

- ***Materials and parts***

To install the reaction force transmission unit inside the MRI scan room with a strong magnetic field, the entire reaction force transmission unit was composed of nonmagnetic materials and parts. Furthermore, all parts used in the gantry of the MRI scanner were composed of nonmetallic materials (i.e., plastic and wood). These parts were brought into the MRI scan room and confirmed to be MRI safe (i.e., they did not cause magnetic adsorption, heat generation, or noise in the MRI images).

- ***Setup***

The rotating shaft connected to the reaction force generation unit was introduced into the MRI scan room by penetrating a dedicated waveguide installed in the penetration panel. The shaft was subsequently made to pass through three shaft support stands installed on

the floor and two stands installed on the MRI bed. The rotation torque was configured to be transmitted to the steering wheel in the hands of the participant (Fig. 2.2). In the gap between the waveguide and the shaft, plastic ball bearings were positioned at both the ends of the waveguide to prevent it from rubbing with the shaft. The height of the floor of the motor output shaft of the reaction force generation unit was made equal to that of the steering shaft that could be held by the participant in the MRI gantry in a steering operation posture. Because the penetration panel was not installed on the extended line of the central axis in the MRI scan room in the left–right direction, the angle of the rotating shaft was changed by approximately 10° using the universal joints on each of the two shaft support bases installed on the floor, and the edge of the shaft reached the penetration panel.

- ***Rotating shaft***

Considering the abovementioned configuration, the length of the rotating shaft needed to be approximately 5 m. To ensure that the steering reaction force controlled by the characteristics of the steering force intended by the experimenter was reproduced, the material of the rotating shaft needed to fulfill the requirements of high torsional rigidity and small moment of inertia. Therefore, we used carbon fiber-reinforced plastic (CFRP) as the material for the rotating shaft. As CFRP is nonmagnetic and nonmetallic, it was expected to fulfill the abovementioned requirements.

- ***Steering posture***

The steering posture is shown in Fig. 2.3 together with the steering wheel. The gripping

part of the steering wheel was made of wood that was easy to process into an arbitrary shape and was nonmagnetic. The diameter of the steering wheel at its outermost end was 370 mm, identical to the steering wheel diameter of a normal automobile. With regard to the shape of the steering wheel, at the point where the steering wheel was held at a rotation angle of zero, the gripping part was secured such that it reproduced the normal grip of an automobile; the other parts were shaped to omit the upper and lower circular arcs so that these parts did not interfere with the participant's body and the MRI gantry during steering rotation.

- ***Adjustments for differences in physique***

Because the participant's head was fixed, the position of the steering wheel, where the participants could choose an appropriate steering posture, was different for participants with different physiques. In general, the taller a participant was, the farther the steering wheel was from his/her head. This dimensional difference was adjusted by using shafts of different lengths, and by increasing or decreasing the gap of the shaft's connecting part.

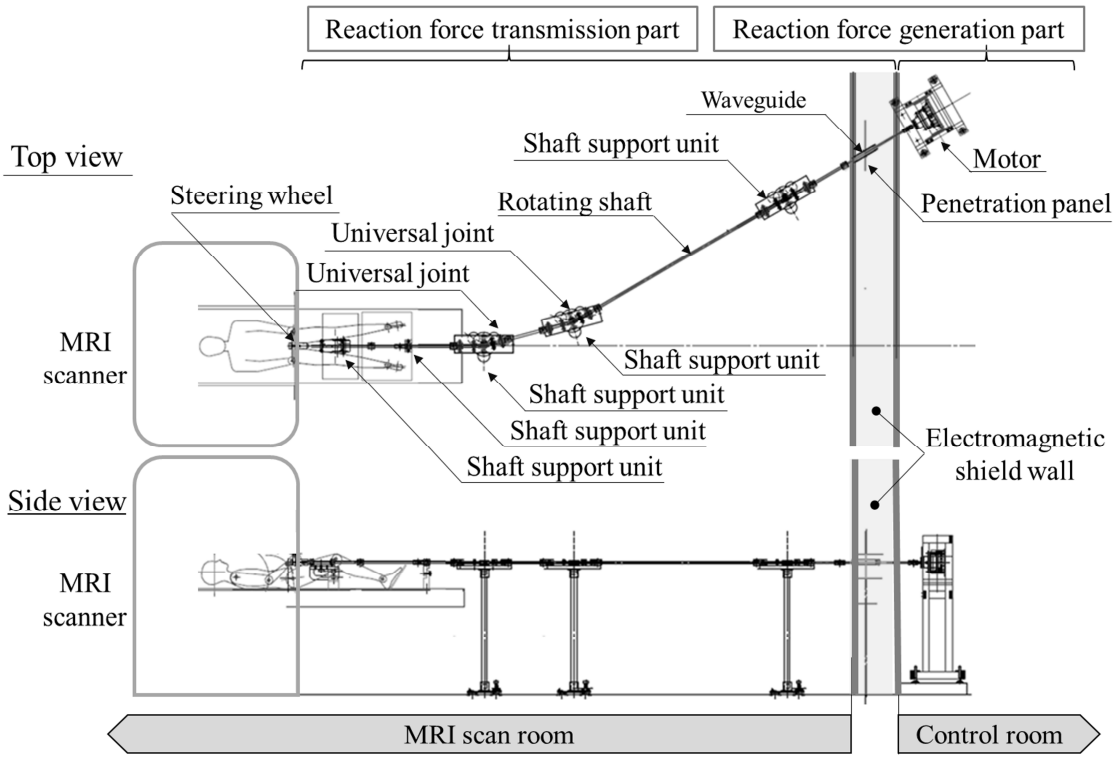

Fig. 2.2. Configuration of fMRI-compatible steering reaction force generation unit.

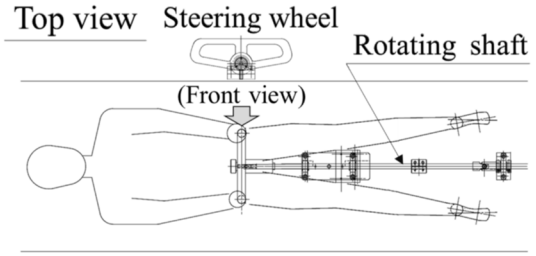

Fig. 2.3. Steering posture.

2.4. **Verification of steering reaction force generation performance**

2.4.1. Methods

The output of the reaction force generation motor was transmitted to the participant, lying in the MRI scanner and operating the steering wheel, by using the reaction force transmission unit. As this unit consisted of long rotating shafts and universal joints, elastic strain was assumed to have been generated during the transmission of the output of the reaction force generation motor. Therefore, the relationship between the output of the motor and the steering reaction force at the position of the steering wheel in the MRI scanner needed to be measured.

However, as a torque measurement device cannot be brought inside the MRI room because of the strong magnetic field inside, the unit was arranged in a room that had a normal magnetic field, and the layout of which was the same as that of the MRI scan room. The steering effort sensor (01184, Sensor Developments Inc. Chelmsford, MA 01824, USA) was attached to the steering wheel. The output of the reaction force generation motor and the reaction force at the hand of the participant were measured.

We set two conditions—low and high—for stiffness against reaction force around the axis of the steering shaft. In this experiment, we determined the control parameter of the reaction force generation motor such that a predetermined steering reaction force was generated when the steering wheel was rotated by $\pi/6$ rad under each condition. Stiffness was determined as the slope of the linear fit-to-rotation angle-reaction torque profile. The stiffness against the rotation of the steering shaft was 2.8 Nm/rad under the “low”

condition and 6.1 Nm/rad under the “high” condition. For these two conditions, the experimenter rotated the steering wheel by π/6 rad to the left and right using both arms with a period of approximately 4 s. The reaction force at the steering wheel and the output of the reaction force generation motor were recorded at a sampling frequency of 100 Hz.

2.4.2. Results

Fig. 2.4 shows the reaction torque measured with the steering wheel rotated by π/6 rad under conditions of low and high reaction torque stiffness. The characteristics of the frequency domain are also shown in Fig. 2.5. The steering effort sensor (Model 01184, Sensor Developments Inc. Chelmsford, MA 01824, USA) was attached to the wooden steering wheel of the proposed equipment. For each of the nine frequencies from 0.25 Hz to 1.5 Hz, the wheel was steered side to side at a maximum angle of π/6 (rad) for 250 cycles. The steering torque, the steering angle of the steering wheel, the torque, and the rotation angle of the motor were recorded at a sampling frequency of 100 Hz. We then calculated the magnitude and phase delay of the motor torque with respect to the steering torque. The motor installed in the steering reaction force generation unit is controlled to generate the steering torque according to the rotation angle of the motor. The rotation angle is generated by the participant’s steering operation, which applies steering torque. Therefore, we calculated the frequency property using the steering torque as the input and the motor torque as the output. By inspecting the figure of the frequency response, we confirmed that the gain is about 1, and the phase delay is about 5-10°.

Fig. 2.6 shows the scatter plot of the rotational torque measured at the output of the reaction force generation motor. The correlation coefficient was 0.974 under the low

condition and 0.992 under the high condition.

Fig. 2.7 shows the steering rotation angle and the reaction torque measured at the position of the steering wheel; in the figure, time is plotted along the horizontal axis. The correlation between the steering rotation angle and the reaction torque was as shown in Fig. 2.8. A linear approximation formula according to the least-squares method was used to obtain this correlation. The R^2 value was 0.830 under the low condition and 0.958 under the high condition.

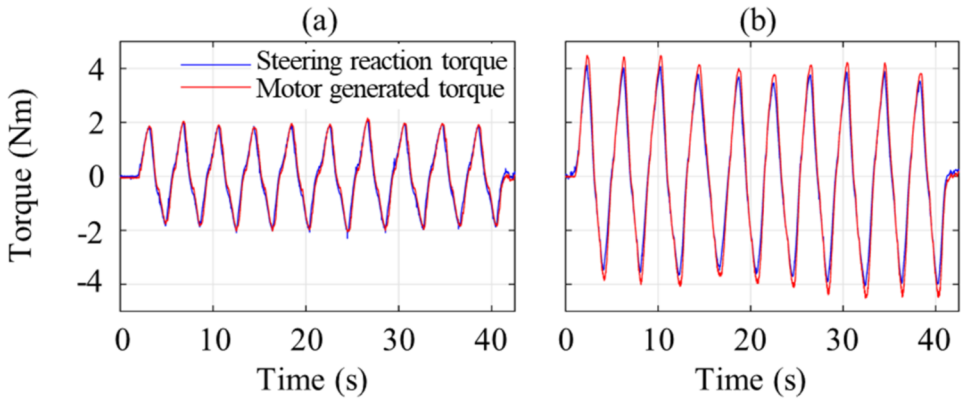

Fig. 2.4. Changes in reaction force with time at motor and steering wheel for (a) low and (b) high reaction force stiffnesses.

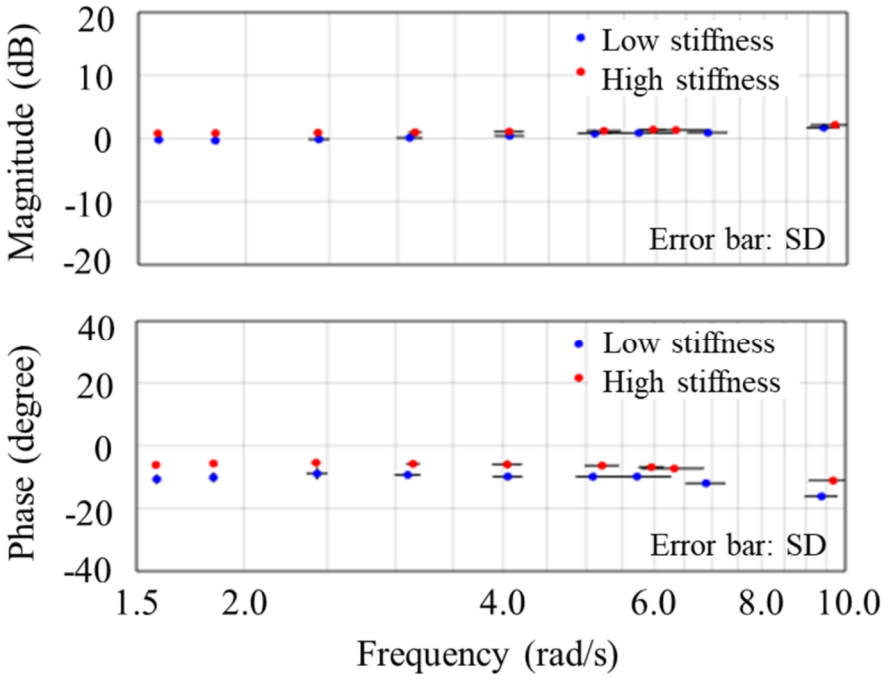

Fig. 2.5. Characteristics of the frequency domain with steering torque as the input and motor rotation torque as the output.

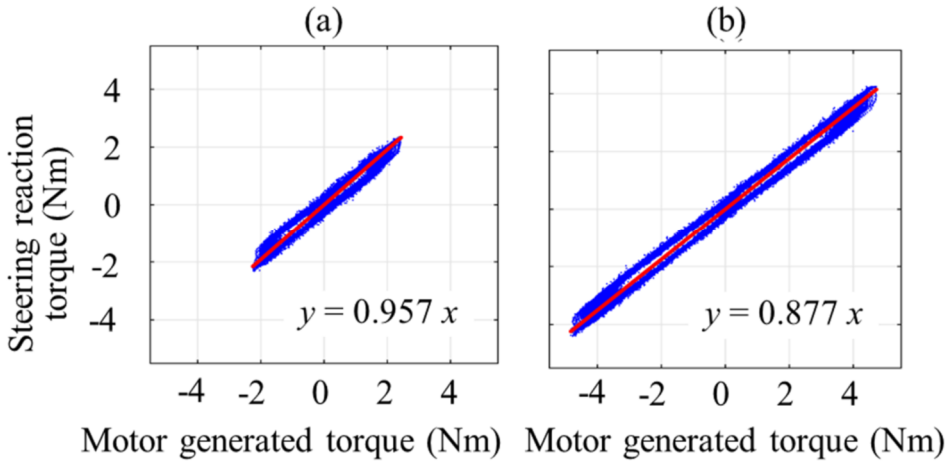

Fig. 2.6. Correlation of reaction force at motor output and steering wheel for (a) low and (b) high reaction force stiffnesses.

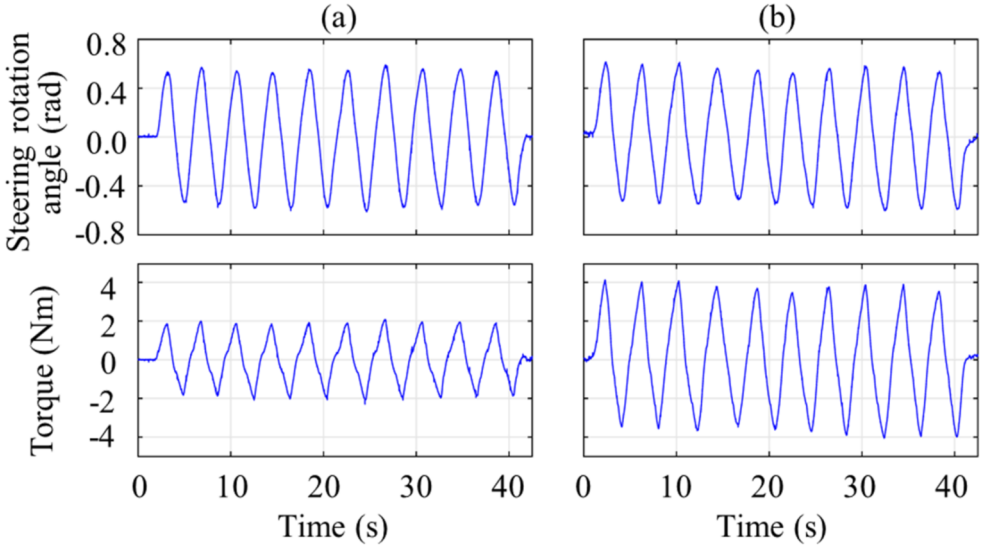

Fig. 2.7. Changes in steering angle and reaction force with time at steering wheel for (a) low and (b) high reaction force stiffnesses.

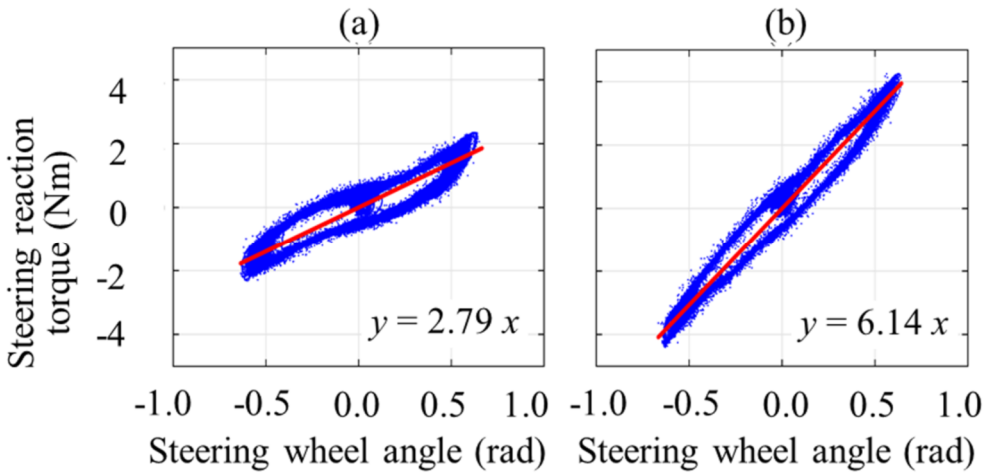

Fig. 2.8. Correlation of steering rotation angle and reaction force at steering wheel for (a) low and (b) high reaction force stiffnesses

2.4.3. Discussion

Although the reaction force generated on the participant's hand against the reaction force generation motor output (see Fig. 2.6) deviated from the linear approximation of a straight line, the correlation coefficient showed a clear relationship between the reaction force generated on the participant's hand and the output of the reaction force generation motor (0.974 under the Low condition and 0.992 under the High condition; ps < 0.001). This indicated that the output of the reaction force generation motor was transmitted accurately to the participant's hand on average.

The reaction force exerted on the hand of the participant with respect to the rotation angle of steering (see Fig. 2.8) also deviated from the linearly approximated straight line. The correlation as transmitted accurately to the participant's hand on average was 0.830 under the low condition and 0.958 under the high condition ($p < 0.001$), indicating that the reaction force was generated exactly with respect to the rotation angle while steering. The slope of the regression line (i.e., reaction force stiffness) under the high condition (6.1 Nm/rad) was approximately 2.2 times that under the low condition (2.8 Nm/rad). This suggested that these two conditions with different steering reaction forces were appropriate for the verification of fMRI performance. It should be noted that some deviations from the regression lines were observed as shown in Figs. 2.6 and 2.8, and there was a phase delay as shown in Fig. 2.5. In future, we intend to reduce the phase delay by using a shaft with higher torsional stiffness and less viscosity.

2.5. Conclusion remarks

In this described that a developed an fMRI-compatible steering reaction force

presentation device. By verifying its performance for steering reaction force generation, we confirmed that the steering reaction force of different magnitudes can be presented at the position of the hand using an MRI scanner.

Chapter 3
Verification of fMRI acquisition performance of fMRI-compatible steering reaction force generation unit

3.1. Introduction

During the operation of the unit, we must consider the following possibilities that might cause the unit to affect MRI imaging performance: (1) an electromagnetic field generated by the reaction force generation motor, and (2) magnetic field disturbance caused by the rotation of members and parts installed in the MRI scan room. To examine these possibilities, we perform two experiments to determine whether fMRI measurement is possible for participants operating the steering under the steering reactive force, and whether brain activity while executing steering operations using the unit is consistent with that reported in previous studies.

The structure of this chapter is as follows. Section 3.2 describes the verification of noise caused by motor operation, Section 3.2.1 describes the experiment, and Section 3.2.2 describes the results and discussion. Section 3.3 describes the verification of functional imaging during steering, Section 3.3.1 describes the experiment, and Section 3.3.2 describes the results and discussion. 3.4 describes the conclusion remarks.

3.2. Noise assessment caused by motor operation

The brain activity of participants at rest with their eyes closed was measured using the apparatus described in the foregoing. We compared brain activities between the conditions when the motor was rotating and when it was not. Through this comparison, we examined the influence of the noise caused by the motor on the functional images.

These experiments were approved by the Research Ethics Committee of Hiroshima University and Mazda Motor Corporation (approval numbers E-965-3 and TRC-151-09). Prior to the experiment, we obtained informed consent from all participants in writing.

3.2.1. Methods

We measured fMRI responses while the participants were not grasping the steering wheel, with the wheel being rotated automatically by the reaction force generation motor.

- ***Participants***

The participants were 21 men (average age: 21.8 ± 1.7 years) with no history of neurological or psychiatric disorders.

- ***Experimental design***

With the unit installed in the MRI scanner, the participants were asked to lie on the bed. The experiment consisted of 20-s blocks during which the motor was not rotated (no-rotation condition) and other blocks of time during which it was (rotation condition). Each experimental run lasted for 430 s. Each run began with five dummy scans (10 s) that were discarded to allow for T1 equilibration effects. Blocks of the no-rotation and the rotation conditions were then alternately repeated 10 times; finally, one block of the no-rotation condition was added following the 10th block of the rotation condition. In the rotation

condition, the motor rotated to the right and left by approximately π/18 rad at intervals of 2 s. The participants wore earplugs and headphones that attenuated noise from the MRI scanner. They were instructed to close their eyes and rest during the experiment. No clues to distinguish the onset of the no-rotation or the rotation condition were presented to them. All participants reported having been unaware of the operation of the motor.

- ***fMRI data acquisition***

A 3.0-T MRI scanner (MAGNETOM Verio, Siemens AG, Munich, Germany) was used to obtain MRI data. The functional images were acquired using a T2*-weighted gradient echo planar imaging (EPI) method. The imaging parameters were as follows: TR = 2000 ms, TE = 24 ms, 30 slices, slice thickness = 4 mm (without gaps), voxel size = 3 × 3 × 4 mm, flip angle = 75°, and field of view (FOV) = 192 mm.

The structural image was acquired using the T1-weighted 3D magnetization-prepared rapid gradient echo imaging method. The imaging parameters were as follows: TR = 2500 ms, TE = 2.98 ms, 176 slices, thickness = 1 mm, voxel size = 1 × 1 × 1 mm, flip angle = 9°, and FOV = 192 mm.

- ***fMRI data analysis***

The data were analyzed using the statistical parametric mapping (SPM) 12 package [27]. From the functional image obtained for each participant, five volumes obtained during the dummy scans were excluded from the analysis and the remaining 110 volumes were analyzed. Spatial correction of the movement of the head was first performed based on the first volume (realignment), and the correction of in the timing of the imaging (slice timing correction) was carried out. The T1-weighted structural image for each participant was then aligned to the first volume of the corresponding participant (co-registered) and

normalized to the Montreal Neurological Institute (MNI) template. Following this, the normalized images of the echo planar were smoothened by a Gaussian kernel (full width at half maximum = 8 mm). The T1-weighted structural image for each participant was then aligned to the first volume of the corresponding participant (co-registered) and normalized to the MNI template.

For pre-processed echo planar images, we performed a statistical analysis using a general linear model. The rotation and no-rotation conditions were modeled by a boxcar function by convolving the hemodynamic response function (HRF). In addition, to remove artifacts related to the movement of the head, six relevant parameters obtained from realignment processing were included as regressors in the model.

Prior to regression analysis, low-frequency fluctuations in the blood oxygenation level-dependent (BOLD) signal were eliminated by applying a high-pass filter with a cutoff of 128 s. Moreover, serial correlations among the scans were estimated using an autoregressive model (AR (1)) to remove high-frequency noise contaminating the EPI time series. The contrast images between the no-rotation and the rotation conditions were calculated for each participant using the fixed-effects model and were then considered in group analysis using a random-effects model.

3.2.2. Results and discussion

To verify whether the noise caused by motor operation affected the acquired functional images, we performed a one-sample t-test on the contrast images between the rotation and no-rotation conditions with a family-wise error (FWE) corrected for $p < 0.05$ as the activity peak threshold. This revealed that no voxel was significantly activated in the

rotation condition compared with the no-rotation condition for 21 participants.

A comparison between brain activities when the motor was operated and when it was not indicated no significant activation for all participants. This suggested that the electromagnetic field generated by the motor does not affect brain imaging.

3.3. Verification of fMRI acquisition performance during steering

The participants performed a steering operation by using their right hands, left hands, or both hands. We looked for brain activity in the motor area on the opposite side of the operating arm, as reported in previous studies (e.g., Roland *et al*. [28] and Kinoshita *et al*. [29]).

This experiment was approved by the Research Ethics Committee of Hiroshima University and Mazda Motor Corporation (approval numbers E-965-3 and TRC-151-09). Prior to the experiment, we obtained informed consent from all participants in writing.

3.3.1. Methods

- ***Participants***

The participants for this experiment were 27 men aged 19–32 years with no history of neurological or psychiatric disorders. The laterality quotient (LQ) was calculated according to the Edinburgh inventory [30]. Two participants with LQ < 0 were regarded as left handed and excluded from the analysis. Six participants whose head movements exceeded 4 mm were excluded as well. As a result, data from 19 participants (average

age: 22.7 ± 2.9 years) were used for analysis.

- ***Experimental design***

Table 3.1 lists the conditions for the arm used for steering and the stiffness in the rotation of the steering shaft. The reaction torque stiffness around the steering axis at the gripping position of the steering wheel operated by the participants was set at two levels: low (2.8 Nm/rad) and high (6.1 Nm/rad). These values were obtained by converting the values of 2.8 Nm/rad in the low condition and 6.1 Nm/rad in the high condition, which had been used to verify reaction force generation performance, into the torque of the steering wheel at the gripping position (0.185 m from the center of rotation). At the high level, participants used both arms for manipulation (High-B condition). At the low level, they used their left arms, right arms, or both (Low-L, Low-R, and Low-B conditions, respectively).

The experimental protocol is shown in Fig. 3.1. The experiment consisted of four sessions. The four conditions (Table 3.1)—Low-L, Low-R, Low-B, and High-B—were used in each session in random order for each participant. Each session lasted for 320 s. Five dummy scans (10 s) were carried out to discard the volumes and allow for T1 equilibration. The rest (10 s) and the task (20 s) blocks were alternately repeated 10 times and, finally, one rest block (10 s) was added (Fig. 3.2).

Prior to each session, the experimenter instructed the participants on which arm(s) to use for steering. Each session began with a fixation cross presented at the center of the screen. After 10 s, bars tilted by $\pi/4$ rad and $-\pi/4$ rad were presented alternately for 1 s each. The color of the bar was a cue for block identification (task or rest block), and the correspondence between the condition and the color was counterbalanced for each

participant.

The participants were instructed to avoid moving their eyes as much as possible from the fixation cross displayed at the center of the screen, and to rotate the steering wheel by π/9 rad to the left and right according to the direction of the bar, when a bar of a specific color was presented. In addition, they were instructed to not release the steering wheel until the session was over, move their heads as little as possible, and not perform any action except the steering operation during each session. Before the experiment, the participants were trained to rotate the steering wheel by π/9 rad in accordance with the experimenter's instruction, so that they could remember the operation during the task blocks.

To reduce the movement of the participants' heads during the steering operation in the task blocks, the face and the head coil were connected using skin tape, and cushions were used on both the sides of the head to suppress movement. This was done with the consent of the participants. Moreover, the participants were instructed to avoid movement of the head by paying attention to the tension in the tape, felt when their heads began to move. Moreover, prior to the first session, the participants performed two practice trials for each condition.

- ***fMRI data acquisition***

We used the 3.0 T MRI scanner used in 3.2.1. The imaging parameters were also the same as those in 3.2.1.

- ***fMRI data analysis***

In each session, we obtained 161 volumes. In the dummy scan, five volumes were discarded from the analysis and the remaining 156 were preprocessed using the procedure

employed in 3.2.1. In the statistical analysis, the task and rest blocks were modeled by a boxcar function by convolving the HRF. The contrast images between the task and the rest of the blocks were calculated for each participant using the fixed-effects model and were then taken into the group analysis using a random-effects model.

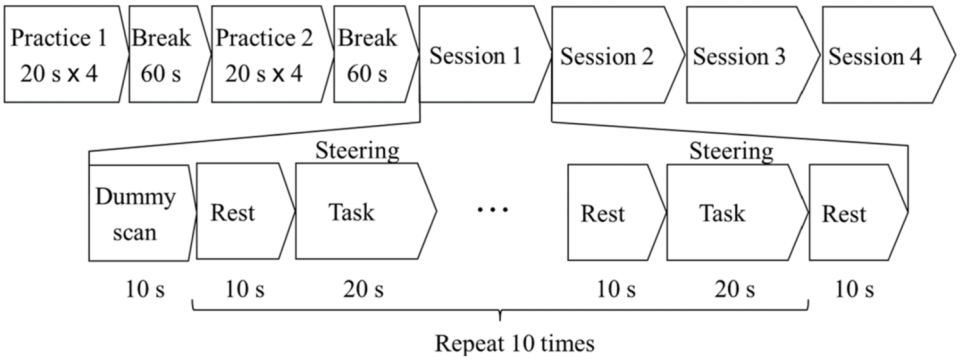

Fig. 3.1. Experimental protocol.

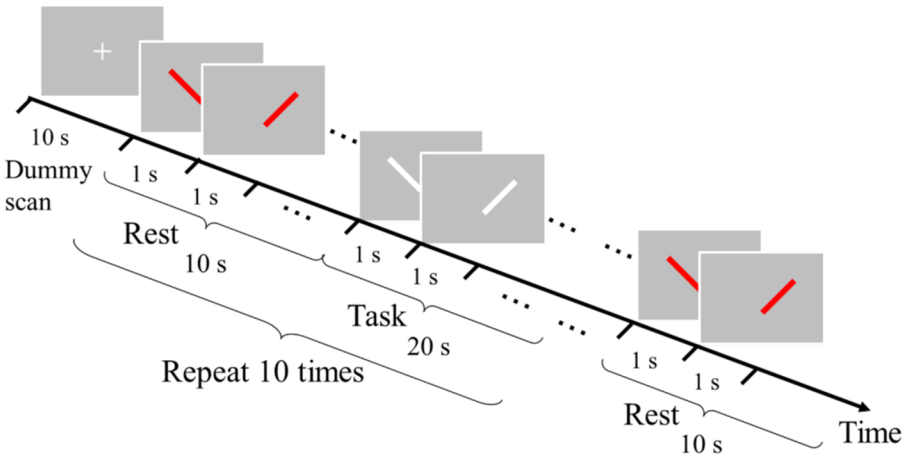

Fig. 3.2. Timeline of experiment. Ten repetitions of the rest (10 s) and task (20 s) blocks. A fixation cross was displayed at the center of the screen throughout the experimental run. Ten seconds after the beginning of the experiment, bars tilted by ±π/4 rad were presented alternately for 1 s each. The participants were instructed to look at the fixation cross and hold the steering wheel. The colors of the bars indicate rest or task block. The participants were instructed to steer in the direction in which the bar was tilted when white bars were presented, and to not steer when red bars were shown. The relationship between the colors and the task/rest block was counterbalanced across participants.

Table 3.1 Experimental conditions for steering arm and reaction torque stiffness

			Steering arm		
			Left arm	Right arm	Both arms
Reaction torque stiffness	Low	2.8 Nm/rad	Low-L	Low-R	Low-B
	High	6.1 Nm/rad	-	-	High-B

3.3.2. Results

Fig. 3.3 shows the displacements of the head calculated in the realignment process during the preprocessing stage of MRI analysis; the results are indicated separately for the analysis target group and the excluded group. In the figure, *Dx, Dy,* and *Dz* represent the displacements along the x, y, and z directions, respectively, and *θ pitch, θ roll,* and *θ yaw* indicate the rotation along the pitch, roll, and yaw directions, respectively.

We compared the contrast images between the task for each condition (Low-L, Low-R, Low-B, and High-B) and the rest blocks. A one-sample t-test with the FWE corrected for $p < 0.05$ (with a cluster extent of $k > 20$ voxels) revealed that common activities occurred in the primary motor cortex and the cerebellum under all conditions. In particular in the primary motor cortex, we observed right hemispheric dominance under the Low-L condition and left hemispheric dominance under the Low-R condition (Table 3.2 and Fig. 3.4).

To examine whether the degree of handedness affected the results, percentage changes in the BOLD signal of the primary motor cortices under the Low-B and the High-B conditions were calculated using MarsBar [32] for 16 participants with LQ > 0.7, which had been used in previous studies as the criterion for determining dextrality (e.g., [33]). For each participant, we summed the percentage change in the BOLD signal in the left and right primary motor cortices.

Fig. 3.5 shows the percentage change in the BOLD signal in the bilateral primary motor cortices averaged over 16 participants under each condition for the reaction force torque stiffness. A paired t-test showed that the percent signal change tended to increase under the High-B condition than under the Low-B condition ($t = 1.378$, $df = 15$, $p = 0.0944$).

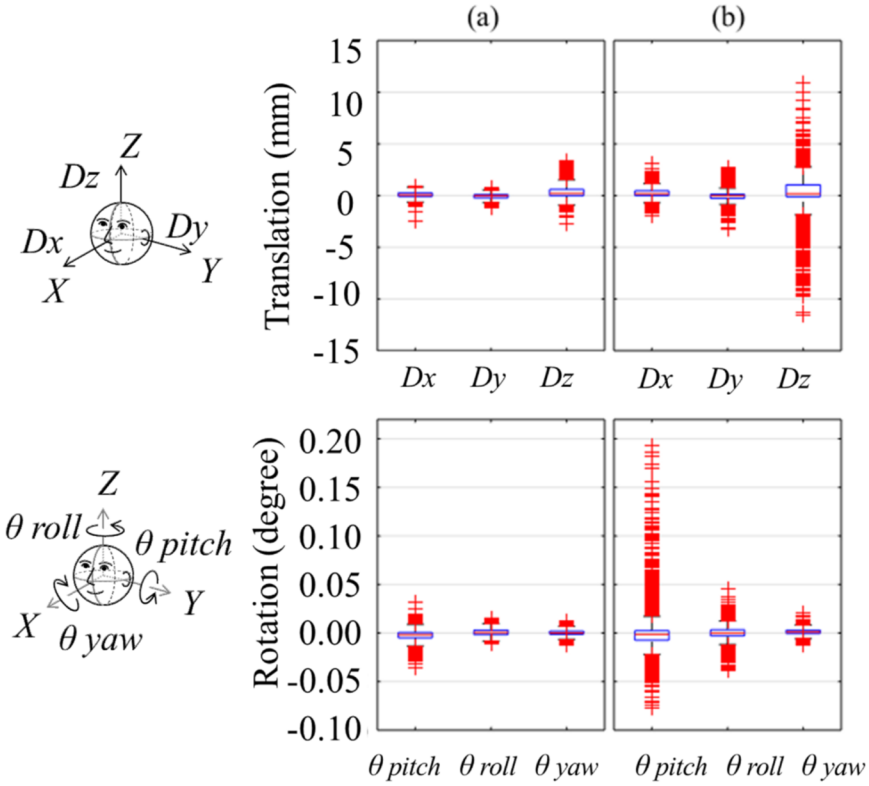

Fig. 3.3. Displacement and rotation of head position for (a) analyzed and (b) excluded volumes. The *X, Y*, and *Z* axes are coordinate axes in the MNI (Montreal Neurological Institute) coordinate system [31], and *θ yaw, θ pitch,* and *θ roll* indicate rotation about the *X, Y*, and *Z* axes, respectively.

Low-L	Low-R
Reaction torque stiffness: Low	
Left arm	Right arm
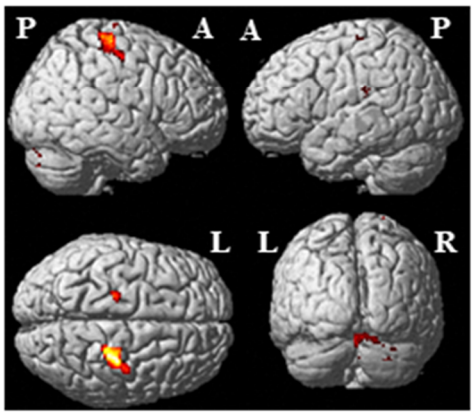	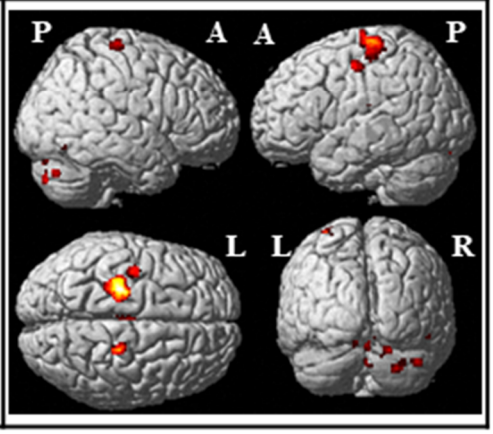

Low-B	High-B
Reaction torque stiffness: Low	Reaction torque stiffness: High
Both arms	
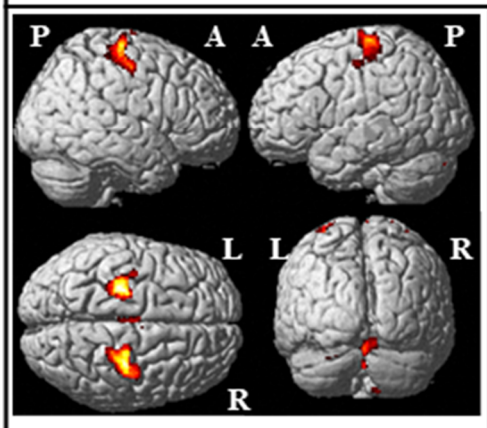	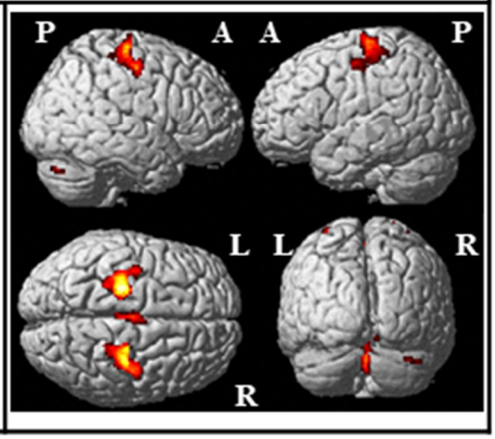

Fig. 3.4. Detected brain activated area.

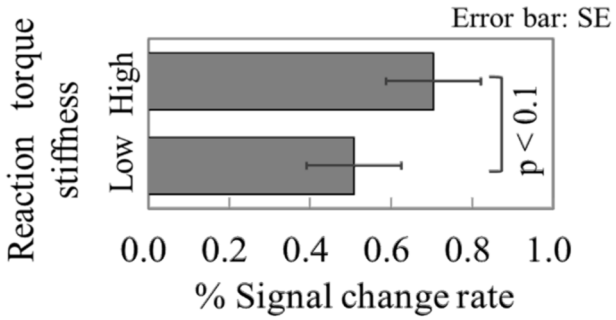

Fig. 3.5. BOLD signal change rate in primary motor cortex for subjects screened with LQ > 0.7.

Table 3.2 Location and volume of activation clusters

X, Y, and Z indicate the coordinates in the MNI coordinate system. As shown in Fig. 3.4, the MNI coordinate system is a right-handed system where the anteroposterior direction of the head is along the x axis, the lateral direction was the y-axis, and the vertical direction is the z -axis. The origin is at 2.5 mm along the x-axis and 4.5 mm along the z-axis from the anterior commissure. The origin was located at the center in the lateral direction of the brain, 74.5 mm from the front end, 106.5 mm from the rear end, 82 mm from the upper end, and 52 mm from the lower end.

	Region	BA	*X* (mm)	*Y* (mm)	*Z* (mm)	Peak Z	Voxels
Low-L	R Precentral gyrus	4/6	28	-24	56	5.79	504
	L Parietal operculum		-40	-28	22	5.53	86
	Cerebellar		-2	-60	-20	5.29	154
	➢ L Cerebellum		-8	-54	-10	5.15	
	➢ L Cerebellum		-12	-48	-16	5.14	
	L Cingulate gyrus		-18	-42	20	5.22	40
	Cerebellar		4	-80	-22	5.18	61
	➢ R Cerebellum		16	-84	-22	5.09	
	L Precentral gyrus	4	-20	-22	66	5.08	46
Low-R	L Precentral gyrus	4/6	-28	-24	54	6.33	658
	L Precentral gyrus	4/6	-40	-12	50	6.15	75
	R Cerebellum		44	-74	-34	5.98	26
	R Precentral gyrus	6	24	-24	68	5.74	122
	R Cerebellum		26	-84	-38	5.59	37
	Cerebellar		2	-60	-20	5.20	79
	➢ R Cerebellum		10	-72	14	4.94	
	R Cerebellum		18	-84	-26	5.19	27
	L Cerebellum		-4	-40	0	5.17	31
	L Supplemental motor area	6	-2	-16	54	5.16	37
Low-B	R Precentral gyrus	4/6	40	-16	52	6.29	843
	L Precentral gyrus	4/6	-26	-24	58	5.91	696
	Cerebellar		0	-60	-20	5.74	230
	Cerebellar		0	-46	2	5.66	102
	R Supplemental motor area	6	8	-22	50	5.33	34
	L Supplemental motor area	6	-4	-14	54	5.25	97
	Cerebellar		4	-78	-22	5.17	88
High-B	R Precentral gyrus	4/6	40	-14	52	6.46	828
	L Precentral gyrus	4/6	-24	-24	60	6.41	1012
	Cerebellar		0	-60	-18	5.85	736
	➢ Cerebellar		2	-74	-30	5.34	
	➢ R Cerebellum		14	-48	-18	5.08	
	L Paracentral lobule	6	-2	-24	52	5.61	327
	R Cerebellum		36	-80	-32	5.23	27
	Cerebellar		0	-44	0	5.21	47

3.3.3. Discussion

The results of fMRI data (Fig. 3.4, Table 3.2) under low reaction torque stiffness (Low-L, Low-R, and Low-B) showed significant brain activity during the task in the right primary motor cortex for steering using the left arm (Low-L), in the left primary motor cortex for steering using the right arm (Low-R), and the bilateral motor cortices for steering using both arms (Low-B). Significant activity was also observed in the cerebellum for all three (Low-L, Low-R, and Low-B) conditions. Under the High-B condition, wherein reaction torque stiffness was high, significant activity was observed relative to the rest block in the bilateral primary motor cortices and the cerebellum, as observed under the Low-B condition. These activated regions were consistent with those reported in many previous studies (e.g., [34]) reporting MRI measurements during hand or arm movements. Furthermore, as these results were obtained with the same peak threshold as that in 3.2.2, the influence of noise due to the operation of the motor was sufficiently small, suggesting that brain activity measurement was not obstructed by the use of the unit. Thus, we confirmed that brain activity related to the movement of the hands can be measured using this unit to yield results consistent with those of previous studies.

Because the steering operation was performed to the left and the right against the reaction force while the participants were lying in the MRI scanner, there was a concern whereby body movements could have become significant. In particular, the displacement in the left and right directions (Dy) as well as the roll direction ($\theta\,roll$) might have become large. However, the magnitude of displacement of the head (Fig. 3.3) indicated that this and the standard deviation along the z direction were large both in the group for analysis

and that to be excluded; in particular in the latter, the displacements along the z and the pitch directions were larger than those in the group for analysis. Moreover, approximately 30% of the participants were excluded from analysis because the maximum displacement of the head for them during imaging was greater than 4 mm. This excessive displacement was only along the z direction.

These results can be interpreted as follows: Because the axis of the steering wheel was along the horizontal direction, changes in the elbow angle because of the steering operation caused a component force in the direction parallel to the axis of the steering wheel, and a reaction force was generated along the z and the pitch directions with respect to the participant's body. This force was generated by the gap between the head coil and the head of the participant. We fixed the participant's head by placing urethane cushions on both the sides of his head, but we did not place a cushion in the gap above the head. Moreover, we used surgical tape on the participant's forehead and the head coil so that he would be aware of head movements by sensing the tension in the tape. However, the tension on the face along the z direction to suppress the movement of the head was difficult to perceive than the tension in the tape along the y direction, and it might have been difficult to perceive head movements along the z direction. By improving methods to suppress the participants' head movement along the z and the pitch directions, the number of participants excluded from analysis can be reduced.

To examine brain activity according to reaction torque stiffness, the rate of change in the BOLD signal in the bilateral primary motor cortices was calculated for 16 participants with LQ > 0.7; this has been used as right-handed reference in previous studies [33]. We found that the activity tended to increase under the High-B condition relative to that under

the Low-B condition (see Fig. 3.5). The results of past studies have indicated that the degree of force exerted and the BOLD signal of the primary motor cortex are positively correlated [18]. The results of this experiment were consistent with those of previous studies.

However, we did not observe statistically significant differences between BOLD responses under the High-B and the Low-B conditions. This can be interpreted as follows: Because this experiment aimed to verify the performance of the proposed unit, the participants were asked to keep the steering operation as simple as possible. However, the operation involves cooperative movement of the arms with multiple degrees of freedom, including the movement of the elbow, the wrist, and the joints of the shoulder. Therefore, the movement is not necessarily simple. For example, it is known that neural crosstalk, which is defined as a mirror image command sent to the homologous muscles of the contralateral limb, exists between the arms; this crosstalk contributes to the learning and stability of performance on bimanual force production tasks, as reported previously by Kennedy *et al*. [35]. Therefore, we can infer that under the Low-B and High-B conditions, where the magnitude of the reaction force changed according to manipulation by both arms, hemodynamic responses related to neural crosstalk were also contaminated. Yokoi *et al*. [36] also reported the difference in role sharing between the dominant and nondominant hands in motor learning with arm coordination. Therefore, if the number of degrees of freedom of the dominant hand differs from that of the nondominant hand, there is a difference in role sharing. We inferred that the hemodynamic responses might have been contaminated in response to this difference. Unlike previous studies analyzing the increase in the BOLD signal of the primary motor cortices depending on the force exerted

on single-arm movements, in this study, the fMRI results might have been contaminated by a factor specific to bimanual coordination. Therefore, using the criterion of right handedness (LQ > 0.7) can reduce this contamination. Taken together, our unit yields satisfactory performance in terms of presenting various reaction forces and can be used in MRI scanners to measure brain activity during simulated driving.

- ***Limitations***

The major limitation of this study is that the steering in MRI was restricted to a supine position, which exerted a significant impact on the state of the muscle. As the proposed device does not affect the magnetic field while imaging brain activity by installing the power source outside the MRI room, the layout configuration of the experimental environment is highly flexible. Therefore, it can be easily combined with Stand-Up MRI [37] and PET [38] which can measure brain activity in the sitting position and solve problems posed by posture restriction. Moreover, we plan to perform experiments using real vehicles to obtain data that complement the MRI measurement, and to clarify the relationships between driving motion in a supine posture under MRI environment and that in a sitting posture during normal driving.

Further, the following problems originating from the fMRI experimental environment must be solved: (i) realizing the feeling of driving immersion, (ii) reducing awkward feelings from fMRI measurement, (iii) reducing the differences between the biomechanical conditions of actual driving environment and the fMRI experimental environment. Regarding problem (i), previous studies [12], [13] derived important scientific insights into brain functions by presenting appropriate driving cues to simulate the driving situation under fMRI experimental environments. The achievements of these

previous studies indicate that a highly realistic simulated environment is not always necessary if the principal cues of a driving situation are provided. In our study, the principal cue is the force feedback. The force feedback not only enabled us to measure the human responses against the force feedback but also increased the feeling of immersion relative to previous studies. Nonetheless, fMRI-compatible virtual reality devices [39] should be developed in the future to further improve the feeling of immersion. Regarding (ii), we tried to reduce awkward feelings caused by the enclosed gantry, loud noises, and physical restraint caused by the fMRI experimental environment. For example, we used active noise-cancelling headphones, and we applied the minimum sufficient head stabilization (i.e., we used cushions to restrain the participant's head by pressing the parietal bone in the minus direction along the y-axis), and supported the participants to maintain the desired posture and decrease fatigue. Regarding (iii), we plan to carry out complementary experiments using EEG (Electroencephalogram e.g., [40]) to clarify the influence of acceleration input on the sense of balance through semicircular canal and vestibular organ.

3.4. **Conclusion remarks**

The fMRI acquisition performance of the fMRI-compatible steering reaction force generation unit was verified by the following. (1) A comparison between brain activities when the motor was operated and when it was not indicated no significant activation for 21 participants. This suggested that the electromagnetic field generated by the motor does not affect brain imaging. (2) The brain activity of 19 participants of an experiment were

measured by using fMRI while they performed steering operations using their arm/arms under various steering forces. The results were consistent with those for motor-related brain activity obtained in past neuroimaging studies. Therefore, it was concluded that the proposed unit can measure brain activity through fMRI in the presence of a steering reaction force.

The results obtained using this novel device can contribute to our understanding of the relationship between the characteristics of the steering force of automobiles and brain activity. Moreover, because our measurement of brain activity is aimed to resolve the effect of drivers' steering operation on the functioning of the motor control and cognitive emotional evaluation systems, this device will help to understand the intrinsic driving pleasure to design a steering control system for a car that is pleasing to drive.

However, to improve the reproducibility of the steering characteristics, the rigidity of the torque transmission shaft should be improved. Moreover, to further improve the imaging accuracy of fMRI, it is desirable to further suppress head movement along the z direction. In future research, we plan to investigate brain activity under more realistic experimental settings—for instance, by presenting visual stimuli generated by a driving simulator. The proposed apparatus can be used to elucidate the relationship between brain function and reaction force, which depends on personal characteristics. Such relationships can be applied to generate appropriate reaction forces to compensate for the burden of visual cognition, and to support cognitive functions of elderly and new drivers.

Chapter 4
Brain activity while waiting for the upcoming steering task

4.1. Introduction

This chapter focuses on brain activity while waiting for steering, assuming it reflects the emotional state of the participants in preparing for the next steering task. We examine the brain mechanism of drivers' anxiety associated with the characteristics of steering reaction force by analyzing data obtained from the verification of fMRI acquisition performance of our steering reaction force unit (chapter 3). We use a block design in which the blocks for steering and standby for steering are repeated, and we visualize brain activity focusing on a block of standby for steering that do not include brain activity directly related to steering movement. It can be assumed that the brain activity while waiting to steer includes the function of preparation for the upcoming steering operation. In addition, the brain activity for preparation may be affected by the upcoming condition of the magnitude of the steering reaction force and the condition of the arm to be used for steering.

The structure of this chapter is as follows. Section 4.2 describes the methods, Section 4.3 describes the results, Section 4.4 describes the discussion and Section 4.5 describes the conclusion remarks.

4.2. Methods

4.2.1. fMRI-compatible steering reaction force generation unit

We used the apparatus reported in our previous study [69] described in chapter 3. Fig. 4.1 shows the experimental environment including the fMRI-compatible simulated steering reaction force generation unit (hereinafter referred to as “the unit”). The unit consisted of a steering reaction force generation part and a reaction force transmission part. The unit simultaneously generated a steering reaction force, calculated based on the vehicle model of the driving simulator, depending on the steering rotation angle, which was fed back to a participant lying in the MRI scanner (Fig. 4.2). Using this unit, we constructed an experimental system that could acquire functional brain images in an experimental situation where participants virtually drove by their steering operation and received the steering reaction forces as feedback.

4.2.2. Measuring brain activities while waiting for the upcoming steering task

In this chapter, we focused while steering standby, analyzed fMRI data obtained from our previous experiment [69] described in chapter 3. Therefore, methodological details, such as participants, experimental design, and fMRI data acquisition and analysis, were the same as in the previous study.

- ***Participants***

The participants were voluntary applicants to the recruitment of participants, who were university or graduate male students and have driver's license. They were 27 men aged

19–32 years with no history of neurological or psychiatric disorders. The laterality quotient (LQ) was calculated according to the Edinburgh inventory [30]. Two participants with LQ < 0 were excluded from the analysis because they could be regarded as left-handed. Six participants whose head movements exceeded 4 mm were excluded for further analysis. Consequently, data from 19 participants (average age: 22.7 ± 2.9 years) were used for analysis.

- ***Experimental design***

Table 4.1 shows the conditions for the arm used for steering and the reaction torque stiffness. The reaction torque stiffness around the steering axis at the gripping position of the steering wheel operated by the participants was set at two levels: low (2.9 Nm/rad) and high (7.1 Nm/rad). At the low level, they used their left arm, right arm, or both (Low-L, Low-R, and Low-B conditions, respectively). At the high level, participants used both arms for manipulation (High-B condition).

The experiment consisted of four sessions. Each of the four conditions (Table 4.1)—Low-L, Low-R, Low-B, and High-B—was assigned in each session in random order for each participant. The protocol of the experiment is shown in Fig. 4.3. Each session lasted for 320 s. Five dummy scans (10 s) were carried out to discard the volumes and allow for T1 equilibration.

As shown in Fig. 4.4, the rest (10 s) and the task (20 s) blocks were alternately repeated 10 times and, finally, one rest block (10 s) was added. Prior to each session, the participants were instructed on which arm(s) to use for the task. Each session began with a fixation cross presented at the center of the screen. After 10 s, bars tilted by π/4 rad and -π/4 rad were presented alternately for 1 s each. The color of the bar was a cue for task or

rest. For each participant, the correspondence between the condition and the color was counterbalanced.

The participants were instructed not to release the steering wheel until the session was over, to move their heads as little as possible, and not to perform any action except the steering operation during a session. They were also instructed to avoid moving their eyes as much as possible from the fixation cross displayed at the center of the screen. When a bar, colored in a designated color as a task block, was presented, they were asked to rotate the steering wheel by $\pi/9$ rad to the left and right according to the direction of the bar. Before the experiment, the participants were trained to rotate the steering wheel by $\pi/9$ rad in accordance with the experimenter's instruction, so that they could remember the operation during the task blocks.

It is important for proper fMRI data acquisition to reduce the movement of the participants' heads during the experiment, especially during the steering operation in the task blocks. Participants' face and the head coil were connected using skin tape, and cushions were used on both the sides of the head to suppress movement. This was done with the consent of the participants. Moreover, the participants were instructed to avoid movement of the head by paying attention to the tension in the tape, so that they can feel their movement when their heads move. Moreover, prior to the first session, the participants performed two practice trials for each condition.

- ***MRI data acquisition***

To obtain MRI data, a 3.0-T MRI scanner (MAGNETOM Verio, Siemens AG, Munich, Germany) was used. The functional images were acquired using a T2*-weighted gradient echo planar imaging (EPI) method. The imaging parameters were as follows: TR = 2000

ms, TE = 24 ms, 30 slices, slice thickness = 4 mm (without gaps), voxel size = 3 × 3 × 4 mm, flip angle = 75°, and field of view (FOV) = 192 mm. The structural image was acquired using the T1-weighted 3D magnetization-prepared rapid gradient echo imaging method. The imaging parameters were as follows: TR = 2500 ms, TE = 2.98 ms, 176 slices, thickness = 1 mm, voxel size = 1 × 1 × 1 mm, flip angle = 9°, and FOV = 192 mm.

fMRI data analysis: For data analysis, the statistical parametric mapping (SPM) 12 package [27] was used. From the functional brain images obtained for each participant, five volumes obtained during the dummy scans were excluded from the analysis and the remaining 156 volumes were analyzed. Spatial correction of the movement of the head was performed based on the first volume (realignment), and the correction in the timing of the imaging (slice timing correction) was carried out. The T1-weighted structural image for each participant was then co-registered to the first volume of the corresponding participant and normalized to the Montreal Neurological Institute (MNI) template. Following this, the normalized images of the echo planar were smoothened by a Gaussian kernel (full width at half maximum = 8 mm).

We performed a statistical analysis using a general linear model for pre-processed echo planar images. The task and rest blocks were modeled by a boxcar function by convolving the hemodynamic response function (HRF). To remove artifacts related to the movement of the head, six relevant parameters obtained from realignment processing were included as regressors in the model.

Low-frequency fluctuations in the BOLD signal were eliminated by applying a high-pass filter with a cutoff of 128 s prior to regression analysis. To remove high-frequency noise contaminating the EPI time series, serial correlations among the scans were

estimated using an autoregressive model (AR (1)). The contrast images between the task and the rest blocks were calculated for each participant using the fixed-effects model and were then considered in group analysis using a random-effects model.

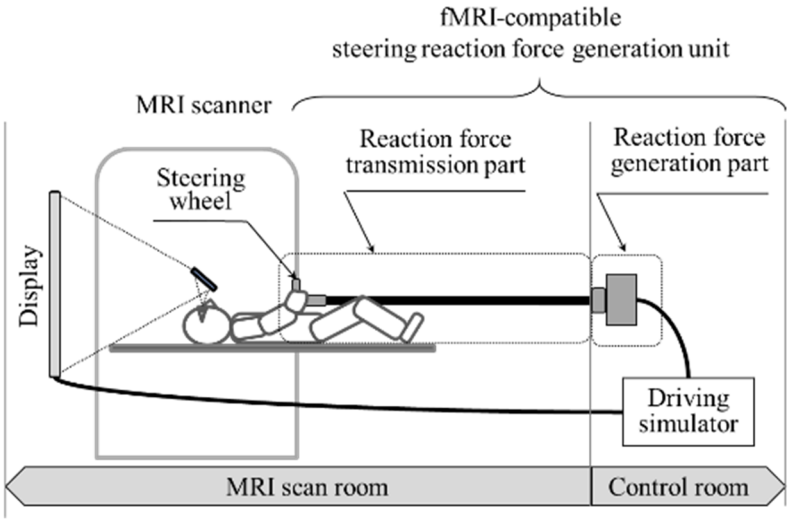

Fig. 4.1. Experimental system consisting of fMRI-compatible steering.

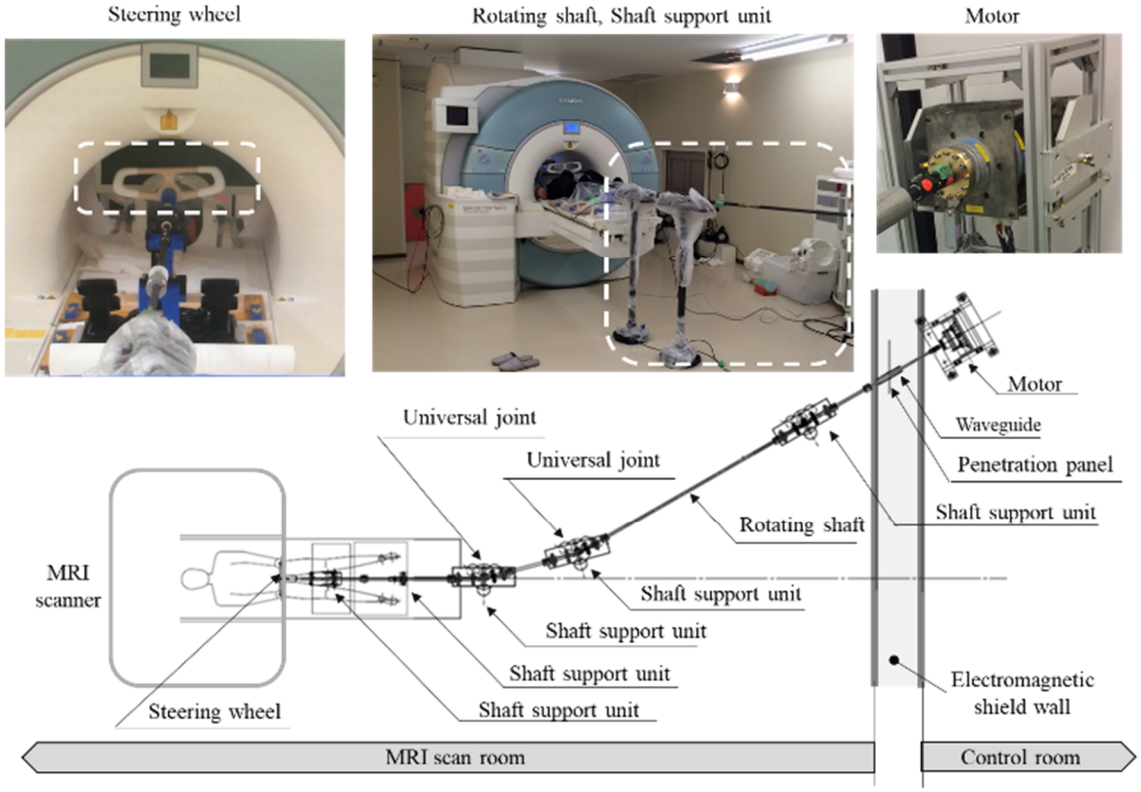

Fig. 4.2. fMRI-compatible steering reaction force generation unit.

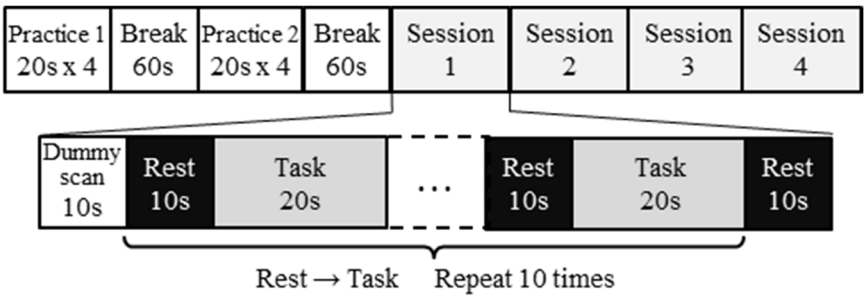

Fig. 4.3. Experimental protocol.

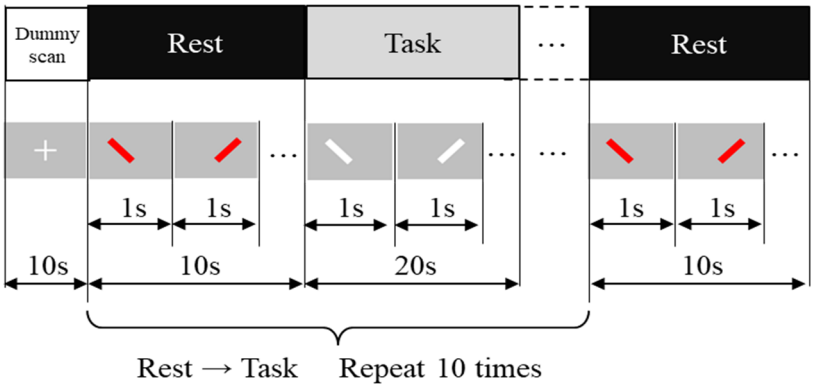

Fig. 4.4. Timeline of experiment. Ten repetitions of the rest (10 s) and task (20 s) blocks were performed. A fixation cross was displayed at the center of the screen throughout the experimental run. Ten seconds after the beginning of the experiment, bars tilted by ±π/4 rad were presented alternately for 1 s each. The participants were instructed to look at the fixation cross and hold the steering wheel. The colors of the bars indicate rest or task block. The participants were instructed to steer in the direction in which the bar was tilted when white bars were presented, and to not steer when red bars were shown. The relationship between the colors and the task/rest block was counterbalanced across participants.

Table 4.1 Experimental conditions for steering arm and reaction torque stiffness.

Steering arm / Reaction torque stiffness		Left arm	Right arm	Both arms
Low	2.8 Nm/rad	Low-L	Low-R	Low-B
High	6.1 Nm/rad	-	-	High-B

4.3. **Results**

To identify the brain region activated more during the rest than during the task for each condition, we created a contrast image that compared the brain activation during rest to that during the task for each condition. Then, we conducted a one-sample t-test using these contrast images. A one-sample t-test with a peak level threshold of uncorrected for multiple comparisons $p < 0.001$ and a cluster-level threshold of false discovery rate (FDR) corrected $p < 0.05$ revealed common activities in the ACC and the insula under all conditions (Table 4.2, Table 4.3, Fig. 4.5, Fig. 4.6, and Fig. 4.7).

The amygdala was active under Low_L condition (Table 4.2 and Fig. 4.6) for 16 participants with LQ > 0.7, used as the criterion for determining dextrality in the previous studies (e.g., [33]). Also, in the supplementary motor cortex, significant activation was observed under the Low_L condition (Table 4.2 and Fig. 4.7). To examine the BOLD signal change rate in the ACC, we conducted a structural region of interest (ROI) analysis. The region definitions used in the ROI analysis were derived from the Automated Anatomical Labeling library [41]. Under Low_B and High_B conditions, a BOLD signal change rate in the ACC, calculated using MarsBar [32] is shown in Fig. 4.8. We conducted paired t-test on BOLD signal changes at ACC during the rest, to examine the differences between High-B and Low-B condition. Paired t-tests showed that the BOLD signal change rate was significantly larger under the High-B condition than under the Low-B condition in the left ACC (t = -2.740, df = 18, p = 0.0067) and in the right ACC (t = -2.187, df = 18, p = 0.0211).

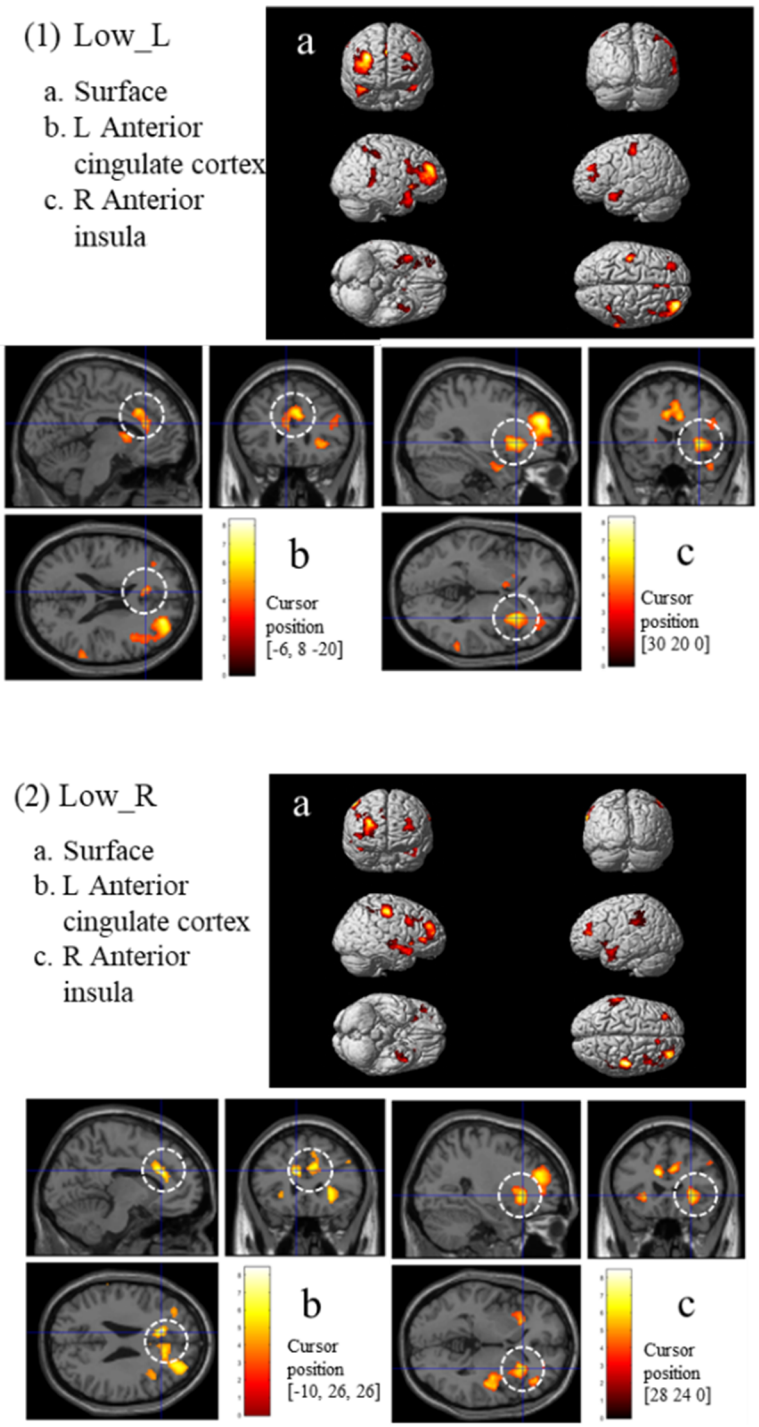

Fig. 4.5. Activation in the anterior cingulate cortex and insula (uncorrected for multiple comparisons $p < 0.001$ with cluster-level corrected FDR $p < 0.05$).

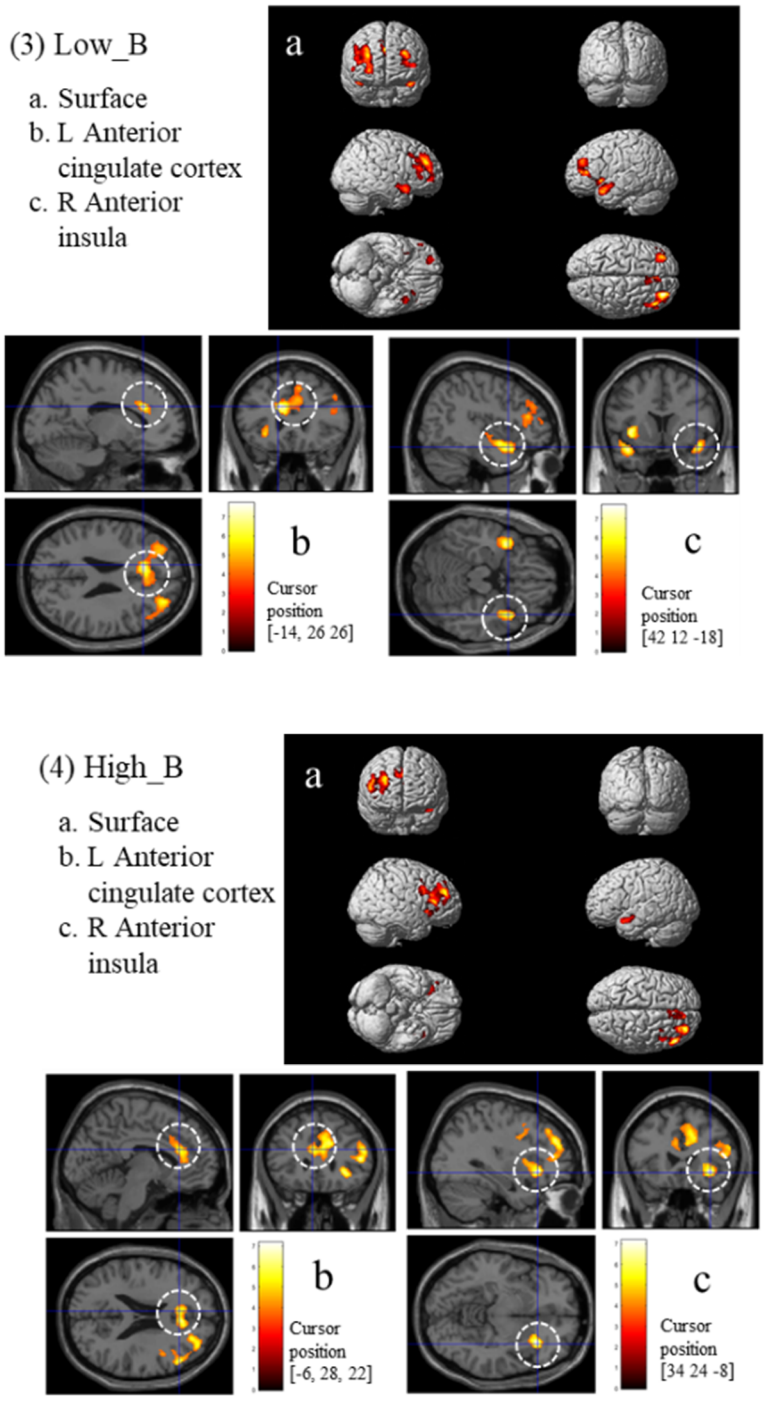

Fig. 4.5. *(Continued.)* Activation in the anterior cingulate cortex and insula (uncorrected for multiple comparisons $p < 0.001$ with cluster-level corrected FDR $p < 0.05$).

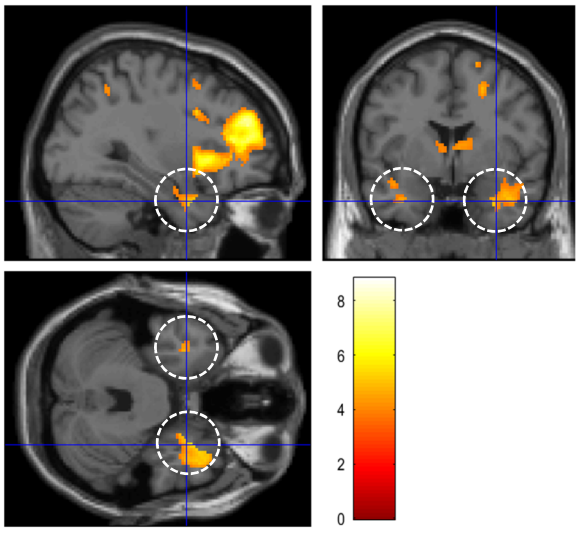

Fig. 4.6. Activation in the amygdala under Low_L condition (LQ > 0.7) (uncorrected for multiple comparisons $p < 0.001$ with cluster-level corrected FDR $p < 0.05$).

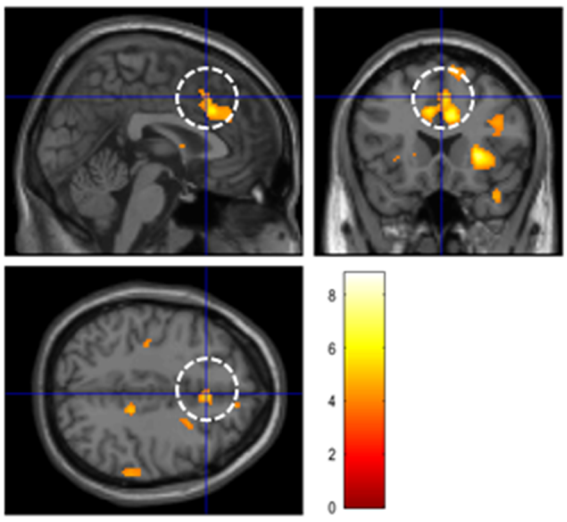

Fig. 4.7. Activation in the supplementary motor area under Low_L condition for participants (LQ > 0.7) (uncorrected for multiple comparisons $p < 0.001$ with cluster-level corrected FDR $p < 0.05$).

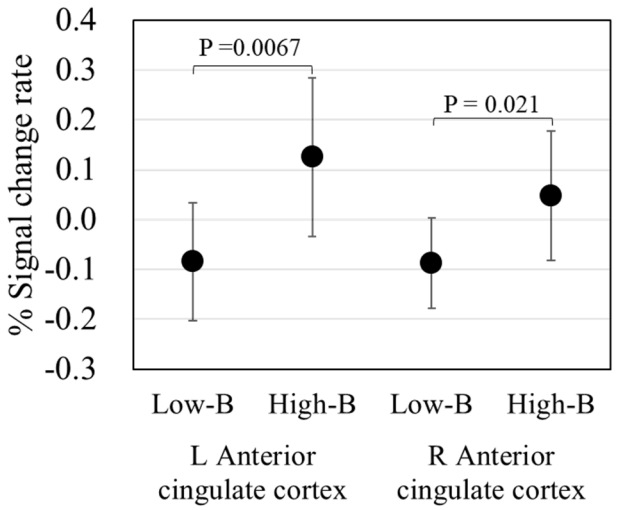

Fig. 4.8. Bold signal change rate in anterior cingulate cortex.

Table 4.2 Activated cluster location and volume under Low_L and Low_R condition

	Region	BA	*X* (mm)	*Y* (mm)	*Z* (mm)	Peak Z	Voxels
Low-L	R Middle cingulate cortex	32	6	24	32	5.25	880
	R Supplementary motor area	6	4	22	40	4.28	
	L Middle cingulate cortex	32	-6	22	34	4.23	
	L Anterior cingulate cortex	24	-6	28	20	4.10	
	R Middle frontal gyrus	10	34	48	28	5.10	2126
	R Anterior insula		30	20	0	4.71	1206
	R Superior temporal pole	38	44	14	-24	4.18	
	L Postcentral gyrus	1/2/3/43	-46	-22	62	4.53	270
	L Middle frontal gyrus	10	-26	46	8	4.22	439
	L Triangular part of inferior frontal gyrus	45	-40	42	6	3.64	
	L Superior temporal pole	38	-42	10	-18	4.05	398
	L Amygdala		-32	0	-28	3.77	
	L Superior temporal gyrus	22	-42	-6	-10	3.61	
	R Caudate		14	-8	8	4.02	475
	L Caudate		-8	8	6	3.98	
Low-R	L Anterior cingulate gyrus	32	-10	26	26	5.30	2116
	R Superior frontal gyrus	8	10	30	44	4.69	
	R Middle frontal gyrus	10	28	44	24	4.66	
	R Posterior insula		34	-12	16	5.24	1822
	R Anterior insula		28	24	0	4.60	
	R Postcentral gyrus	1/2/3/43	50	-18	52	4.92	651
	R Inferior parietal louble	40	54	-44	52	3.65	
	R Superior parietal gyrus	7	44	-50	60	3.57	
	L Hippocampus		-30	-6	-28	4.48	685
	L Middle temporal gyrus	21	-40	4	-32	4.12	
	L Anterior insula		-26	-24	0	4.11	
	L Supramarginal gyrus	40	-64	-36	34	4.42	197
	L Inferior parietal louble	40	-60	-40	44	3.73	
	L Middle frontal gyrus	10	-26	44	12	4.30	345
	L Triangular part of inferior frontal gyrus	45	-34	38	14	4.23	
	R Opercular part of the inferior frontal gyrus	44	42	16	32	3.96	387
	R Middle frontal gyrus	10	34	12	40	3.72	

Table 4.3. Activated cluster location and volume under Low_B and High_B

	Region	BA	*X* (mm)	*Y* (mm)	*Z* (mm)	Peak Z	Voxels
Low-B	L Anterior cingulate cortex	32	-14	26	26	5.06	1865
	L Middle frontal gyrus	10	-30	44	30	4.42	
	L Triangular part of inferior frontal gyrus	45	-36	38	10	3.98	
	R Anterior cingulate cortex	45	8	32	26	3.72	
	L Superior temporal pole	38	-38	10	-20	4.84	570
	L Posterior insula		-40	-6	-10	4.40	
	R Middle frontal gyrus	10	24	52	2	4.79	1526
	L Anterior insula		-36	16	-4	4.79	397
	R Superior temporal pole	38	44	2	-12	4.57	483
	R Anterior insula		42	12	-18	4.54	
	R Posterior insula		38	-8	-10	3.57	
High-B	R Middle frontal gyrus	10	30	48	28	4.87	1580
	R Triangular part of inferior frontal gyrus	45	50	28	12	4.66	
	R Opercularis of the inferior frontal gyrus	44	52	30	22	4.39	
	R Anterior insula		34	24	-8	4.85	389
	R Anterior cingulate cortex	32	12	32	28	4.65	1454
	R Supwerior frontal gyrus	8	10	34	40	4.29	
	L Anterior cingulate cortex	32	-6	28	22	4.25	
	L Superior temporal pole	38	-44	4	-18	3.98	262
	L Temporal pole	38	-36	12	-20	3.90	

4.4. **Discussion**

Analysis of fMRI data focusing on the brain activities while being on standby for steering showed significant activation in the SN including the ACC and insula under all conditions. Although we defined the period of being on standby for steering as 'rest', during this period, the participants held the steering wheel while seeing the fixation point on the display according to the prior instructions. Moreover, participants waited for the cue (a change in the color of the bar presented on the display) to start the steering operation. Thus, this period cannot be just considered as 'rest'. The activations in the ACC and insula during this period are consistent with our hypothesis. Menon *et al*. [24] argued that the SN switches the state of the intrinsic brain networks. It is known that the DMN is dominant when people are idle, or during mind-wandering (e.g. [42]). When participants have to prepare for an upcoming task, the SN is activated to switch the DMN to the CEN related to task engagement. In the present study, during the 'rest' period, the participants were required to pay attention to the change in the external stimulus to perform the predetermined task immediately when the change occurred. Thus, the activation in the SN during the 'rest' period can be interpreted as the function of the SN to switch the brain network into the executive mode in order to engage in the upcoming operation task.

There were significant differences between Low_B and High_B conditions in the left and right ACC. This indicates that the magnitude of the stiffness of the steering reaction force affected the SN during the 'rest' period where the steering operation was not performed directly. When the participants were preparing for starting the steering operation with a large resistance, the activity in the SN, particularly in the ACC, would

be enhanced. Previous studies have reported that the ACC is active in correlation with the score of anxiety [43] [44]. Therefore, our results suggested that during the standby for steering where greater force exertion was required, the participants felt more anxiety.

Significant activation in the amygdala, which is known to be associated with negative emotions [45], was observed in the condition (Low_L) in which the pure right-handed participants (LQ > 0.7) steered with only their left arm. In addition, for the pure right-handed participants under Low_L condition (Low_L), significant activation was observed in the supplementary motor area (SMA). The SMA is known to be involved in the initiation and suppression of voluntary movement [46]. These activations in the amygdala and SMA might reflect the negative emotion associated with the additional resource required to prepare for the movement initiation of the left hand, which the right-handed participants were not accustomed to use for the steering operation.

The major limitation of this study is that the results were obtained from a very simple comparison of conditions. In the experiment, participants were required to pay attention to the change in the color of the bar as a cue to start or stop the steering operation, and to perform the simple task following the cue. There was no subjective evaluation of the handling of the maneuvering. Therefore, it might have been difficult to maintain their motivation to perform the task. In actual driving situation, drivers feel positive emotions, as well as negative emotions such as anxiety. The brain mechanism underlying drivers' positive emotions could be applied for the development of a vehicle that enhances drivers' positive emotions during driving, leading to a novel control technology for vehicles. Therefore, in future research, we will improve the experimental design, such as the feedback from the maneuvering, for example changes of front scene along the various

simulated testing course by steering operation, during the experiment, which can elicit a positive emotional change in the form of a sense of accomplishment in driving.

4.5. Conclusion remarks

In this chapter, we focused on the brain activity of participants while they waited to steer. We observed activations in the SN, including the ACC and insula. When the steering reaction force was large, the BOLD signal change rate in the ACC increased during the standby period.

When the pure right-handed participants were waiting for steering operation using only their left arm, the amygdala and SMA were significantly activated, suggesting that the participants felt a negative emotion associated with the additional resource needed to prepare for the initiation of the movement of the left hand.

These results showed for the first time that the magnitude of the steering reaction force and the difference in arms used for steering operation influence the brain activity during the standby period for steering.

Chapter 5
Brain activity during driving operations modulated by the viscoelastic characteristics of a steering wheel

5.1. Introduction

In this chapter, using a developed MRI-compatible unit for steering reaction force generation, we investigate changes in human brain activity induced by varying the viscoelastic characteristics associated with manipulating a car steering wheel.

Achieving a steering feeling within a range of small steering angles up to about 10 degrees is an important issue in vehicle development because this range is mainly used in daily driving; therefore, we focused on this range in our experiment. We used a simple linear relationship between steering angle and steering reaction force, whereas existing commercial vehicles have a comparatively more complex relationship. As the first step toward clarifying the neural basis for driving, we aimed to delineate the effects of stiffness and viscosity on driving behavior and brain activity by performing simple comparisons among conditions with different levels of stiffness and viscosity. Therefore, based on the linear approximation of the non-linear relationship between steering angle and reaction force used in existing commercial vehicles, we used a steering force that was characteristic of a linear relationship between the steering angle and the reaction force.

Stiffness and viscosity parameters of the steering wheel were varied to examine how viscoelastic parameters affect motor control strategies. We investigated the neural basis of driving; in particular, motor planning and control associated with changing physical conditions and emotions related to driving pleasure. Changes in stiffness and viscosity characteristics of steering, which are mechanical, can be assumed to affect brain activity related to motor control. Furthermore, if the steering wheel characteristics impact the ease of driving, negative feelings should be elicited when a vehicle's response to the steering wheel input is not as expected, whereas positive feelings should be elicited when a vehicle response is as expected. Given that driving is considered a kind of goal-directed visuomotor behavior, drivers evaluate their task performance by monitoring prediction errors with respect to the vehicle's response. If a mechanical characteristic of the steering wheel is difficult to control, the driver's motivation may be affected and he or she may become irritated by being unable to reduce prediction error. In contrast, if a vehicle response is as expected, drivers can operate the vehicle without stress and can maintain their motivation, resulting in a positive feeling. Altogether, it can be expected that varying steering characteristics while driving should activate brain regions associated not only with motor control, but also with emotional processing caused by evaluation of prediction error in vehicular responses to steering operations.

The structure of this chapter is as follows. Section 5.2 describes the methods, Section 5.3 describes the results, Section 5.4 describes the discussion, Section 5.5 describes the conclusion remarks, and Section 5.6 describes appendix.

5.2. Methods

5.2.1. Apparatus

- ***Overall structure***

Fig. 5.1 shows an experimental setting in which the steering reaction force can be manipulated in a simulated driving environment in an MRI scanner. The experimental system was configured using an MRI-compatible steering reaction force generation unit [69], which we will refer to as “the unit”. The unit consisted of a steering reaction force generation component and a reaction force transmission component, both of which made of non-magnetic materials. The unit generates force against the rotation and rotational velocity of the steering wheel according to preset mechanical characteristics. We improved the unit from the previous study [69] in three ways: (i) we increased the rigidity of the rotating shaft by improving the manufacturing method of the fiber reinforced plastic (FRP) material, (ii) we improved the stability of the shaft support component, and (iii) we replaced the motor with a specialized substitute that allowed for torque control.

- ***Presentation of simulated road images***

The driving simulator presented road images seen from a car traveling at a constant speed. Participants were allowed to operate the wheel to steer the car left and right in a supine posture, as shown in Fig. 5.2. An MRI-compatible 32-inch liquid crystal display (LCD) monitor (NordicNeuroLab, Norway) with a resolution of 1,920 × 1,080 pixels was placed at the head side of the MRI scanner (left side of Fig. 5.1 (a)), upon which the simulated road images were presented with the left and right sides reversed. Participants could watch the images through a mirror attached to the head coil. These configurations allowed

participants to see the road images by naturally looking forward. In the experiment, we used a simple vehicle model because we needed our experimental design in a driving environment to be as simple as possible. In this model, a "camera" placed at the driver's point of view was set about 1300 mm above the road. When the vehicle moved, the camera position was translated forward at a constant speed, and the camera direction was rotated according to the yaw angle proportional to the steering angle. We used the OpenGL graphic library to render the camera view, which also included the road and the poles located on the road.

- ***Reaction force generation***

The reaction force was presented to participants according to the compliance control method given by equation (5.1). In this manuscript, we have used the terms stiffness and viscosity. In equation (5.1), stiffness refers to the element of the reaction force generated in proportion to the magnitude of the rotation angle θ, which is generated by a steering operation. Viscosity is used as a term representing the element of the reaction force generated in proportion to θ velocity.

$$\frac{d^2\theta}{dt^2} = \frac{1}{J}\left(F - K_{stiff}\theta - \frac{d\theta}{dt}B_{visc}\right) \qquad (5.1)$$

where

K_{stiff}: Stiffness coefficient, B_{visc}: Viscosity coefficient,

$\frac{d^2\theta}{dt^2}$: Angular acceleration = Motor control target value,

J: Inertia, and F: Measured torque

The reaction force generation component was installed outside the MRI scan room,

separated by an electromagnetic shield, thereby preventing electromagnetic noise generated by the motor from affecting the MRI images (Fig. 5.1 (b)). The rotating shaft of the reaction force generating motor was connected to the reaction force transmission component in the MRI scan room via a waveguide. To generate reaction force, we used a reaction force generation motor (Torque Actuator UNISERVO SVM-80 reduction rate 1/50 type, ROBOTEC Inc., Tokyo, Japan) and controller (SVC-80, ROBOTEC Inc., Tokyo, Japan). The torque-servo installed in this system allowed us to measure and control the torque at the output shaft.

5.2.2. Experiment

Two sets of experiments were performed to investigate the neurobehavioral effects of manipulating the steering reaction forces using three different levels of stiffness and viscosity parameters, represented by K_{stiff} and B_{visc} in equation (5.1), respectively. Hereafter, these sets of experiments will be referred to as the stiffness condition and the viscosity condition, respectively.

- ***Participants***

The participants consisted of 23 men (average age: 25.9 years (SD 5.2)) for the stiffness condition and 22 men (average age: 27.1 years (SD 5.2)) for the viscosity condition, none of whom had a history of neurological or psychiatric disorders. All participants were right-handed, as confirmed by the Edinburgh Handedness Inventory [30], had a driver's license and were driving on a daily basis.

These experiments were approved by the Research Ethics Committee of Hiroshima University and Mazda Motor Corporation (approval numbers E-965-5 and TRC-152-6).

Prior to the experiment, we obtained written informed consent from all participants.

- ***Experimental design***

Table 5.1 shows the experimental parameters of the stiffness and viscosity conditions. K_{stiff} and B_{visc} in Table 5.1 are the stiffness coefficient and viscosity coefficient shown in equation (5.1). Each stiffness and viscosity coefficient conditions consisted of three levels. In the first level of the stiffness condition (S1), both coefficients were set to zero; in the first level of the viscosity conditions (V1), only the viscosity was set to zero. We considered S1 and V1 as the reference levels to examine the effects of stiffness and viscosity. The second level of stiffness condition (S2) was then implemented by converting the steering angle-steering force characteristic into a simple linear relationship, based on the value of the steering angle-reaction force characteristic of existing commercial vehicles within a small steering angle range up to 10 degrees. In our preliminary pilot experiment outside the scanner, we confirmed that with the reaction force generated at this level, it was easy to steer in the supine posture, which was required for this experiment to be performed inside an MRI scanner. The third level of stiffness condition (S3) was the level at which the steering reaction force was felt to be slightly large in the supine position, which was achieved by setting the stiffness coefficient (K_{stiff}) in equation (5.1) to twice the value used for S2. We also confirmed that a large exertion force was not required for steering operations in the pilot experiment. For the three levels of the viscosity condition (V1-V3), the stiffness coefficients were the same as the second level of the stiffness condition (S2). In the first level of the viscosity condition (V1), the viscosity coefficient was set to zero; in the second level (V2), the viscosity coefficient was set to a value that gave a moderate response to participants, which made them feel

the viscosity. The third level (V3) was the level that made participants feel a slightly excessive viscosity. The viscosity coefficient value used for V3 was twice of that for V2, and this viscosity was felt to be slightly high in the supine position, although we confirmed that participants could perform this task without much difficulty due to steering delay. Regarding the number of levels for each condition, we determined one condition with three levels that would fulfill the minimum requirement for our study aim, considering participants' fatigue.

The experimental protocol is shown in Fig. 5.3. The experiment consisted of six runs. The three levels of the parameters used for each condition are shown in Table 5.1 (K_{stiff}: S1, S2, S3 in the stiffness condition; B_{visc}: V1, V2, V3 in the viscosity condition). Each of the three levels of the parameters was randomly assigned to six runs, but we avoided assigning the same level to successive runs by assigning it only to the first or latter three runs.

As shown in Fig. 5.3, each run consists of practice and task phases. In the practice phase, participants practiced driving tasks and subjective evaluation using the visual analog scale (VAS). In the task phase, participants performed six trials. After each trial, participants performed a subjective evaluation of each trial using VAS (hereinafter referred to as VAS4). At the end of the run, participants performed a subjective evaluation of six trials using VAS (hereinafter referred to as VAS7). Rest periods were inserted before Trial 1 and Trial 4, and after Trial 6.

In the driving practice, participants were instructed to trace a lane of a winding road. Participants' views of the road were rendered according to their steering inputs. The level of the steering parameter used in the practice trial was the same as that used in the

subsequent trials.

In the subjective evaluation practice, participants practiced the subjective VAS7 evaluation by rotating the steering wheel (described later). Table 5.2 shows all evaluation words we asked participants to use, seven of which were used in VAS7. Six evaluation words, “self-efficacy”, “unpleasantness”, “pleasantness”, “arousal”, “expectation”, and “excitement” were commonly used in the stiffness and viscosity conditions. The evaluation word “self-efficacy” was selected to ask participants to evaluate how well their steering control matched their intention; that is, how they felt that about being able to demonstrate their ability to accomplish the task. We also asked participants to evaluate their valence and arousal [47] while performing the task. The pleasantness and unpleasantness were evaluated separately because we considered the possibility that these factors may not exist on the same axis. The evaluation word “expectation” was selected to ask the participants how well they expected to perform the task. The evaluation word “excitement” (described as “waku-waku” in Japanese) was selected to ask them to gauge how much excitement they felt while performing the task. One word differed between the stiffness and viscosity conditions; we used “anxiety” in the stiffness condition and “motivation” in the viscosity condition. The evaluation word “motivation” in the viscosity condition was selected because we considered that a delay in the response of the vehicle due to an increase in viscosity could decrease a participant’s motivation to accurately perform the task. On the other hand, the evaluation word “anxiety” in the stiffness condition was selected because vehicle development engineers have an empirical belief that when the reaction force from the steering wheel is too low, drivers often experience anxiety. In the VAS4 period, participants evaluated their feelings while performing each

trial in terms of four evaluation words: “self-efficacy”, “pleasantness”, “nimbleness”, and “smoothness” (Table 5.2). Two of the four evaluation words (“self-efficacy” and “pleasantness”) were commonly seen in the VAS7 evaluations. The remaining two words, “nimbleness” and “smoothness” are generally used by vehicle development engineers to evaluate steering performance.

In VAS7, after the final rest period in each run, participants were asked to perform a subjective evaluation of how they felt during the overall run. At the beginning of VAS7, an instruction for an evaluation word and a VAS scale (Fig. 5.4) were presented to participants, next they moved the cursor on the scale to the left or right by rotating the steering wheel to score each word. The order of the seven evaluation words was randomized, and the initial position of the cursor for each word was randomized around 50 (near the center of the scale), with a range of ±5 to eliminate the possibility of biasing the rating value by fixing the initial value of the cursor. If the cursor did not move for 2 s, the position was fixed and recorded as the rating score.

For the rest of the phases, a fixation cross was shown at the center of the display (the leftmost display shown in the lowest row in Fig. 5.3), and participants instructed to look at it.

Each trial consisted of “ready”, “countdown”, “straight”, “gate”, score feedback, and subjective evaluation (VAS4) periods. In the ready period, the word “Ready” was displayed for 1 s prior to the start of the countdown period (the second display from the left in the lowest row in Fig. 5.3). In the countdown period, the number decremented by one every 1 s starting from three; this was shown at the center of the display (the third display from the left in the lowest row in Fig. 5.3) and disappeared 1 s after the countdown

reached 1 s. The vehicle automatically started to move when the timer reached zero. Participants were instructed to prepare for the upcoming task and to imagine how well they would perform a task in which they were required to pass through the center of a gate (described later) as smoothly as possible. In the "straight" period, participants were instructed to trace the white line in the center of the road. In the "gate" period, participants were instructed to control the vehicle to pass through the center of the gate as precisely and smoothly as possible. During this period, five gates were presented one at a time; the first, third, and fifth gates were presented at the center of the road, whereas the second and fourth gates randomly appeared on the left or right side of the white line at the center of the road. In the feedback period, the difference of the x-coordinates between the center of the gate and the position where the center of the car passed through the gate (excluding the first and fifth gates) was calculated. The calculated value was converted to 0-100 and presented to the participants as a feedback score to assess the task performance of the trial. The score was presented for a randomly selected duration of time of 1, 3, or 5 s. After each trial, participants performed subjective evaluations of the last trial (VAS4) in the same manner as in VAS7.

- ***Steering reaction force characteristics***

Fig. 5.5 shows the steering reaction force characteristics presented to participants. To measure the steering torque using a torque sensor that could not be used in a strong magnetic field in the MRI gantry, the same layout was reproduced outside the MRI scan room. In the reproduced setting, using a steering effort sensor (Model 01184, Sensor Developments Inc. Chelmsford, MA 01824, USA) mounted on the steering wheel, we measured the steering torque relative to the steering angle while performing one run of

the driving task. The upper row of Fig. 5.5 shows that the stiffness parameters changed the slopes of the regression lines but did not affect the hysteresis. The lower row of Fig. 5.5 shows that the viscosity parameters changed the hysteresis but did not affect the slope of the regression line corresponding to stiffness. These observations confirmed that the parameters in equation (5.1) could independently determine the stiffness and viscosity of the steering wheel. The measured value was confirmed to be in agreement with the steering angle output from the steering force sensor attached to the steering wheel within the steering angle and operating speed range shown in Fig. 5.5.

- ***fMRI data acquisition***

A 3.0 T MRI scanner (MAGNETOM Verio, Siemens AG, Munich, Germany) was used to obtain MRI data. The functional images were acquired using a T2*-weighted gradient echo planar imaging method. The acquisition parameters were as follows: repetition time (TR) = 1,000 ms, echo time (TE) = 30 ms, 42 slices, slice thickness = 3.2 mm (without gaps), voxel size = 3 × 3 × 3.2 mm, flip angle = 80°, and field of view (FOV) = 192 mm. The structural image was acquired using the T1-weighted 3D magnetization-prepared rapid gradient echo imaging method. The acquisition parameters were as follows: TR = 2,500 ms, TE = 2.98 ms, 176 slices, thickness = 1 mm, voxel size = 1 × 1 × 1 mm, flip angle = 9°, and FOV = 192 mm. To reduce head movement caused by steering when using both arms during fMRI measurements, we used a suction-type fixed bag (ESF-19, Engineering System Co., Ltd, Nagano, Japan) in the head coil. In addition, we used a cushion to fill the gap between the head coil and the sides of both ears and the top of the head as much as possible.

- ***fMRI data analysis***

Data were analyzed using Statistical Parametric Mapping version 12 (SPM12) software (Wellcome Department of Cognitive Neurology, London, UK.) [27]. The first five volumes of functional images obtained in each run were discarded to allow for T1 equilibration; the remaining volumes were analyzed. Spatial correction of the movement of the head was performed based on the first volume (realignment). The T1-weighted structural image for each participant was then aligned to the first volume of the echo-planar images (EPIs) for the corresponding participant (co-registered) and normalized to the Montreal Neurological Institute (MNI) template.

In this study, it was difficult to regress out the motion parameters based on SPM during measurement of brain activity because the noise caused by the movement of the head associated with the steering wheel operation was very large. Therefore, we modified the Human Connectome Project (HCP) pipeline so that their MultiRunFIX [48] could be applied to data preprocessed by the SPM software. The independent components were extracted by Multi-Run sICA (spatial independent component analysis) from the normalized EPI data, which were concatenated from six runs. The reason for linking the 6-run data is that it is more advantageous to have more time points in order to improve the noise and signal separation performance for sICA. This reduces the risk of removing not only noise but also task-related activities due to low separation performance. To the extracted independent components, automatic labeling based on machine learning was not performed; instead we performed manual labeling based on a study by Griffanti *et al*. [49]. In the last noise component removal step, using the FIX cleanup procedures described by Griffanti *et al*. [48] described later, motion regression was performed using

24 parameters for each signal and noise component, and concatenated data from which the effects of motion artifacts were more effectively removed were obtained. The concatenated data were divided and returned to the data of each run, and the process was then returned to the SPM12 software.

In the cleanup procedures with FIX, the following three steps were performed, similar to that in the "soft" approach described by Griffanti *et al*. [48]: (1) We regressed out the full space of the motion confounds from both the data and all the ICA component timeseries; (2) we estimated the contribution of both good and bad components via multiple regression of the data against all (motion-cleaned) ICA timeseries; and (3) the unique contribution of the bad components was removed from the data, employing only the bad ICA components' timeseries and regression coefficients. The 24 parameters used for the above motion regression were motion estimation (R = [X, Y, Z, pitch, yaw, roll]), the derivatives (R′) of these factors, and their squares (R^2, R'^2).

Following this procedure, the normalized EPIs were smoothed by a Gaussian kernel (full width at half maximum = 8 mm). For pre-processed EPIs, we performed statistical analysis using a general linear model. The "countdown", "straight", "gate," "feedback," and "VAS" periods were modeled as a boxcar function convolved with the canonical hemodynamic response function. Fig. 5.6 shows an example of the design matrix for the 1st and 2nd level analyses of one run of the "gate" period. In the 1st level analysis, each trial was modeled as one regressor for each run in the "gate" period, and 36 regressors were created for each subject (total of six runs). For each "countdown," "straight," "feedback," and "VAS" period, six trials in each run were modeled as one regressor. Similarly, in the analysis focused on the "countdown" and "straight" periods, we created

different design matrices for each; the “countdown” or “straight” period in each trial was modeled as one regressor. For each of the other periods, six trials were modeled as one regressor. A one-way ANOVA within subjects was performed for the 2nd level analysis. To reduce the variance caused by the fluctuations in subjective ratings for each trial, the principal component scores of the VAS4 evaluations after each trial (described below) were adopted as covariates of no interest. Prior to the regression analysis, low-frequency fluctuations in the blood oxygenation level-dependent (BOLD) signal were eliminated by applying a high-pass filter with a cutoff of 128 s. Moreover, serial correlations among scans were estimated using an autoregressive model (AR (1)) to remove high-frequency noise contaminating the EPI time-series. The contrast images for the “countdown”, “straight”, and “gate” periods were calculated for each participant using the fixed-effects model and were then considered in the group analysis using a random-effects model. The anatomical region was identified using SPM Anatomy toolbox 2.2b (Forschungszentrum Jülich GmbH, Jülich, Germany) [50], [51], [52] and Talairach Client 2.4.3 (Research Imaging Institute, San Antonio, TX 78229, USA) [53], [54].

- ***Subjective ratings***

A principal component analysis (PCA) was performed for the subjective rating data obtained in the stiffness and viscosity conditions. For VAS7, six evaluation words common to both conditions were used in the PCA. One participant rated with extreme values for all evaluation words in most trials in the viscosity condition; this participant gave ratings of 100 in 96.5% of his VAS4 evaluations, and 0 (for anxiety) or 100 (for other words) for 95.2% of his VAS7 evaluations. Thus, we excluded this participant from the analysis because the PC could not be calculated.

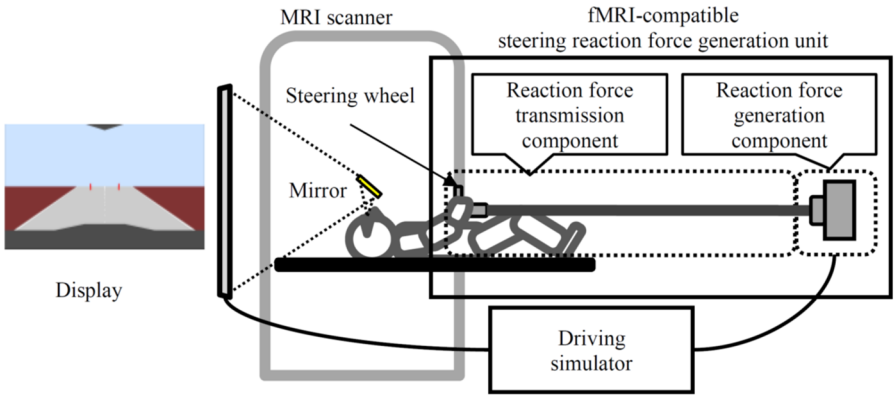

(a) Experimental system consisting of a functional magnetic resonance imaging (fMRI)-compatible steering reaction force generation and transmission unit.

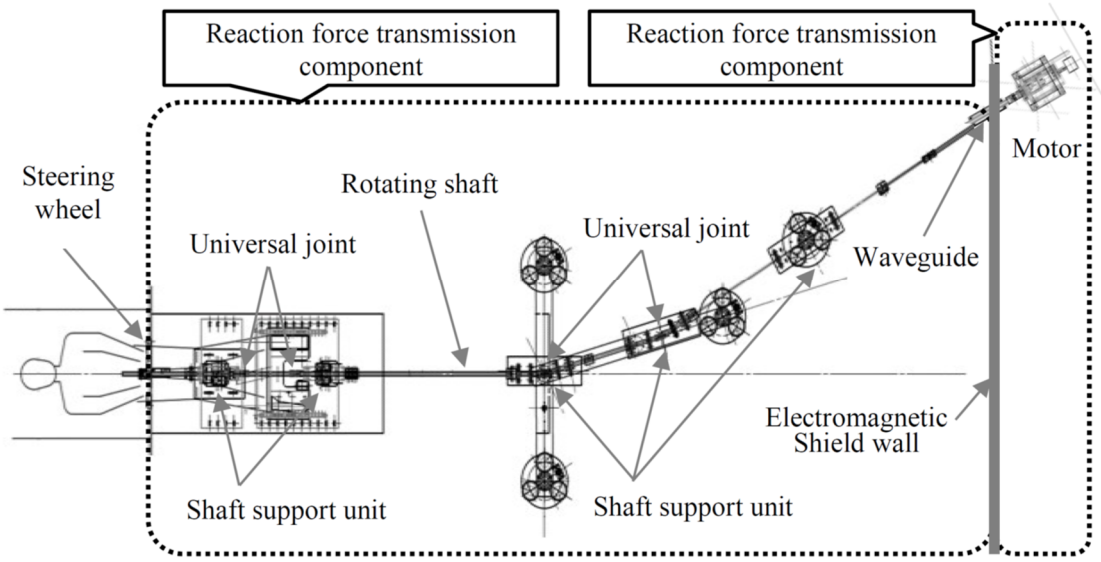

(b) Configuration of the fMRI-compatible steering reaction force generation system.

Fig. 5.1. Experimental system for presenting steering reaction forces during simulated driving in a magnetic resonance imaging (MRI) scanner.

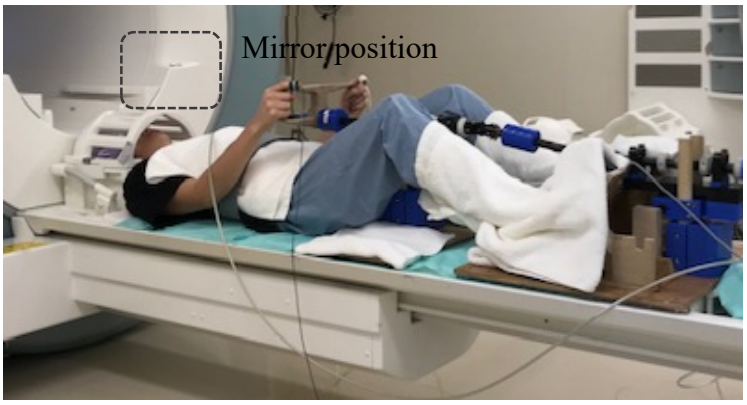

Fig. 5.2. Steering posture with the participant in a supine position inside the gantry.

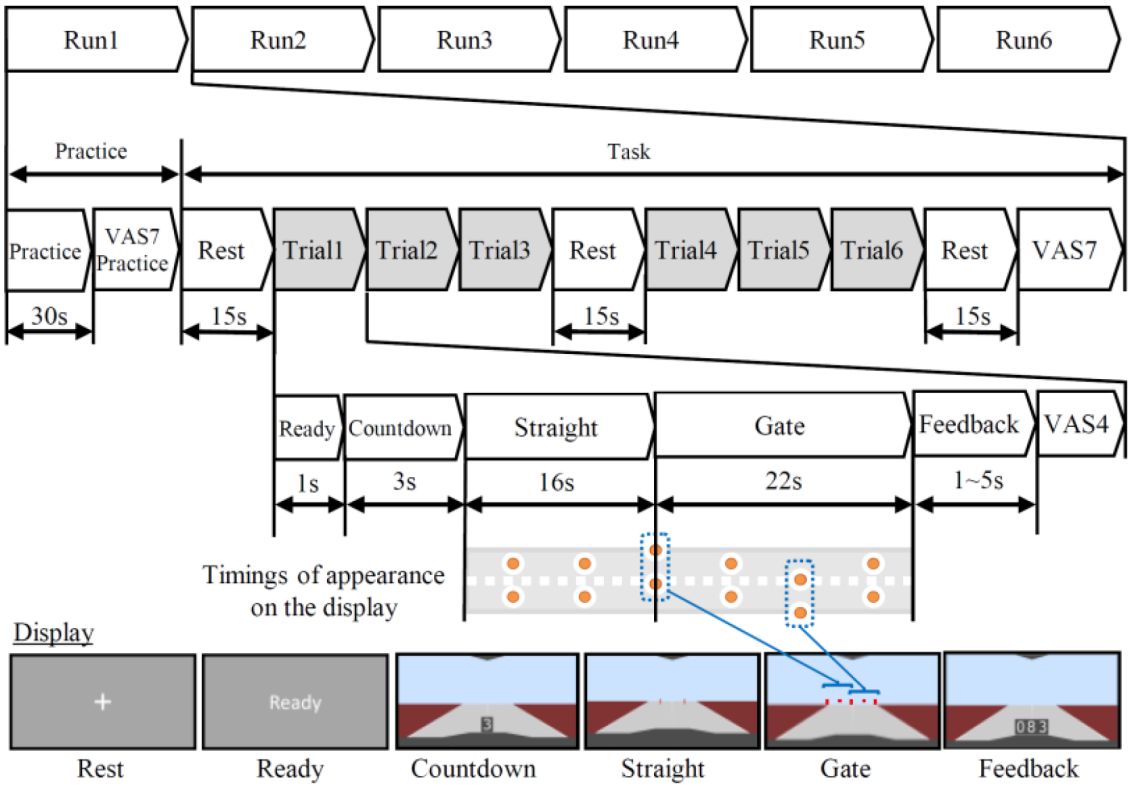

Fig. 5.3. Schematic of the experimental protocol showing the timing and duration of each phase. VAS = visual analog scale.

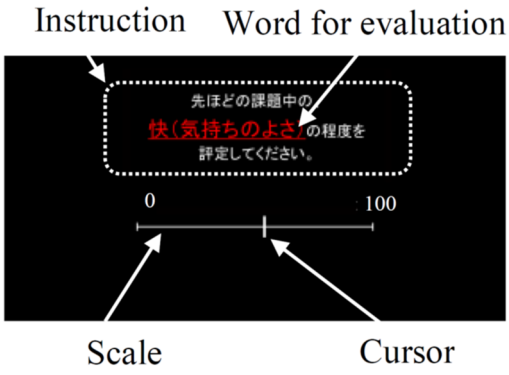

Fig. 5.4. Example of the screen of the input interface shown to the participants during the subjective evaluation of performance based on certain descriptive words using a visual analog scale (VAS).

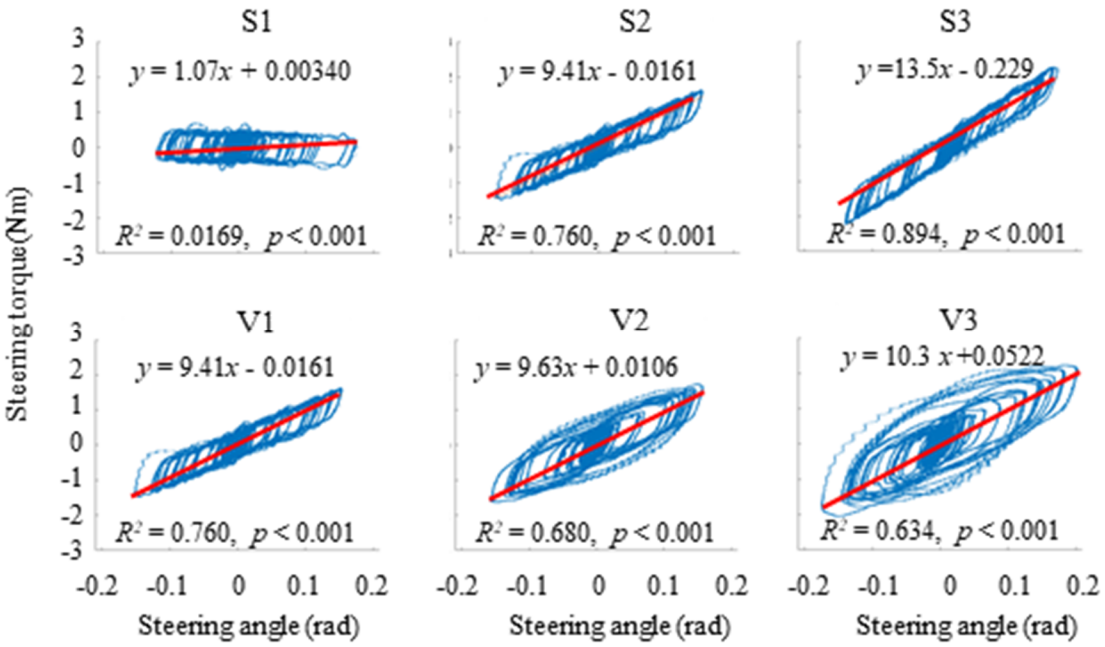

Fig. 5.5. Measured steering torques for each stiffness (top row) and viscosity (bottom row) experimental conditions. Prior to the experiment, steering reaction force characteristics were measured by an experimenter outside the magnetic resonance imaging (MRI) scan-room for one run comprised of six trials. The result of the linear regression equation for each condition is shown by a red line.

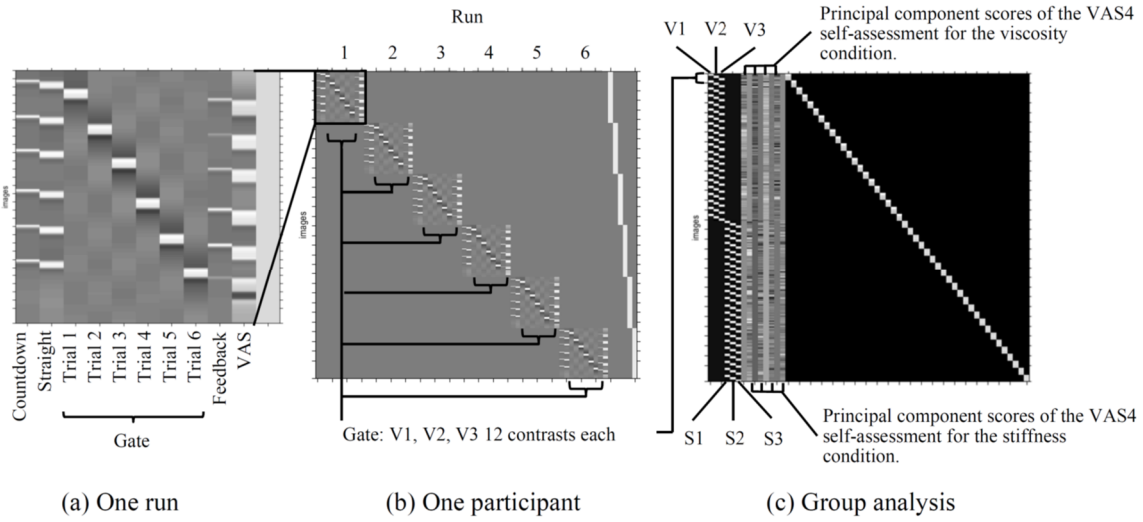

Fig. 5.6. Design matrix showing each phase of one run (a), all runs each subject participated in (b), and group analysis.

Table 5.1 Experimental condition: Motor control for reaction force generation.

	Stiffness condition			Viscosity condition		
	S1	S2	S3	V1	V2	V3
K_{stiff} (Nm/rad)	0.00	12.8	25.5	12.8		
B_{visc} (Nms/rad)	0.00			0.00	2.00	4.00
	$J = 0.02$ (Nms^2/rad)					

K_{stiff}: Stiffness coefficient, B_{visc}: Viscosity coefficient, J: Inertia

Table 5.2 Words for subjective evaluation.

	Stiffness condition	Viscosity condition
VAS4	Self-efficacy Pleasantness Nimbleness Smoothness	Self-efficacy Pleasantness Nimbleness Smoothness
VAS7	Unpleasantness Self-efficacy Pleasantness Arousal Expectation Excitement Anxiety	Unpleasantness Self-efficacy Pleasantness Arousal Expectation Excitement Motivation

VAS = visual analog scale.

5.3. Results

5.3.1. Steering behaviors

Fig. 5.7 shows the time-series of steering angles in each trial. (a) to (d) are examples of sections from Countdown to Gate. Since the appearance of the two gates on the left or right in Fig. 5.3 is random, there are four possible combinations of gate appearances. Therefore, (a) to (d) represent four selected ways from the six trials of a certain participant. (e) and (f) show the mean and standard deviation of all subjects' trials under all conditions of stiffness and viscous conditions, respectively. Since the gates appear randomly on the left or right, the average and standard deviation between trials were calculated using the absolute value of the steering angle.

5.3.2. Common brain activity in the stiffness and viscosity conditions

To examine the brain activity related to each period in the driving task, we calculated the signals during the “countdown”, “straight”, and “gate” periods. Fig. 5.8 shows the brain regions that exhibited significant activations at the thresholds of family-wise error (FWE) with a corrected $p < 0.05$ at the voxel level in the stiffness and viscosity conditions during the “countdown”, “straight”, and “gate” periods. We performed FWE corrections for each predefined contrast. The MNI coordinates of activation clusters are shown in Appendix Table S1 and Appendix Table S2. In both stiffness and viscosity conditions, we found significant activations in the visual cortex, somatosensory area, primary motor area, somatosensory association area, and cerebellum during the “countdown” period. During the “straight” period, we found significant activations in the visual cortex, somatosensory

area, somatosensory association area, and cerebellum. During the “gate” period, we found significant activations in the visual cortex, somatosensory area, primary motor area, somatosensory association area, and cerebellum.

5.3.3. Subjective ratings and performance scores

Fig. 5.9 shows the performance scores of the task that indicate how close to the center of the gate the participants were able to pass through. A repeated measures ANOVA revealed no significant main effect of the levels in the stiffness condition (F (2, 22) = 0.601, p = 0.549), but a significant main effect of the levels in the viscosity condition (F (2, 21) = 13.344, $p < 0.01$).

Fig. 5.10 shows the result of the subjective evaluations obtained from VAS4 (for each trial). Fig. 5.10 (a) shows the mean rating scores for each evaluation word under the stiffness condition, and Fig. 5.10 (b) shows those under the viscosity condition. Under the stiffness condition, a repeated measures ANOVA with levels of stiffness as a factor revealed a significant main effect for all evaluation words, including “self-efficacy” (F (2, 22) = 51.384, $p < 0.01$), “pleasantness” (F (2, 22) = 21.699, $p < 0.01$), ”nimbleness” (F (2, 22) = 38.777, $p < 0.01$), and “smoothness” (F (2, 22) = 28.601, $p < 0.01$). Under the viscosity condition, a repeated measures ANOVA revealed no significant main effect of levels of viscosity for any evaluation words, “self-efficacy” (F (2, 20) = 2.424, p = 0.089), “pleasantness” F (2, 20) = 0.575, p = 0.563), ”nimbleness” (F (2, 20) = 1.084, p = 0.339), and “smoothness” (F (2, 20) = 2.109, p = 0.122). The results of Tukey’s post-hoc tests comparing the levels in each condition are shown in the figure.

Fig. 5.10 (c) shows the factor loadings of each PC for each evaluation word and the

contributions for each PC obtained by the PCA. The subjective rating data obtained from VAS4 (for each trial) for the stiffness and viscosity conditions were analyzed by PCA. The factor loading of the first PC was positive for evaluation words related to a positive affective state. Therefore, this PC can be interpreted as being a component reflecting positive feelings. The second PC reflected high self-efficacy with low nimbleness. The third PC reflected a feeling of comfort associated with low smoothness. The fourth PC was related to maneuverability, with high nimbleness and low smoothness.

The results of the analyses of VAS7 ratings (for each run) are shown in Fig. 5.11. Fig. 5.11 (a) shows the mean rating scores for each evaluation word under the stiffness condition, and (b) those under the viscosity condition. Under the stiffness condition, a repeated measures ANOVA with stiffness level as a factor revealed a significant main effect for four words: “anxiety,” “self-efficacy,” “pleasantness,” and “excitement” (“unpleasantness” (F (2, 22) = 0.846, p = 0.433), “anxiety” (F (2, 22) = 6.474, p < 0.01), “self-efficacy” (F (2, 22) = 16.240, p < 0.01), “pleasantness” (F (2, 22) = 5.925, p < 0.01), “arousal” (F (2, 22) = 2.676, p = 0.076), “expectation” (F (2, 22) = 4.562, p = 0.014), and “excitement” (F (2, 22) = 8.971, p < 0.01). Under the viscosity condition, a repeated measures ANOVA revealed no significant main effect of viscosity levels for any evaluation words (“unpleasantness” (F (2, 20) = 0.045, p = 0.956), “anxiety” (F (2, 20) = 0.601, p = 0.552), “self-efficacy” (F (2, 20) = 0.536, p = 0.588), “pleasantness” (F (2, 20) = 1.071 p = 0.349), “arousal” (F (2, 20) = 0.497, p = 0.611), “expectation” (F (2, 20) = 0.165, p = 0.848), and “excitement” (F (2, 20) = 1.701, p = 0.191)). The results of Tukey’s post-hoc tests comparing the levels in each condition are shown in Fig. 5.11 (a).

Fig. 5.11 (c) shows the factor loadings of each PC for each evaluation word and the

contributions for each PC obtained by PCA. For the subjective ratings for each run (VAS7), we performed PCA using six evaluation words common in the stiffness and viscosity conditions. In the subjective ratings for each trial and for each session, the factor loading of the first PC was positive for evaluation words related to a positive affective state (except for discomfort), but negative only for "discomfort" related to a negative affective state. Therefore, the first PC can be interpreted as a component reflecting positive feelings. For subjective evaluations of each session, the second PC meant that participants had a high level of discomfort, with low self-efficacy. The third PC reflected a high self-efficacy, but a high degree of discomfort and low arousal, while the fourth PC reflected high expectation and excitement, the fifth a high degree of pleasantness but low self-efficacy and arousal, and the sixth a degree of high excitement and low expectation.

To examine the correlation between subjective ratings (VAS4) and performance scores, we performed regression analyses with ratings for each evaluation word as the objective variable and performance score as the explanatory variable. Under the stiffness condition, regression analyses revealed significant relationships between performance scores and the ratings of evaluation words, including "self-efficacy" ($R^2 = 0.100, \beta = 0.769, t = 9.581, F$ (1, 826) = 91.804, $p < 0.01$), "pleasantness" ($R^2 = 0.118$, $\beta = 0.834$, $t = 10.512$, F (1, 826) = 110.495, $p < 0.01$), "nimbleness" ($R^2 = 0.079$, $\beta = 0.664$, $t = 8.415$, F (1, 826) = 70.819, $p < 0.01$), and "smoothness" ($R^2 = 0.114$, $\beta = 0.829$, $t = 10.299$, F (1, 826) = 106.073, $p < 0.01$). Under the viscosity condition, regression analyses revealed significant relationships between performance scores and the ratings of evaluation words, including "self-efficacy" ($R^2 = 0.095$, $\beta = 0.558$, $t = 8.880$, F (1, 754) = 78.846, $p < 0.01$), "pleasantness" ($R^2 = 0.043$, $\beta = 0.365$, $t = 5.794$, F (1, 754) = 33.569, $p < 0.01$),

"nimbleness" (R^2 = 0.064, β = 0.425, t = 7.205, F (1, 754) = 51.916, $p < 0.01$), and "smoothness" (R^2 = 0.079, β = 0.501, t = 8.066, F (1, 754) = 65.058, $p < 0.01$).

Overall, these results showed significant correlations between subjective evaluations and objective performance scores. This suggests that the subjective ratings reflected not only the participants' mental state during steering, but also that the steering performance scores fed back to affect perceptions of performance after the steering trials ended. These confounders are possibly associated with brain activation related to subjective ratings. Therefore, we did not examine the relationship between the subjective ratings and brain activity.

5.3.4. Brain activity correlated with physical parameters

To examine the brain regions showing activity depending on stiffness and viscosity parameters, we compared the brain activity between S3 and S1 and also between V3 and V1 during the "gate" period.

We performed FWE corrections for each predefined contrast for both stiffness and viscosity. A significant effect of stiffness was observed in the somatomotor and sensorimotor cortices at the threshold of FWE with a corrected $p < 0.05$ at the voxel level (Fig. 5.12 (a)). In the left primary motor cortex (M1), we found a cluster shown in the blue rectangles with peak activation occurring at MNI coordinates -48, -24, 62, corresponding to the location of the central sulcus opening near a region suggested to be involved in controlling movement of the wrist by Germann *et al*. [55]. The MNI coordinates of this cluster are shown in Appendix Table S3. Fig. 5.12 (b) shows the percent signal change of this left M1 cluster for each stiffness level. Fig. 5.12 (c) shows

the spatial relationship between the peak activation observed at MNI coordinates -48, -24, 62 and the central sulcus.

A significant effect of viscosity was observed in the somatomotor and sensorimotor cortices at the threshold of FWE with a corrected $p < 0.05$ at the voxel level (Fig. 5.13 (a)). One of the three significantly activated clusters included the left premotor cortex with a peak activation at MNI coordinates -26, -18, 58. The MNI coordinates of this cluster are shown in Appendix Table S4. In Fig. 5.13 (b), the percent signal change in the activation of a cluster at MNI coordinates -22, -30, 62 for each viscosity level is shown relative to the cluster shown in Fig. 5.13 (a). This area is involved in controlling movement of the shoulder, as reported by Colebatch *et al*. [56]. Fig. 5.13 (c) shows the spatial relationship between significant activation in the contrasts of V3 > V1 and S3 > S1 with the peak activation in the left premotor cluster with MNI coordinates of -22, -30, 62.

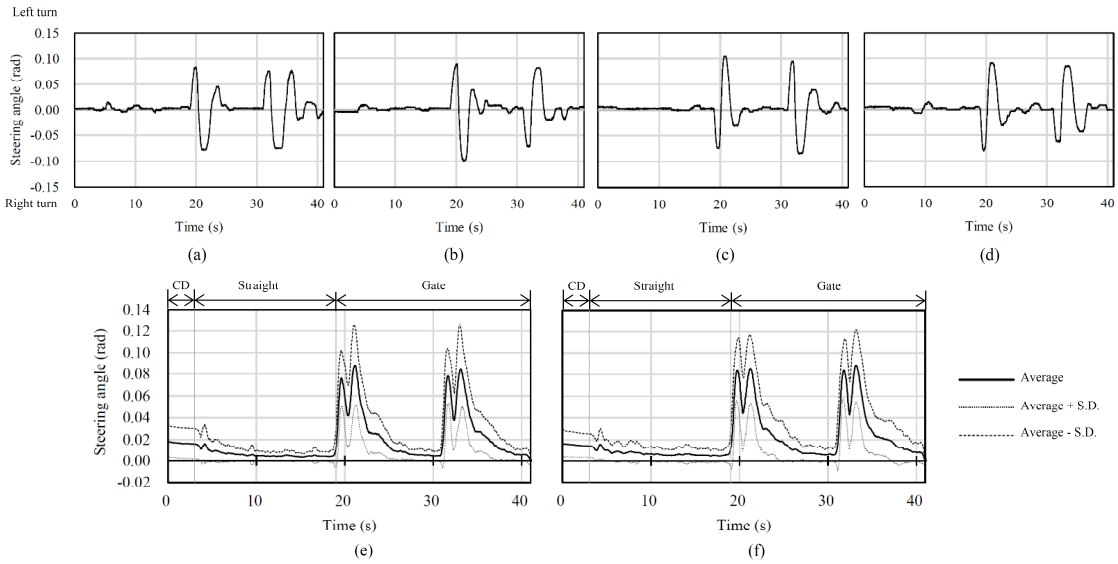

Fig. 5.7. Time-series examples of steering angle during the driving task. (a) to (d) are examples of one trial under one viscosity condition (V2). These examples correspond to four patterns of combinations of two gates that appear randomly on the left or right during a single trial. (a) An example of a trial in which both gates appeared on the left. (b) An example of a trial in which the first gate appeared on the left, the second on the right. (c) An example of a trial in which the first gate appeared on the right, the second on the left. (d) An example of a trial in which both gates appeared on the right. (e) and (f) show the average and standard deviation of the absolute values of steering angles over all trials of all subjects for each stiffness and viscosity condition. (e) shows the time series under the stiffness condition, and (f) under the viscosity condition. These measurements were performed with the steering angle meter built in the reaction force generation motor. The measured values showed good agreement with those measured at the steering position under the measurement conditions shown in Fig. 5.5. CD = Countdown.

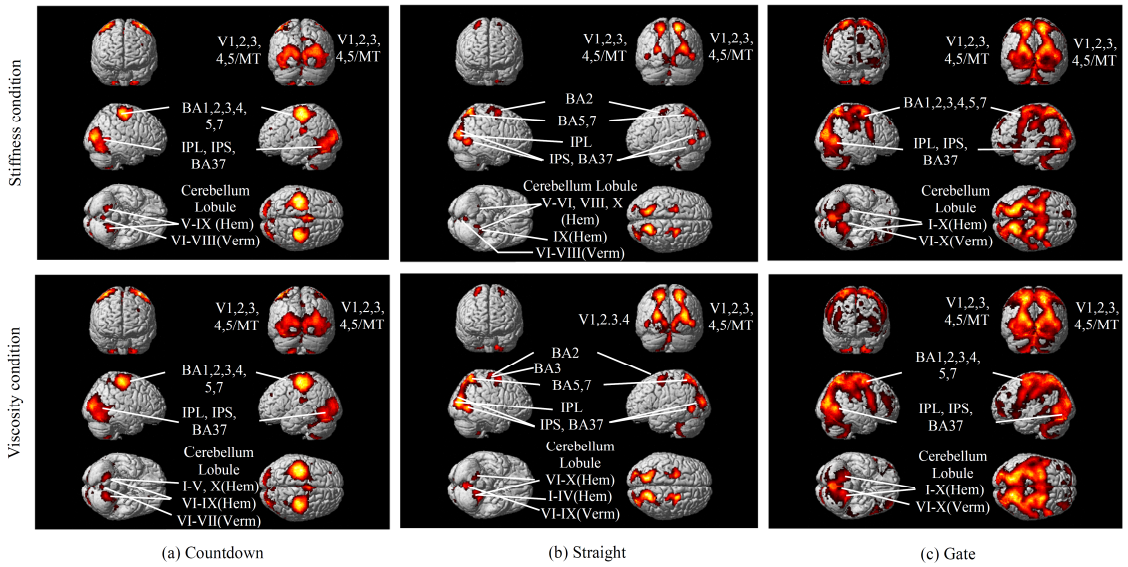

Fig. 5.8. Brain regions significantly activated at the thresholds of family-wise error (FWE) with a corrected $p < 0.05$ at the voxel level in the stiffness (top row) and viscosity (bottom row) conditions during the "countdown" (a), "straight" (b), and "gate" (c) periods. BA: Brodmann area, IPL: Inferior parietal lobule, IPS: Intraparietal sulcus, V1: Primary visual, cortex, V2: Secondary visual cortex, V3: Tertiary visual cortex, V4: Quaternary visual cortex, V5/MT: Middle temporal visual area, Hem: Hemisphere, Verm: Vermis

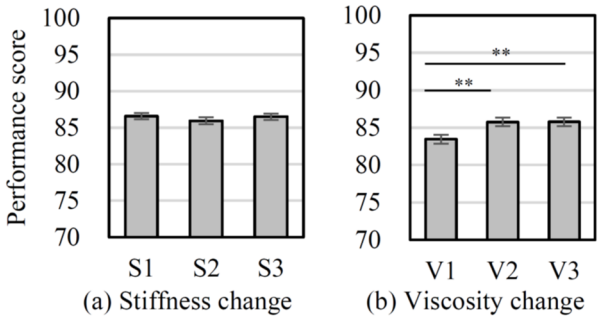

Fig. 5.9. Performance scores for each of the three stiffness (a) and viscosity (b) condition parameters. **: $p < 0.01$. Error bar: SEM.

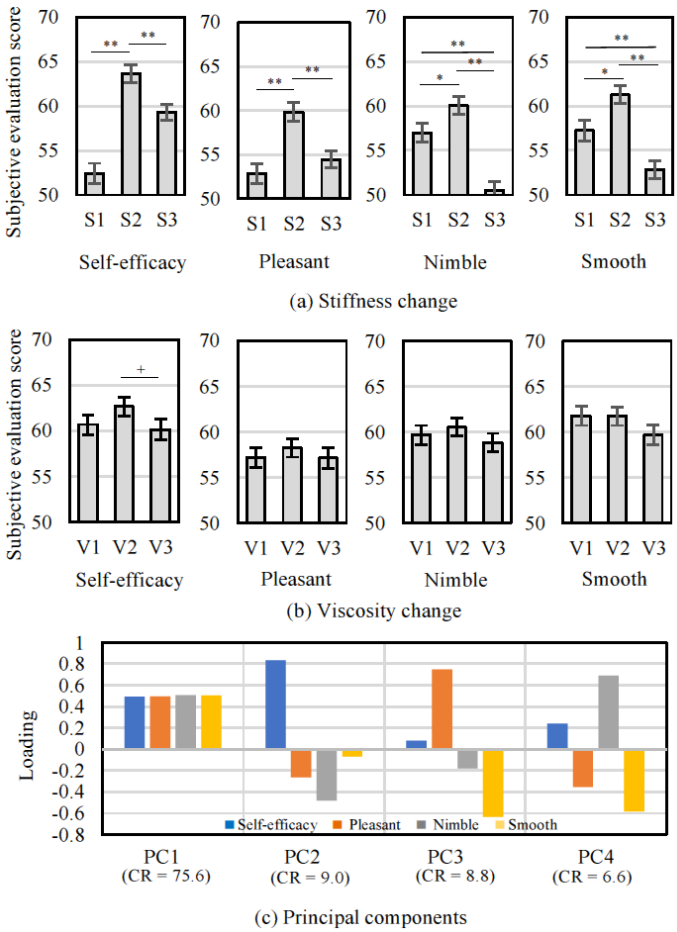

Fig. 5.10. VAS4 subjective evaluation scores for trials based on a visual analog scale (VAS) for each descriptive word for stiffness (a) and viscosity (b) conditions. The factor loading and contribution ratios for each principal component based on descriptive words are shown in (c). **: $p < 0.01$, *: $p < 0.05$, +: $p < 0.1$, Error bar: SEM. CR: Contribution ratio.

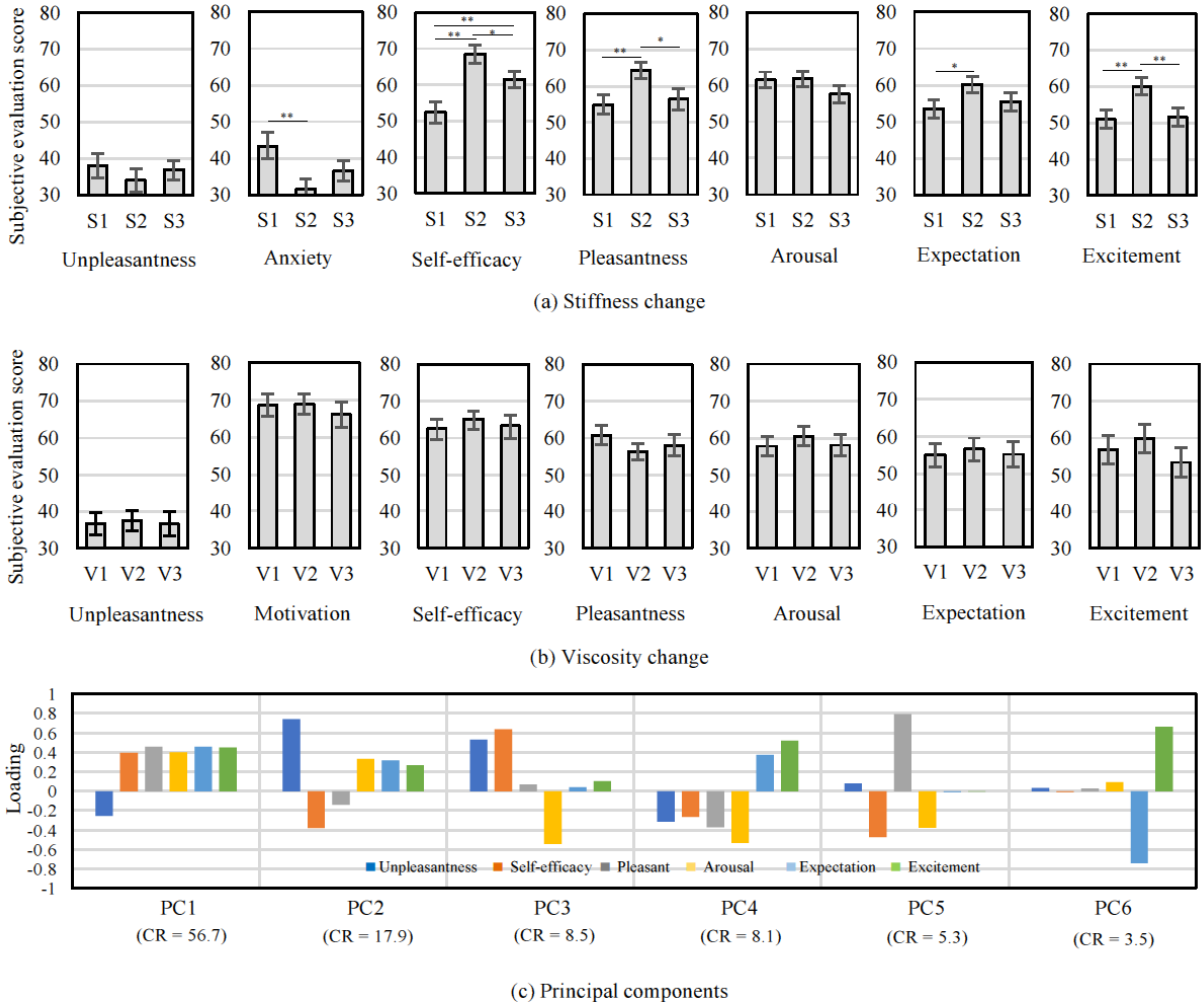

Fig. 5.11. VAS7 subjective evaluation scores at the end of the run based on a visual analog scale (VAS) for each descriptive word for the stiffness (a) and viscosity (b) conditions. The factor loadings and contribution ratios for each principal component based on the descriptive words are shown in (c). **: $p < 0.01$, *: $p < 0.05$, Error bar: SEM. CR: Contribution ratio.

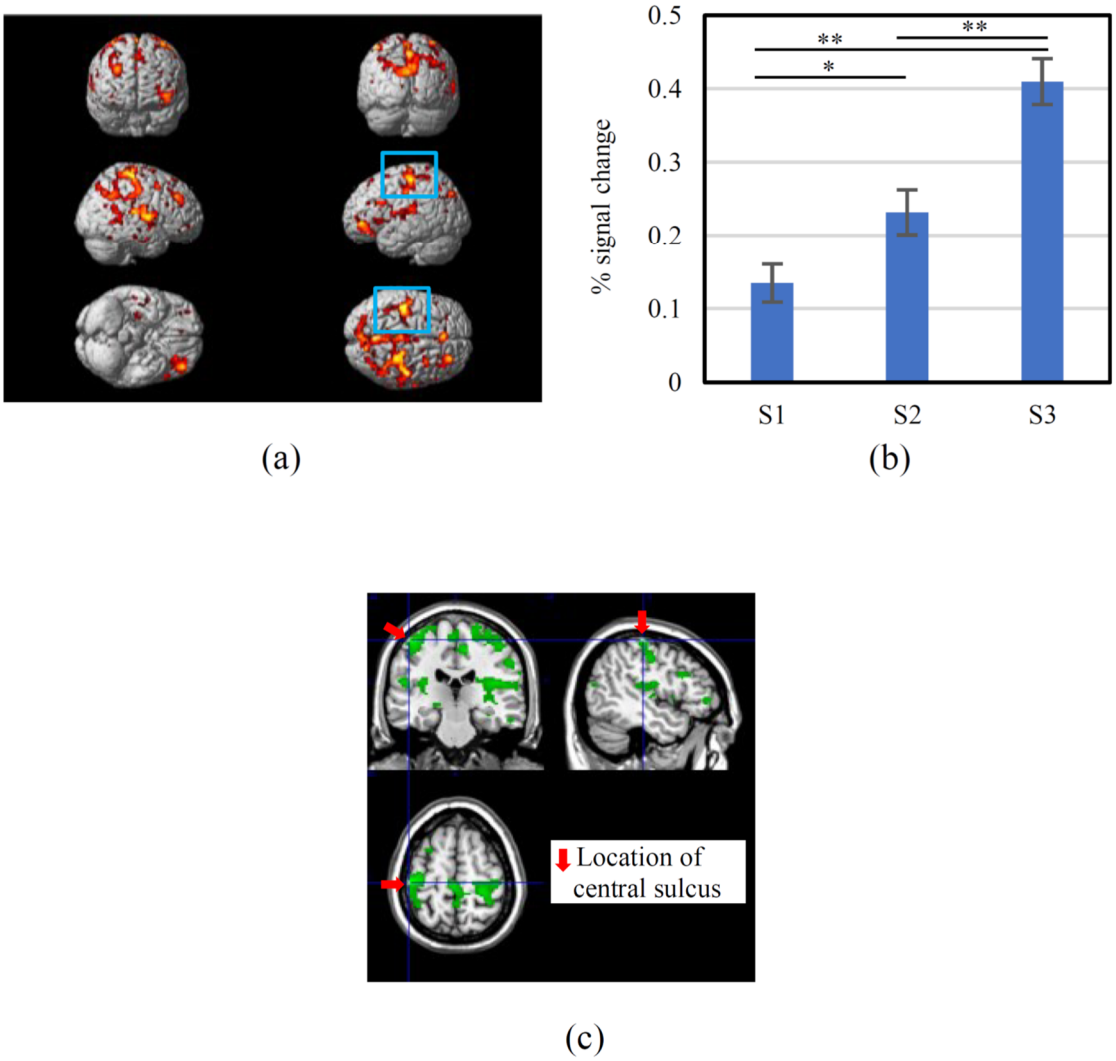

Fig. 5.12. (a) Significant brain activation in the contrast of S3 > S1 in the stiffness condition during the gate period at the threshold of family-wise error (FWE) with a corrected $p < 0.05$ at the voxel level. The blue rectangles indicate a left motor cortex cluster containing the Montreal Neurological Institute (MNI) coordinates -48, -24, 62. (b) Percent signal change in the activated cluster in the contrast of S3 > S1. (c) Spatial relationship between activation peaks observed at MNI coordinates: -48, -24, 62 and the central sulcus. **: $p < 0.01$, *: $p < 0.05$, Error bar: SEM.

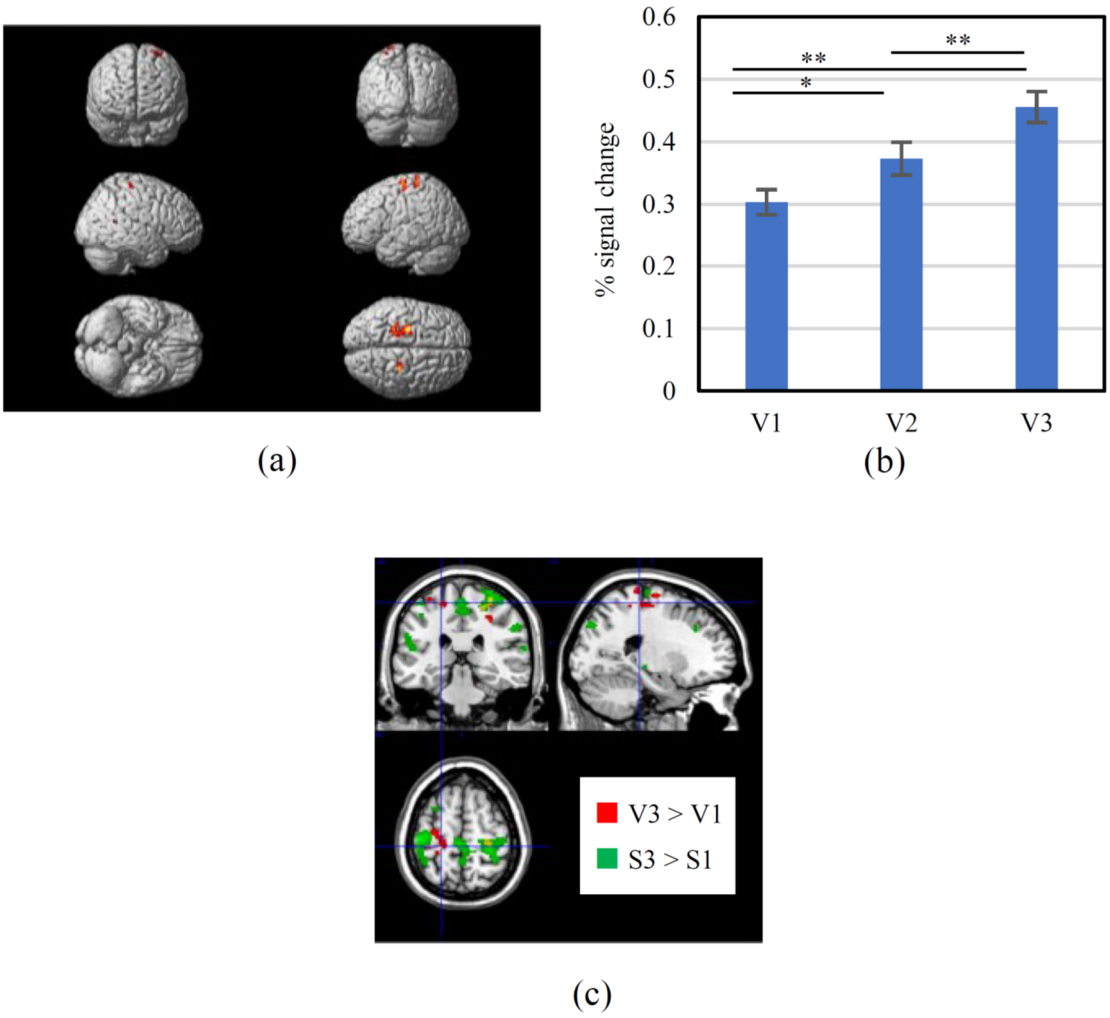

Fig. 5.13. (a) Significant brain activation in the contrast of V3 > V1 in the viscosity condition during the gate period at the threshold of family-wise error FWE with a corrected $p < 0.05$ at the peak level. (b) Percent signal change in the activated cluster in the contrast of V3 > V1. (c) Spatial relationship between significant activation in the contrast of V3 > V1 with the peak activation in the left premotor cluster including the Montreal Neurological Institute (MNI) coordinates -22, -30, 62 and the significant activation in the contrast of S3 > S1. **: $p < 0.01$, *: $p < 0.05$, Error bar: SEM.

5.4. Discussion

5.4.1. Validity of fMRI data

In the “countdown,” “straight,” and “gate” periods, it was predicted that there would be activation in the brain regions involved in task-related visual and motor processing; indeed, these periods were associated with significant activation in the visual cortex (see Fig. 5.8). In the “countdown” period, we observed activations in the visual cortices, somatosensory areas, primary motor area, parietal somatosensory association area, and cerebellum. During this period, participants were required to prepare for the upcoming task by grasping the steering wheel and viewing the countdown numbers. Processing in this task would require motor planning and the sensory perception necessary for grasping the steering wheel. This result was consistent with our prediction.

In the “straight” period, we observed activations in the primary somatosensory cortex, parietal somatosensory association area, and cerebellum, as well as the visual cortices. This result can be interpreted as force modulation based on the processing of visual information (e.g., [57]), since the participants were required to maintain a constant force on the steering wheel to trace the straight white line.

During the “gate” period, participants performed a kind of a visuomotor task in which they needed to steer and maintain control of the virtual vehicle to pass through the center of the gates. This led to the prediction that the brain regions involved in motor and visual processing would be engaged because the task would require the coordination of both hands in accordance with the timing of the car’s passage through the gate. This task required the participant to process sensorimotor information based on the steering

reaction force and visual information. The brain regions activated during the "gate" period included the parieto-motor regions and the cerebellum. Engagement of these regions is consistent with those reported in a study by Schweizer *et al*. [13] in which they used an fMRI-compatible driving simulator, requiring participants to make a turn. This suggests that similar cognitive resources associated with visuospatial and motor coordination were recruited in the "gate" period in our study as those activated when making a turn. The activations observed in various brain regions in each period of the task can be reasonably interpreted based on the predicted functional requirement for performance in each period.

Since more brain regions were active in the contrasts of S3 > S1 than in that of V3 > V1 (see Figs. 5.12 and 5.13), a change in the stiffness condition had greater effects on brain activity than changes in the viscosity condition. This is supported by the fact that in the stiffness condition, many evaluation words had a significant main effect ($p < 0.01$), whereas in the viscosity condition, no evaluation words showed a significant main effect (see Figs. 5.10 and 5.11). Therefore, the range of affective changes in the participants was larger under the stiffness condition than under the viscosity condition. In future studies, we plan to examine the relationship between subjective evaluation and brain activity by dissociating participants' mental state during steering and brain activation from other factors, such as the steering performance scores fed back after the end of the steering trials.

5.4.2. Brain activity correlated with viscoelastic conditions

We found that changes in stiffness covaried with changes in activation in the M1 region associated with the hand representation (inverted omega sign, Yousry *et al*. [58]) (Fig.

5.12). Functional neuroimaging studies revealed somatomotor body representation of the M1 region, including distal representation in the ventral portion of M1 and proximal representation in the dorsal portion of M1 (Colebatch *et al.* [56]; Grafton *et al*. [59]). The well-known morphological sign for the hand region (distal representation) is the inverted omega sign (Yousry *et al*. [58]). Recently, Germann *et al*. [55] showed that the central sulcus is composed of five distinct sulcal segments and that each segment relates systematically to the sensorimotor representation of distinct parts of the body. Thus, stiffness of the wheel is mainly associated with driving control mediated by the distal muscles (i.e., the hand).

In contrast, changes in viscosity covaried with driving-related activation in the dorsal premotor cortex and the dorsal M1 region associated with hand representation (Fig. 5.13). According to Germann *et al*. [55], the precentral gyrus dorsal to the hand area with the inverted omega sign represents the proximal muscles. Studies involving lesions of the dorsal premotor cortex showed weakness of the contralateral shoulder or hip muscles, and uncoordination of movements requiring temporal adjustment between proximal muscle activations on both sides of the body (limb-kinetic apraxia) (Freund [60]). Thus, viscosity affects driving control mediated by the proximal muscles.

The mechanical characteristics of the steering reaction force in the experiment reflected that of a quadratic linear system (i.e., a spring-mass-damper system, with the torque input and the angle output consisting of inertia, stiffness and viscosity parameters). In this case, the damping ratio decreases as the stiffness increases, and, conversely, increases as the viscosity increases. Also, the natural angular frequency increases in proportion to the square root of the stiffness (e.g., [61]). Therefore, a steering system has a quicker response

when the stiffness becomes larger, thus requiring distal force tuning. On the other hand, the system has a slower response when the viscosity becomes larger, thus requiring proximal force tuning.

In this study, we demonstrated for the first time that distinct parameters representing the physical characteristics of the steering wheel, namely stiffness and viscosity, can affect vehicular control during driving by engaging different muscular systems.

From the viewpoint of human physical characteristics, the forearms and hands are operated by distal muscles and are suitable for controlling fast movement because the corresponding inertia of the forearm and hand is rather small. On the other hand, proximal muscles have a large body inertia, which is suitable for controlling slow movements [62]. Therefore, our results show that these different muscular systems were reasonably utilized for each condition according to participants' force feeling information in the driving task, as a kind of visuo-motor control tool, rather than a simple power exertion. In contrast, in the context of visuo-motor control, when we exert an action, we predict sensory feedback and modify the motor signals based on the prediction error (e.g. [63], [64]). Likewise, the vehicle response results in less prediction error to steering operation based on driving intention; thus, a driver can maintain motivation without stress, which eventually leads to positive emotions. Moreover, drivers might make predictions based on an internal model [64] acquired from their past experience driving vehicles. In this case, a steering wheel's viscoelasticity can be a control factor for drivers to adapt to the prediction error between the vehicle's reaction expected from their internal model of a vehicle, such as a small car, a large car, and a sporty car, depending on their experiences, as well as age and gender. In recent years, a model-based approach has gained importance for efficient and high-

quality product development (e.g. [65]), and for future model-based development, accumulating knowledge on the brain mechanism for the input-output relationship associated with driving will be useful.

In this study, despite using a simplified relationship between steering angles and reaction force, we found a fundamental difference in the effects of stiffness and viscosity on driving behavior and brain activity. To extend our findings, in a future study, we will conduct an experiment using complex steering force characteristics (e.g. Takemura *et al*. [3]) that closely resemble real vehicles. Participants were instructed to steer as if they were actually driving; however, they were not given detailed information on the vehicle, such as whether it was large or small. However, the kind of vehicle they intend to drive might affect steering feelings. To clarify the effects of steering force characteristics on the steering feeling, it will be necessary to define the characteristics of the target vehicle and to use a corresponding vehicle model.

5.4.3. Subjective perceptions

Regarding the results of VAS4 shown in Fig. 5.10, in the stiffness condition, S2 was rated significantly positive for all VAS4 evaluation words, as predicted by our preliminary pilot study, which can be interpreted as the moderate reaction force being important for positive steering feeling in comparison with S1 and S3. In contrast, regarding the viscous condition, self-efficacy tended to be significantly higher in V2 than in V3. Since V2 was determined as a characteristic with moderate viscosity, it might mean that excessive viscosity might hinder the desired steering. In addition, from the results of principal component analysis (PCA), participants' evaluation followed a single axis reflecting

positive-negative feeling.

As for VAS7 after six trials, anxiety was rated significantly higher in S1 than in S2 in the stiffness condition, as shown in Fig. 5.11 (a). This suggests that participants felt anxiety if they experienced no reaction force. In addition, self-efficacy, pleasantness, and excitement were rated significantly higher in S2 than in S1 and S3. This tendency that ratings for positive evaluation words increased in S2 was consistent with the results of VAS4, suggesting that moderate stiffness is related to positive feelings. As for VAS7, in the viscosity condition, there was no significant difference among the three levels as shown in Fig. 5.11 (b). In the PCA results shown in Fig. 5.11 (c), the first principal component can be interpreted as a positive feeling and the second as unpleasant, with the cumulative contribution rate of the first and second principal components being around 75%. Therefore, these results suggested that the evaluation on a positive-negative feeling was dominant both in VAS4 and VAS7.

Note that the task performance scores presented at the end of each trial resulted in a bias to the steering feeling. Nevertheless, at least the negative-positive feeling varied by changing the viscoelastic characteristics of the reaction force even in the measurement environment using MRI. In addition, the significant change in anxiety rating in VAS7 by different stiffness coefficients may reflect that participants performed the driving task with a mindset to drive a vehicle even in this simple driving simulation.

5.4.4. Limitations

Our experimental settings markedly differed from real-life driving conditions; for instance, participants' postures were supine and the driving task required no acceleration

input. To generalize our results to actual driving, we should consider implementing the following improvements in future studies: (1) establishing a method to verify the findings obtained by fMRI in a vehicular driving environment mimicking the real world; (2) improving the driving task to enhance participants' driving pleasure, possibly by using steering reaction force characteristics such that participants may feel the steering reaction force changing linearly with their steering operation (e.g. [3]) and by adopting a challenging driving course. Furthermore, subjective evaluations in this experiment were influenced by the performance score presented after each trial as well as the driving feeling during the trial, because the subjective evaluation was performed after presentation of the performance score at the end of each trial. Therefore, it is difficult to extract brain activity purely related to the driving feeling, and in future work, the experimental design needs to be improved so that participants can perform a subjective evaluation purely reflecting their feelings while performing the driving task; and (3) examining the effects of individual differences in driving ability, such as skills and experience. Moreover, although this experiment targeted only young men to obtain reliable results within a homogeneous subject group, it is necessary to expand the scope of research because of the clear differences in driving behavior and emotional/affect states caused by age and gender [66], [67], [68]. Considering these issues will lead to a better understanding of the neural mechanisms related to driving pleasure.

5.5. **Conclusion remarks**

This chapter described the first experiment to perform fMRI measurements of brain activity during steering operations in a simulated driving task with variable steering

reaction forces. By changing the viscoelastic characteristics of the steering reaction force, we found that the stiffness of the handle mainly affected the distal muscles, whereas the viscosity affected driving control mediated by the proximal muscles. It is possible that these novel and basic findings could provide a neuroscientific method for optimizing steering characteristics based on brain activity.

5.6. **Appendix**

Table S1 Location and volume of active clusters in the stiffness condition

Brain regions significantly activated at the family-wise error (FWE) thresholds with a corrected $p < 0.05$ at the voxel level.

(a) Countdown period

Region	Area	*X* (mm)	*Y* (mm)	*Z* (mm)	Peak *Z*	Voxels
L Postcentral Gyrus	3b	-42	-22	58	Inf	4295
L Precentral Gyrus	6	-36	-20	70	Inf	
L Rolandic Operculum		-44	-24	22	7.49	
L Superior Parietal Lobule	5L (SPL)	-28	-46	56	6.61	
R Middle Occipital Gyrus	hOc4lp	32	-86	10	Inf	14074
R Calcarine Gyrus	hOc1 [V1]	12	-80	6	Inf	
L Superior Occipital Gyrus	hOc1 [V1]	-8	-98	4	Inf	
R Cuneus	hOc2 [V2]	14	-94	14	Inf	
L Calcarine Gyrus	hOc1 [V1]	-10	-82	2	Inf	
R Cerebelum (IV-V)	Lobule VI (Hem)	24	-50	-18	Inf	
L Cerebelum (IV-V)	Lobule VI (Hem)	-26	-46	-22	Inf	
L Middle Occipital Gyrus	hOc4lp	-28	-90	8	Inf	
L Inferior Occipital Gyrus	19	-42	-66	-8	Inf	
L Superior Occipital Gyrus	hOc4d [V3A]	-16	-94	18	Inf	
L Fusiform Gyrus	hFG1	-32	-60	-14	Inf	
L Lingual Gyrus	18	16	-74	-6	Inf	
R Occipital Fusiform Gyrus	37	26	-70	-12	Inf	
R Lingual Gyrus	18	-16	-72	-10	Inf	
L Calcarine Cortex	18	-6	-92	-4	Inf	
R Inferior Occipital gyrus	37	50	-70	-8	6.99	
R Precentral Gyrus		38	-26	70	Inf	2246
R Precentral Gyrus	4	40	-18	54	Inf	
R Precentral Gyrus	4	36	-26	58	Inf	
R Precentral Gyrus	6	46	-18	62	Inf	
R Precentral Gyrus	6	30	-20	68	Inf	
R Superior Frontal Gyrus	6	32	-4	68	Inf	
R Superior Frontal Gyrus		36	-8	66	Inf	
R Precentral Gyrus		40	-6	62	7.67	
L Posterior-Medial Frontal	6	-2	-2	54	Inf	2316
L MCC	5	-10	-26	48	Inf	
L Posterior-Medial Frontal	6	-6	-18	50	Inf	
R MCC	6	12	-24	46	7.76	
L MCC	5M (SPL)	-12	-38	52	6.39	
R Cerebelum (VIII)	Lobule VIIIb (Hem)	20	-56	-56	7.58	249
L Cerebelum (VIII)	Lobule VIIIb (Hem)	-22	-48	-56	6.46	323
L Cerebelum (VIII)	Lobule VIIIb (Hem)	-28	-42	-54	6.25	
Cerebellar Vermis (6)	Lobule VI (Verm)	0	-60	-22	6.43	241
Cerebellar Vermis (8)	Lobule VIIIa (Verm)	2	-64	-32	5.98	
L Thalamus	Thal: Prefrontal	-14	-20	8	5.50	34
L Rolandic Operculum	6	-46	0	8	5.32	27
L Middle Frontal Gyrus	10	-38	46	28	5.06	17
R Lingual Gyrus	36	12	-40	-2	4.63	3
L Putamen		-14	10	-10	4.63	2
R Caudate Nucleus		16	16	-10	4.62	1
L Superior Parietal Lobule	7	-16	-68	46	4.60	7

(b) Straight period

Region	Area	*X* (mm)	*Y* (mm)	*Z* (mm)	Peak *Z*	Voxels
R Superior Parietal Lobule	7A (SPL)	18	-60	60	Inf	4848
R Superior Occipital Gyrus	19	28	-84	20	Inf	
R Middle Temporal Gyrus	19	44	-64	0	Inf	
R Lingual Gyrus	hOc3v [V3v]	14	-76	-8	Inf	
L Lingual Gyrus	hOc3v [V3v]	-12	-80	-8	Inf	
L Lingual Gyrus	hOc1 [V1]	-10	-84	-2	Inf	
R Superior Occipital Gyrus	7	26	-72	34	Inf	
R Superior Parietal Lobule	7P (SPL)	22	-78	50	5.74	
Cerebellar Vermis (6)	Lobule V (Hem)	0	-62	-20	5.71	
Cerebellar Vermis (6)	Lobule VI (Verm)	2	-70	-14	5.43	
L Superior Parietal Lobule	7A (SPL)	-18	-60	58	Inf	1979
L Superior Parietal Lobule	7A (SPL)	-20	-56	56	Inf	
L Precuneus	7A (SPL)	-14	-62	70	Inf	
L Middle Occipital Gyrus	19	-24	-84	14	Inf	
L Superior Parietal Lobule	7A (SPL)	-16	-78	52	7.61	
L Middle Occipital Gyrus	7	-26	-66	28	6.10	
L Middle Occipital Gyrus	19	-42	-66	0	Inf	342
RPrecentral Gyrus	6	30	-6	52	Inf	862
R Superior Frontal Gyrus	6	24	0	62	Inf	
RPrecentral Gyrus		28	-22	60	7.67	
R Superior Frontal Gyrus	6	20	-14	76	7.64	
R Superior Frontal Gyrus	6	20	-14	66	7.22	
L Superior Frontal Gyrus	6	-22	-4	54	Inf	617
L Cerebelum (IX)	Lobule VIIIb (Hem)	-16	-48	-50	7.48	188
L Cerebelum (VIII)	Lobule X (Hem)	-22	-36	-48	6.71	
L Cerebelum (VIII)	Lobule VIIIb (Hem)	-28	-40	-50	6.00	
L Cerebelum (VI)	Lobule VI (Hem)	-30	-36	-36	5.85	
L Cerebelum (VI)	Lobule VI (Hem)	-32	-40	-32	5.83	
L Cerebelum (VIII)	Lobule VIIIa (Hem)	-32	-42	-50	5.32	
L Cerebelum (X)	Lobule V (Hem)	-26	-32	-40	5.27	
Cerebellar Vermis (8)	Lobule VIIIa (Verm)	0	-70	-34	7.36	101
R Cerebelum (VIII)	Lobule VIIIb (Hem)	28	-42	-48	4.95	11
L Superior Occipital Gyrus	hOc2 [V2]	-8	-98	8	4.94	2
L Precentral Gyrus		-26	-22	58	4.82	5
L Precentral Gyrus	6	-56	6	38	4.68	3

(c) Gate period

Region	Area	*X* (mm)	*Y* (mm)	*Z* (mm)	Peak *Z*	Voxels
R Superior Parietal Lobule	7A (SPL)	18	-60	60	Inf	49362
R Superior Occipital Gyrus	19	26	-84	20	Inf	
R Lingual Gyrus	hOc2 [V2]	12	-78	-6	Inf	
L Lingual Gyrus	hOc3v [V3v]	-8	-82	-8	Inf	
R Superior Occipital Gyrus	hOc4d [V3A]	22	-88	16	Inf	
R Cuneus	18	18	-92	12	Inf	
L Middle Occipital Gyrus	hOc4d [V3A]	-20	-90	16	Inf	
L Superior Parietal Lobule	7A (SPL)	-16	-60	60	Inf	
L Superior Parietal Lobule	5L (SPL)	-26	-50	56	Inf	
R Middle Temporal Gyrus	hOc5 [V5/MT]	46	-64	0	Inf	
R Middle Temporal Gyrus	hOc5 [V5/MT]	44	-68	0	Inf	
L Inferior Occipital Gyrus	19	-42	-68	2	Inf	
R Superior Frontal Gyrus	6	24	-2	62	Inf	
L Superior Parietal Lobule	7	-18	-68	44	Inf	
L Superior Frontal Gyrus	6	-22	-4	62	Inf	
L Superior Frontal Gyrus	6	-24	-4	54	Inf	
L Thalamus	Thal: Prefrontal	-12	-20	10	Inf	999
L Putamen		-24	-6	8	6.08	
L Thalamus	Thal: Prefrontal	-8	-24	-2	5.81	
N/A	Thal: Prefrontal	-18	-6	6	5.81	
L Thalamus	Thal: Prefrontal	-14	-8	-2	5.39	
L Superior Medial Gyrus	9	-8	58	34	Inf	299
L Superior Frontal Gyrus		-12	52	42	6.81	
L Superior Frontal Gyrus	8	-12	44	46	6.00	
R Thalamus	Thal: Prefrontal	12	-18	8	Inf	570
R Putamen		28	-12	6	7.46	
L Superior Medial Gyrus	Fp2	-8	56	2	6.51	105
L ACC	Fp2	-6	54	-2	6.33	
L Mid Orbital Gyrus	Fp2	-10	50	-10	5.91	
R Superior Orbital Gyrus	11	14	54	-14	6.50	41
R Superior Medial Gyrus	Fp2	12	58	0	5.69	
R Superior Medial Gyrus	9	8	54	40	5.84	45
R Caudate Nucleus		4	8	-4	5.80	36
N/A		4	2	-6	5.28	
R Caudate Nucleus		10	16	-6	5.07	
N/A		-4	4	-4	4.96	
L Superior Frontal Gyrus	8	-14	30	58	5.66	16
L Middle Frontal Gyrus	10	-32	54	24	5.63	37
L Middle Frontal Gyrus	10	-38	52	14	4.89	
R Insula Lobe	13	34	20	10	5.44	13
R Middle Orbital Gyrus	10	38	48	-14	5.28	6
L Middle Temporal Gyrus	TE 3	-62	-16	0	5.07	11
R Superior Frontal Gyrus	8	14	36	50	4.88	7
N/A	Thal: Parietal	20	-26	-4	4.87	7
L Insula Lobe		-30	18	10	4.80	6
R Middle Orbital Gyrus	10	44	50	-12	4.79	2
N/A		20	-14	-6	4.67	2
R IFG (p. Orbitalis)	47	38	26	-18	4.58	1
L IFG (p. Triangularis)		-48	38	22	4.57	2
L PCC		0	-44	28	4.51	1
L Caudate Nucleus		-14	24	-8	4.50	1

Table S2 Location and volume of active clusters in the viscosity condition

Brain regions significantly activated at the family-wise error (FWE) thresholds with a corrected $p < 0.05$ at the voxel level.

(a) Countdown period

Region	Area	*X* (mm)	*Y* (mm)	*Z* (mm)	Peak Z	Voxels
L Postcentral Gyrus	3b	-42	-20	56	Inf	4188
L Precentral Gyrus	6	-40	-18	66	Inf	
L Precentral Gyrus	6	-32	-20	64	Inf	
L Superior Frontal Gyrus		-18	4	72	5.69	
L Superior Frontal Gyrus	6	-24	0	70	5.62	
L Superior Parietal Lobule	7PC (SPL)	-26	-54	60	4.67	
R Middle Occipital Gyrus	hOc4lp	32	-86	10	Inf	15964
R Calcarine Gyrus	hOc1 [V1]	14	-80	4	Inf	
R Cuneus	hOc2 [V2]	14	-94	10	Inf	
L Superior Occipital Gyrus	hOc1 [V1]	-8	-98	6	Inf	
L Calcarine Gyrus	hOc1 [V1]	-10	-82	2	Inf	
R Cuneus	hOc1 [V1]	16	-96	6	Inf	
R Cerebelum (VI)	Lobule VI (Hem)	26	-52	-20	Inf	
L Inferior Occipital Gyrus	FG2	-44	-64	-12	Inf	
R Fusiform Gyrus	FG1	30	-64	-16	Inf	
L Inferior Occipital Gyrus	FG2	-40	-70	-12	Inf	
L Fusiform Gyrus	FG1	-34	-62	-16	Inf	
R Cuneus	18	16	-72	-6	Inf	
L Lingual Gyrus	18	-16	-74	-10	Inf	
L Cerebellum Exterior		-20	-56	-18	Inf	
R Temporal lobe	37	40	-60	-16	Inf	
L Middle Occipital Gyrus	19	-30	-82	16	Inf	
R Precentral Gyrus	6	38	-20	64	Inf	2983
R Precentral Gyrus	6	30	-22	74	Inf	
R Precentral Gyrus	6	30	-18	72	Inf	
R Superior Parietal Lobule	7PC (SPL)	32	-50	64	5.61	1868
L Posterior-Medial Frontal	6	-2	-2	52	Inf	
R Posterior-Medial Frontal	6	10	-22	48	7.10	
L MCC	31	-8	-26	48	7.06	
L Posterior-Medial Frontal	6	-6	-22	50	6.85	
L MCC	5M (SPL)	-14	-40	50	5.65	
R Paracentral Lobule	5	16	-40	50	5.43	
L Posterior-Medial Frontal	6	-2	-4	70	5.07	
R Cerebelum (VIII)	Lobule VIIIb (Hem)	22	-54	-56	Inf	330
L Cerebelum (VIII)	Lobule VIIIb (Hem)	-22	-52	-58	Inf	506
L Cerebelum (VIII)	Lobule VIIIb (Hem)	-26	-44	-56	Inf	
L Rolandic Operculum		-48	-22	22	7.53	266
L Lingual Gyrus		-8	-42	-2	6.23	90
R Lingual Gyrus	36	10	-40	0	6.01	92
R Calcarine Gyrus	18	18	-52	4	5.86	102
R Lingual Gyrus	hOc1 [V1]	8	-56	8	5.15	
L Middle Frontal Gyrus	10	-32	44	34	5.68	24
L Rolandic Operculum	6	-42	-2	12	5.29	19
L Thalamus	Thal: Prefrontal	-16	-22	8	4.84	7
L Precentral Gyrus	6	-52	4	36	4.80	8
L Middle Orbital Gyrus	Fo3	-20	36	-16	4.70	4
L Precuneus	5M (SPL)	0	-52	62	4.69	4
R Putamen		16	14	-8	4.67	6

(b) Straight period

Region	Area	*X* (mm)	*Y* (mm)	*Z* (mm)	Peak Z	Voxels
L Lingual Gyrus	Area hOc1 [V1]	-10	-86	-2	Inf	10956
R Superior Parietal Lobule	Area 7A (SPL)	22	-58	56	Inf	
R Middle Occipital Gyrus	19	34	-84	14	Inf	
L Superior Parietal Lobule	Area 7A (SPL)	-16	-64	54	Inf	
R Middle Temporal Gyrus	39	42	-64	2	Inf	
R Calcarine Gyrus	Area hOc1 [V1]	12	-84	0	Inf	
L Middle Occipital Gyrus	19	24	-84	18	Inf	
R Lingual Gyrus	Area hOc3v [V3v]	14	-78	-6	Inf	
R Superior Parietal Lobule	Area 7A (SPL)	22	-60	70	Inf	
L Lingual Gyrus	Area hOc3v [V3v]	-16	-80	-8	Inf	
R Cuneus	Area hOc1 [V1]	14	-92	8	Inf	
L Occipital Pole	18	-8	-98	8	Inf	
Cerebellar Vermis	Lobules VI-VII (Verm)	0	-70	-32	Inf	
L Cerebellum Exterior		-8	-68	-46	5.57	
L Inferior Occipital Gyrus	18	-32	-92	-4	4.97	
L Middle Occipital Gyrus	19	-42	-64	2	Inf	498
R Superior Frontal Gyrus	6	24	0	56	Inf	1222
R Precentral Gyrus	6	24	-14	74	Inf	
R Precentral Gyrus		28	-22	56	7.51	
R Precentral Gyrus		28	-22	64	7.36	
L Superior Frontal Gyrus	6	-24	-2	56	Inf	1037
L Precentral Gyrus		-28	-24	62	5.86	
L Precentral Gyrus		-26	-22	56	5.60	
L Cerebelum (IX)	Lobule IX (Hem)	-14	-48	-50	Inf	647
L Cerebelum (VIII)	Lobule VIIIb (Hem)	-28	-40	-50	Inf	
L Cerebelum (VI)	Lobule VI (Hem)	-30	-36	-34	Inf	
L Cerebelum (Crus 1)	Lobule VI (Hem)	-38	-42	-36	7.53	
L Cerebelum (X)	Lobule V (Hem)	-26	-32	-40	7.19	
L Cerebelum (VI)	Lobule VI (Hem)	-28	-42	-30	7.17	
L Cerebelum (VIII)	Lobule VIIIb (Hem)	-18	-38	-54	6.16	
L Cerebelum (VIII)	Lobule VIIIb (Hem)	-24	-50	-56	6.03	
R Cerebelum (IX)	Lobule IX (Hem)	16	-50	-48	7.57	164
R Cerebelum (VIII)	Lobule VIIIb (Hem)	28	-42	-50	6.32	
R Cerebelum (VIII)	Lobule VIIIb (Hem)	18	-38	-52	5.58	

Table S2 ***(Continued.)*** Location and volume of active clusters in the viscosity condition

(c) Gate period

Region	Area	*X* (mm)	*Y* (mm)	*Z* (mm)	Peak *Z*	Voxels
L Calcarine Gyrus	hOc1 [V1]	-8	-86	-2	Inf	61302
R Lingual Gyrus	hOc2 [V2]	12	-80	-4	Inf	
R Superior Parietal Lobule	7A	22	-60	56	Inf	
R Middle Occipital Gyrus	19	32	-78	18	Inf	
L Middle Occipital Gyrus	19	-32	-86	18	Inf	
L Superior Parietal Lobule	7A	-18	-64	52	Inf	
R Cuneus	hOc1 [V1]	14	-92	8	Inf	
R Middle Temporal Gyrus	hOc5 [V5/MT]	44	-66	2	Inf	
R Cuneus	18	20	-90	14	Inf	
R Fusiform Gyrus	hOc4v [V4(v)]	26	-74	-10	Inf	
L Middle Temporal Gyrus	19	-42	-66	2	Inf	
L Inferior Occipital Gyrus	19	-44	-66	-2	Inf	
R Superior Frontal Gyrus	6	26	-2	56	Inf	
L Superior Frontal Gyrus	6	-24	-2	56	Inf	
L Superior Frontal Gyrus	6	-22	-4	62	Inf	
R Precentral Gyrus		30	-24	58	Inf	
L Thalamus	Thal: Prefrontal	-12	-18	8	Inf	2848
R Thalamus	Thal: Prefrontal	12	-16	10	Inf	
R Thalamus	Thal: Prefrontal	16	-20	14	Inf	
L Putamen		-24	-8	8	7.23	
N/A		-6	-26	-2	6.86	
N/A	Thal: Prefrontal	8	-22	-4	6.68	
N/A		6	-28	-4	6.50	
N/A	Thal: Prefrontal	-8	-18	-4	6.21	
R Pallidum		22	-4	6	6.11	
R Putamen		28	-16	4	5.90	
N/A		-12	2	10	5.59	
R Thalamus		18	-28	-6	5.34	
L Middle Orbital Gyrus	10	-40	56	-6	Inf	788
L IFG (p. Orbitalis)	10	-38	48	-14	Inf	
L IFG (p. Orbitalis)	47	-42	46	-14	Inf	
L Middle Orbital Gyrus	10	-36	52	-12	Inf	
L Middle Frontal Gyrus	10	-32	58	14	7.70	
L Superior Medial Gyrus	10	-8	62	20	6.87	
L Middle Frontal Gyrus	10	-36	58	2	6.57	
L Superior Frontal Gyrus	Fp1	-18	62	14	5.60	
L Superior Medial Gyrus	10	-4	58	30	5.58	
R Superior Medial Gyrus	Fp2	2	56	4	5.05	
L Superior Medial Gyrus	10	-6	58	6	5.02	
L Insula Lobe	13	-30	16	10	Inf	124
R Middle Frontal Gyrus	10	44	50	14	7.42	778
R Middle Frontal Gyrus	9	38	40	26	6.91	
R Middle Frontal Gyrus	10	44	54	0	6.83	
R Middle Orbital Gyrus	10	42	52	-12	6.61	
R Middle Frontal Gyrus	10	38	42	14	6.48	
R Middle Frontal Gyrus		34	52	28	5.91	
R Middle Orbital Gyrus	Fo3	26	38	-14	5.85	
R Middle Frontal Gyrus	9	38	36	36	5.70	
R IFG (p. Orbitalis)	Fo3	30	34	-16	5.31	
R IFG (p. Orbitalis)	Fo3	26	32	-16	5.24	
L Superior Medial Gyrus	8	-10	44	46	6.40	77
R Superior Frontal Gyrus	8	22	48	42	5.77	20
L Middle Frontal Gyrus	9	-40	34	34	5.78	88
L Middle Frontal Gyrus	9	-46	36	28	5.47	
R IFG (p. Orbitalis)	47	32	28	-18	5.61	10
R IFG (p. Orbitalis)	47	42	24	-18	4.56	
R Superior Frontal Gyrus	Fp1	30	62	6	5.57	11
R Superior Frontal Gyrus	Fp1	26	62	8	5.21	
L IFG (p. Orbitalis)	Fo3	-32	22	-20	5.51	16
L IFG (p. Orbitalis)	Fo3	-34	26	-20	5.48	
L IFG (p. Orbitalis)	47	-34	30	-18	4.88	
R MCC		0	-12	30	5.32	39
L Superior Frontal Gyrus	9	-16	54	36	5.18	10
R Superior Medial Gyrus	9	8	60	28	5.04	36
R Middle Frontal Gyrus		20	60	26	4.90	
L Middle Orbital Gyrus	Fo3	-22	40	-16	4.92	2
L Cerebellum (Crus 2)		-36	-70	-46	4.85	5
R IFG (p. Orbitalis)	47	46	22	-16	4.78	2
R Insula Lobe	Fo3	34	22	-20	4.59	1
Left Posterior Cingulate Gyrus		0	-30	28	4.59	3
L Superior Frontal Gyrus	8	16	38	50	4.58	1
R Superior Medial Gyrus	9	8	56	34	4.52	1

Table S3 Location and volume of active clusters

Stiffness condition S3 > S1 at Cluster 1

Region	Area	*X* (mm)	*Y* (mm)	*Z* (mm)	Peak Z	Voxels
L Postcentral Gyrus	1	-46	-24	62	7.43	826
L Precentral Gyrus		-38	-20	64	6.44	
L Postcentral Gyrus	3b	-50	-16	42	5.81	
L Precentral Gyrus		-26	-22	76	5.69	
L Postcentral Gyrus	1	-44	-36	64	5.56	
L Precentral Gyrus		-30	-22	74	5.41	
L Superior Parietal Lobule	7PC	-38	-48	62	5.22	
L Postcentral Gyrus	1	-40	-42	66	5.10	
L Precentral Gyrus		-18	-18	78	4.88	
L Postcentral Gyrus		-52	-12	52	4.87	

Brain regions significantly activated at the family-wise error (FWE) thresholds with a corrected $p < 0.05$ at the voxel level.

Table S4 Location and volume of active clusters

Viscosity condition V3 > V1

Region	BA	*X* (mm)	*Y* (mm)	*Z* (mm)	Peak Z	Voxels
L Precentral Gyrus		-26	-18	58	5.97	220
L Precentral Gyrus		-24	-14	70	5.68	
L Postcentral Gyrus		-20	-34	76	5.59	120
L Postcentral Gyrus	4a	-32	-32	68	5.25	
L Postcentral Gyrus	2	-24	-40	60	4.84	
R Postcentral Gyrus		28	-28	60	5.49	102
R Postcentral Gyrus		22	-63	52	4.76	

Brain regions significantly activated at the family-wise error (FWE) thresholds with a corrected $p < 0.05$ at the voxel level and false discovery rate (FDR) with a corrected $p < 0.05$ at the cluster level.

Chapter 6
Conclusions

This dissertation described the elucidation of the effect of steering reaction force in human brain activity measured by fMRI, which can measure activity throughout the brain with high spatial resolution.

The author newly developed an fMRI-compatible steering reaction force generation unit, verified its performance, and confirmed that it could measure brain activity through fMRI in the presence of a steering reaction force. In the analysis of brain activity while waiting for a simple steering task, it was shown that the steering reaction force and the hand used for steering operation may influence brain activity while waiting for the upcoming steering task. By changing the viscoelastic characteristics of the steering reaction force during steering operations in a simulated driving task, it was found that the stiffness of the handle mainly affected the distal muscles, whereas the viscosity affected driving control mediated by the proximal muscles.

The following is a summary of this paper, an overview of each chapter, and conclusions.

Chapter 2 described the expected performance, implementation and verification of steering reaction force generation performance of the fMRI-compatible steering reaction force generation unit. To avoid disturbance due to the electromagnetic field of the MRI, the unit was configured as follows: A motor installed outside a scan room generated a reaction force that was transmitted to a steering wheel placed in the hands of a subject using a nonmagnetic transmission unit. Although the reaction force generated on the

participant's hand against the reaction force generation motor output deviated from the linear approximation of a straight line, the correlation coefficient showed a clear relationship between the reaction force generated on the participant's hand and the output of the reaction force generation motor (0.974 under the Low condition and 0.992 under the High condition; *ps* < 0.001). This indicated that the output of the reaction force generation motor was transmitted accurately to the participant's hand on average.

Chapter 3 described the verification of fMRI acquisition performance. To verify whether the noise caused by motor operation affected the acquired functional images, the author performed a one-sample t-test on the contrast images between the rotation and no-rotation conditions with a family-wise error (FWE) corrected for $p < 0.05$ as the activity peak threshold. This revealed that no voxel was significantly activated in the rotation condition compared with the no-rotation condition for 21 participants. Furthermore, regarding the verification of functional imaging during steering, the results of fMRI data under low reaction torque stiffness showed significant brain activity during the task in the right primary motor cortex for steering using the left arm (Low-L), in the left primary motor cortex for steering using the right arm (Low-R), and the bilateral motor cortices for steering using both arms (Low-B). Significant activity was also observed in the cerebellum for all three (Low-L, Low-R, and Low-B) conditions. Under the High-B condition, wherein reaction torque stiffness was high, significant activity was observed relative to the rest block in the bilateral primary motor cortices and the cerebellum, as observed under the Low-B condition. These activated regions were consistent with those reported in many previous studies reporting MRI measurements during hand or arm movements. Therefore, these results indicate that reasonable functional imaging was

performed.

Chapter 4 described the results newly show that the steering reaction force and the hand used for steering operation may influence brain activity while waiting for the upcoming steering task. During the standby period, it was observed that the activations in the SN, including the ACC and insula, and when the steering reaction force was large, the BOLD signal change rate in the ACC increased. These results suggested that during the standby for steering where greater force exertion was required, the participants felt more anxiety. Furthermore, when the pure right-handed participants were waiting for steering operation using only their left arm, the amygdala and SMA were significantly activated, suggesting that the participants felt a negative emotion associated with the additional resource needed to prepare for the initiation of the movement of the left hand.

Chapter 5 described that distinct parameters representing the physical characteristics of the steering wheel, namely stiffness and viscosity, can affect vehicular control during driving by engaging different muscular systems. Changes in stiffness covaried with changes in activation in the M1 region associated with the hand representation. Functional neuroimaging studies revealed somatomotor body representation of the M1 region, including distal representation in the ventral portion of M1 and proximal representation in the dorsal portion of M1. The well-known morphological sign for the hand region (distal representation) is the inverted omega sign. Recently, Germann *et al*. [55] showed that the central sulcus is composed of five distinct sulcal segments and that each segment relates systematically to the sensorimotor representation of distinct parts of the body. Thus, stiffness of the wheel is mainly associated with driving control mediated by the distal muscles (i.e., the hand). In contrast, changes in viscosity covaried with driving-related

activation in the dorsal premotor cortex and the dorsal M1 region associated with hand representation. According to Germann *et al*. [55], the precentral gyrus dorsal to the hand area with the inverted omega sign represents the proximal muscles. Studies involving lesions of the dorsal premotor cortex showed weakness of the contralateral shoulder or hip muscles, and uncoordination of movements requiring temporal adjustment between proximal muscle activations on both sides of the body (limb-kinetic apraxia). Thus, viscosity affects driving control mediated by the proximal muscles.

It is thought that based on the research results of brain activity measurement by MRI during steering, provide a neuroscientific method for optimizing steering characteristics based on brain activity, and a first step to model based development by brain science.

The following three points can be considered as future issues.

The first issue is originating from the fMRI experimental environment: (i) realizing the feeling of driving immersion, (ii) reducing awkward feelings from fMRI measurement, (iii) reducing the differences between the biomechanical conditions of actual driving environment and the fMRI experimental environment.

The second issue is improving the driving task to enhance participants' driving pleasure. It will achieve possibly by using steering reaction force characteristics such that participants may feel the steering reaction force changing linearly with their steering operation and by adopting a challenging driving course. In addition, the experimental design needs to be improved so that participants can perform a subjective evaluation purely reflecting their feelings while performing the driving task.

The third is the issue related to the diversity of experimental participants. It is necessary examining the effects of individual differences in driving ability, such as skills and experience. Moreover, although this experiment targeted only young men to obtain reliable results within a homogeneous subject group, it is necessary to expand the scope of research because of the clear differences in driving behavior and emotional/affect states caused by age and gender. Considering these issues will lead to a better understanding of the neural mechanisms related to driving pleasure.

By solving these problems, the author believes that it will be possible to provide driving pleasure that suits the sensibility mechanism of all automobile users, and that a bright future will open up in which people can live a lively life with automobile.

Publications concerning this dissertation are listed in the bibliography [69], [70], and [71].

Bibliography

[1] Center of KANSEI Innovation Nurturing Mental Welfare [Online]. Available: https://www.jst.go.jp/coi/etc/COI-brochure2020.10EN.pdf, pp. 27-28, Accessed on: Dec. 11. 2020.

[2] A. W. Burton, "Innovation drivers for electric power-assisted steering," *IEEE Control Syst. Mag.*, vol. 23, no. 6, pp. 30–39, Dec. 2003, 10.1109/MCS.2003.1251179.

[3] K. Takemura, N. Yamada, A. Kishi, K. Nishikawa, T. Nouzawa, Y. Kurita, and T. Tsuji, "A subjective force perception model of humans and its application to a steering operation system of a vehicle," *Proceedings - 2013 IEEE Int. Conf. Syst. Man Cybern., SMC 2013*, Manchester, United Kingdom, 2013, pp. 3675–3680, 10.1109/SMC.2013.626.

[4] J. Dang, H. Chen, B. Gao, Q. Li, M. Li, T. Watanabe, R. Hayama, L. Lou, and S. Nakano, "Optimal design of on-center steering force characteristic based on correlations between subjective and objective evaluations," *SAE Int. J. Passeng. Cars-Mech. Syst.*, vol. 7, no. 3, pp. 992–1001, Jun. 2014, 10.4271/2014-01-0137.

[5] A. J. Pick and D. J. Cole, "Neuromuscular dynamics in the driver–vehicle system," *Veh. Syst. Dyn.*, vol. 44, no. sup1, pp. 624–631, 2006. 10.1080/00423110600882704.

[6] C. Dijksterhuis, K. A. Brookhuis, and D. De Waard, "Effects of steering demand on lane keeping behaviour, self-reports, and physiology. A simulator study," *Accid. Anal. Prev.*, vol. 43, no. 3, pp. 1074–1081, May 2011, 10.1016/j.aap.2010.12.014.

[7] A. Lanatà, G. Valenza, A. Greco, C. Gentili, R. Bartolozzi, F. Bucchi, F. Frendo, and E. P. Scilingo, "How the autonomic nervous system and driving style change with incremental stressing conditions during simulated driving," *IEEE Trans. Intell. Transp. Syst.*, vol. 16, no. 3, pp. 1505–1517, Jun. 2015, 10.1109/TITS.2014.2365681.

[8] J. Navarro, E. Reynaud, and F. Osiurak, "Neuroscience and Biobehavioral Reviews Neuroergonomics of car driving: A critical meta-analysis of neuroimaging data on the human brain behind the wheel," *Neurosci. Biobehav. Rev.*, vol. 95, pp. 464–479, Dec. 2018, 10.1016/j.neubiorev.2018.10.016.

[9] P. A. Hancock and J. L. Szalma, "The future of neuroergonomics," *Theor. Issues Ergon. Sci.*, vol. 4, no. 1–2, pp. 238–249, Jan. 2003, 10.1080/1463922021000020927.

[10] R. Parasuraman, "Neuroergonomics: Research and practice," *Theor. Issues Ergon. Sci.*, vol. 4, no. 1–2, pp. 5–20, 2003, 10.1080/14639220210199753.

[11] V. D. Calhoun and G. D. Pearlson, "A selective review of simulated driving studies: Combining naturalistic and hybrid paradigms, analysis approaches, and future directions," *NeuroImage*, vol. 59, no. 1. pp. 25–35, Jan. 2012, 10.1016/j.neuroimage.2011.06.037.

[12] K. Kan, T. A. Schweizer, F. Tam, and S. J. Graham, "Methodology for functional MRI of simulated driving," *Med. Phys.*, vol. 40, no. 1, p. 12301, 2013, 10.1118/1.4769107.

[13] T. A. Schweizer, K. Kan, Y. Hung, F. Tam, G. Naglie, and S. J. Graham, "Brain activity during driving with distraction: An immersive fMRI study," *Front. Hum.*

Neurosci., vol. 7, p. 53, Feb. 2013, 10.3389/fnhum.2013.00053.

[14] Y. Uchiyama, K. Ebe, A. Kozato, T. Okada, and N. Sadato, "The neural substrates of driving at a safe distance: A functional MRI study," *Neurosci. Lett.*, vol. 352, no. 3, pp. 199–202, Dec. 2003, 10.1016/j.neulet.2003.08.072.

[15] M. Mader, A. Bresges, R. Topal, A. Busse, M. Forsting, and E. R. Gizewski, "Simulated car driving in fMRI—Cerebral activation patterns driving an unfamiliar and a familiar route," *Neurosci. Lett.*, vol. 464, no. 3, pp. 222–227, Oct. 2009, 10.1016/j.neulet.2009.08.056.

[16] H. J. Spiers and E. A. Maguire, "Neural substrates of driving behaviour," *Neuroimage*, vol. 36, no. 1, pp. 245–255, May 2007, 10.1016/j.neuroimage.2007.02.032.

[17] J. Z. Liu, T. H. Dai, T. H. Elster, V. Sahgal, R. W. Brown, and G. H. Yue, "Simultaneous measurement of human joint force, surface electromyograms, and functional MRI-measured brain activation," *J. Neurosci. Methods*, vol. 101, no. 1, pp. 49–57, Aug. 2000, 10.1016/S0165-0270(00)00252-1.

[18] T. H. Dai, J. Z. Liu, V. Saghal, R. W. Brown, and G. H. Yue, "Relationship between muscle output and functional MRI-measured brain activation," *Exp. Brain Res.*, vol. 140, no. 3, pp. 290–300, Oct. 2001, 10.1007/s002210100815.

[19] Y. Tanaka, N. Fujimura, T. Tsuji, M. Maruishi, H. Muranaka, and T. Kasai, "Functional interactions between the cerebellum and the premotor cortex for error correction during the slow rate force production task: An fMRI study," *Exp. Brain Res.*, vol. 193, no. 1, pp. 143–150, Feb. 2009, 10.1007/s00221-008-1682-4.

[20] R. Gassert, R. Moser, E. Burdet, and H. Bleuler, "MRI/fMRI-compatible robotic

system with force feedback for interaction with human motion," *IEEE/ASME Trans. Mechatronics*, vol. 11, no. 2, pp. 216–224, Apr. 2006, 10.1109/TMECH.2006.871897.

[21] F. Sergi, A. C. Erwin, and M. K. Omalley, "Interaction control capabilities of an MR-compatible compliant actuator for wrist sensorimotor protocols during fMRI," *IEEE/ASME Trans. Mechatronics*, vol. 20, no. 6, pp. 2678–2690, 2015, 10.1109/TMECH.2015.2389222.

[22] J. P. Mehta, M. D. Verber, J. A. Wieser, B. D. Schmit, and S. M. Schindler-Ivens, "A novel technique for examining human brain activity associated with pedaling using fMRI," *J. Neurosci. Methods*, vol. 179, no. 2, pp. 230–239, May 2009, 10.1016/j.jneumeth.2009.01.029.

[23] J. E. Taylor, "The extent and characteristics of driving anxiety," *Transp Res Part F Traffic Psychol Behav*, vol. 58, pp. 70–79, Oct. 2018, 10.1037/a0029516.

[24] V. Menon and L. Uddin, "Saliency, switching, attention and control: a network model of insula function," *Brain Struct Funct*, vol. 214, no. 5-6, pp. 655–667, Jun. 2010, 10.1007/s00429-010-0262-0.

[25] M. R. Delgado, L. E. Nystrom, C. Fissell, D. C. Noll, and J. A. Fiez, "Tracking the hemodynamic responses to reward and punishment in the striatum," *J. Neurophysiol.*, vol. 84, no. 6, pp. 3072–3077, Dec. 2000, 10.1152/jn.2000.84.6.3072.

[26] S. Y. Saori, C. Tanaka, K. Doya, G. Okada, K. Ueda, Y. Okamoto, and S. Yamawaki, "Prediction of immediate and future rewards differentially recruits cortico-basal ganglia loops," *Nat. Neurosci.*, vol. 7, no. 8, pp. 887–893, Jul. 2004, 10.1007/978-

[27] Wellcome Department of Cognitive Neurology, London, UK. [Online]. Available: www.fil.ion.ucl.ac.uk/spm. Accessed on: March 23, 2016. 4-431-55402-8_22.

[28] P. E. Roland, B. Larsen, N. A. Lassen, and E. Skinhøj, "Supplementary motor area and other cortical areas in organization of voluntary movements in man," *J. Neurophysiol*., vol. 43, no. 1, pp. 118–136, Jan. 1980, 10.1152/jn.1980.43.1.118.

[29] H. Kinoshita, N. Oku, K. Hashikawa, and T. Nishimura, "Functional brain areas used for the lifting of objects using a precision grip: A PET study," *Brain Res.*, vol. 857, no. 1–2, pp. 119–130, Feb. 2000, 10.1016/S0006-8993(99)02416-6.

[30] R. C. Oldfield, "The assessment and analysis of handedness: The Edinburgh inventory," *Neuropsychologia*, vol. 9, no. 1, pp. 97–113, Mar. 1971, 10.1016/0028-3932(71)90067-4.

[31] J. K. Mai and M. Majtanik, Human Brain in Standard MNI Space: A Comprehensive Pocket Atlas, UK: Academic Press, 2017, pp. 4-5.

[32] M. Brett, J.-L. L. Anton, R. Valabregue, and J.-B. Poline, "Region-of-interest analysis using an SPM toolbox," *Abstract Presented at the 8th International Conference on Functional Mapping of the Human Brain*, June 2–6, 2002, Sendai, Japan, Neuroimage, vol. 16, no. 2, Abstract 497, 2002.

[33] R. M. Bilder, R. S. Goldman, D. Robinson, G. Reiter, L. Bell, J. A. Bates, E. Pappadopulos, D. F. Willson, J. M. J. Alvir, M. G. Woerner, S. Geisler, J. M. Kane, and J. A. Lieberman, "Neuropsychology of first-episode schizophrenia: Initial characterization and clinical correlates," *Am. J. Psychiatry*, vol. 157, no. 4, pp. 549–559, Apr. 2000, 10.1176/appi.ajp.157.4.549#.

[34] M. Lotze, P. Montoya, M. Erb, E. Hülsmann, H. Flor, U. Klose, N. Birbaumer, and

W. Grodd, “Activation of cortical and cerebellar motor areas during executed and imagined hand movements: An fMRI study,” *J. Cogn. Neurosci*., vol. 11, no. 5, pp. 491–501, Sep. 1999, 10.1162/089892999563553.

[35] D. M. Kennedy, J. B. Boyle, C. Wang, and C. H. Shea, “Bimanual force control: Cooperation and interference?” *Psychol. Res.*, vol. 80, no. 1, pp. 34–54, Jan. 2016, 10.1007/s00426-014-0637-6.

[36] A. Yokoi, M. Hirashima, and D. Nozaki, “Lateralized sensitivity of motor memories to the kinematics of the opposite arm reveals functional specialization during bimanual actions,” *J. Neurosci.*, vol. 34, no. 27, pp. 9141–9151, Jul. 2014, 10.1523/JNEUROSCI.2694-13.2014.

[37] Stand-Up MRI of Deer Park, P.C., NY, [Online]. Available: https://www.standupmriofdeerpark.com/, Accessed on: March 9, 2018.

[38] Hamamatsu Photonics K.K., Hamamatsu, JP, [Online]. Available: https://www.hamamatsu.com/jp/en/hamamatsu/overview/bsd/central_research_laboratory/health_and_medical_care_field.html, Accessed on: March 9, 2018.

[39] S. V. Adamovich, K. August, A. Merians, and E. Tunik, “A virtual reality-based system integrated with fmri to study neural mechanisms of action observation-execution: a proof of concept study,” *Restor. Neurol. Neurosci.*, vol. 27, no. 3, pp. 209–223, 2009, 10.3233/RNN-2009-0471.

[40] E. Biagioni, E. Mercuri, M. Rutherford, F. Cowan, D. Azzopardi, Maria F. Frisone, G. Cioni, and L. Dubowitz, "Combined use of electroencephalogram and magnetic resonance imaging in full-term neonates with acute encephalopathy," *Pediatrics*, vol. 107, no. 3, pp. 461–468, Mar. 2001, 10.1542/peds.107.3.461.

[41] N. Tzourio-Mazoyer, B. Landeau, D. Papathanassiou, F. Crivello, O. Etard, N. Delcroix, B. Mazoyer, and M. Joliot, “Automated anatomical labeling of activations in SPM using a macroscopic anatomical parcellation of the MNI MRI single-subject brain,” *NeuroImage*, vol. 15, no. 1, pp. 273–289, Jan. 2002, 10.1006/nimg.2001.0978.

[42] M. F. Mason, M. I. Norton, J. D. Van Horn, D. M. Wenger, S. T. Grafton, and C. N. Macrae, “Wandering minds: Stimulus-independent thought,” *Science*, vol. 315, pp. 393–395, Jan. 2007, 10.1126/science.1131295.

[43] W. W. Seeley, V. Menon, A. F. Schatzberg, J. Keller, G. H. Glover, H. Kenna, A. L. Reiss and M. D. Greicius, “Dissociable intrinsic connectivity networks for salience processing and executive control,” *J. Neurosci.*, vol. 27, no. 9, pp. 2349–2356, Feb. 2007, 10.1523/jneurosci.5587-06.

[44] T. Straube, S. Schmidt, T. Weiss, H. J. Mentzel and W. H. R. Miltner, “Dynamic activation of the anterior cingulate cortex during anticipatory anxiety,” *Neuroimage*, vol. 44, no. 3, pp. 975–981, Feb. 2009, 10.1016/j.neuroimage.2008.10.022

[45] E. A. Phelps, “Emotion and Cognition: Insights from Studies of the Human Amygdala,” *Annu. Rev. Psychol.*, vol. 57, no. 1, pp. 27–53, 2006, 10.1146/annurev.psych.56.091103.07023

[46] P. Sumner and M.Husain, ”At the edge of consciousness: automatic motor activation and voluntary control,” *Neuroscientist*, vol. 14, no. 5, pp. 474–486, Oct. 2008, 10.1177/1073858408314435

[47] J. A. Russel, “A Circumplex Model of Affect,” *J. Pers. Soc. Psychol.*, vol. 39, no.

6, pp. 1161–1178, 1980, 10.1037/h0077714.

[48] L. Griffanti, G. S. Khorshidi, C. F. Beckmann, E. J. Auerbach, G. Douaud, C. E. Sexton, E. Zsoldos, K. P. Ebmeier, N. Filippini, C. E. Mackay, S. Moeller, J. Xu, E. Yacoub, G. Baselli, K. Ugurbil, K. L. Miller, and S. M. Smith, "ICA-based artefact removal and accelerated fMRI acquisition for improved resting state network imaging," *NeuroImage*, vol. 95, pp. 232–247, Jul. 2014, 10.1016/j.neuroimage.2014.03.034.

[49] L. Griffanti, G. Douaud, J. Bijsterbosch, S. Evangelisti, F. A. Almagro, M. F. Glasser, E. P. Duff, S. Fitzgibbon, R. Westphal, D. Carone, C. F. Beckmann, and S. M. Smith, "Hand classification of fMRI ICA noise components," *NeuroImage*, vol. 154, pp. 188–205, Jul. 2017, 10.1016/*j.neuroimage.*2016.12.036.

[50] S. B. Eickhoff, K. E. Stephan, H. Mohlberg, C. Grefkes, G. R. Fink, K. Amunts, and K. Zillesa, "A new SPM toolbox for combining probabilistic cytoarchitectonic maps and functional imaging data," *NeuroImage*, vol. 25, no. 4, pp. 1325–1335, May 2005, 10.1016/j.neuroimage.2004.12.034.

[51] S. B. Eickhoff, S. Heim, K. Zilles, and K. Amunts, "Testing anatomically specified hypotheses in functional imaging using cytoarchitectonic maps," *NeuroImage*, vol. 32, no. 2, pp. 570–582, Aug. 2006, 10.1016/j.neuroimage.2006.04.204. Epub 2006 Jun 14.

[52] S. B. Eickhoff, T. Paus, S. Caspers, M.H. Grosbras, A. C. Evans, K. Zilles, and K. Amunts, "Assignment of functional activations to probabilistic cytoarchitectonic areas revisited," *NeuroImage*, vol. 36, no. 3, pp. 511–521, Jul. 2007, 10.1016/j.neuroimage.2007.03.060.

[53] J. L. Lancaster, M. G. Woldorff, L. M. Parsons, M. Liotti, C. S. Freitas, L. Rainey, P. V. Kochunov, D. Nickerson, S. A. Mikiten, and P. T. Fox, "Automated Talairach Atlas labels for functional brain mapping," *Hum. Brain Map.*, vol. 10, no. 3, pp. 120–131, June 2000, 10.1002/1097-0193(200007)10:3<120::aid-hbm30>3.0.CO;2-8.

[54] J. L. Lancaster, L. H. Rainey, J. L. Summerlin, C. S. Freitas, P. T. Fox, A .C. Evans, A. W. Toga, and J. C. Mazziotta, "Automated labeling of the human brain: A preliminary report on the development and evaluation of a forward-transform method," *Hum. Brain Map.*, vol. 5, no. 4, pp. 238–242, 1997, 10.1002/(SICI)1097-0193(1997)5:4<238::AID-HBM6>3.0.CO;2-4.

[55] J. Germann, M. M. Chakravarty, D. L. Collins, and M. Petrides, "Tight Coupling between Morphological Features of the Central Sulcus and Somatomotor Body Representations: A Combined Anatomical and Functional MRI Study," *Cereb. Cortex*, vol. 30, no. 3, pp. 1843–1854, Mar. 2020, 10.1093/cercor/bhz208

[56] J. G. Colebatch, M. P. Deiber, R. E. Passingham, K. J. Friston, and R. S. J. Frackowiak, "Regional cerebral blood flow during voluntary arm and hand movements in human subjects," *J Neurophysiol*, vol. 65, no. 6, pp. 1392–1401, Jun. 1991, 10.1152/jn.1991.65.6.1392.

[57] D. E. Vaillancourt, K. R. Thulborn, and D. M. Corcos, "Neural basis for the processes that underlie visually guided and internally guided force control in humans," *J. Neurophysiol.*, vol. 90, no. 5, pp. 3330–3340, Dec. 2003, 10.1152/jn.00394.2003.

[58] T. A. Yousry, U. D. Schmid, H. Alkadhi, D. Schmidt, A. Peraud, A. Buettner, and

P. Winkler, “Localization of the motor hand area to a knob on the precentral gyrus. A new landmark,” *Brain*, vol. 120, no. 1, pp. 141–157, Jan. 1997, 10.1093/brain/120.1.141.

[59] S. T. Grafton, R. P. Woods, and J. C. Mazziotta, “Within-arm somatotopy in human motor areas determined by positron emission tomography imaging of cerebral blood flow,” *Exp. Brain Res.*, vol. 95, no. 1, pp. 172–176, Jul. 1993, 10.1007/bf00229666.

[60] H. J. Freund, “Clinical aspects of premotor function,” *Behav Brain Res*, vol. 18, no. 2, pp. 187–191, Nov.-Dec. 1985, 10.1016/0166-4328(85)90074-9.

[61] Chassis Handbook, 1st ed., Springer Fachmedien Wiesbaden GmbH, Wiesbaden, BRD, 2011.

[62] R. F. Chandler, C. E. Clauser, J. T. McConville, H. M. Reynolds, and J. W. Young, “Investigation of inertial properties of the human body,” *National Highway Traffic Safety Administration*, vol. no. 00, pp. 1–169, Mar. 1975.

[63] T. Tsuji and Y. Tanaka, “Bio-mimetic impedance control of robotic manipulator for dynamic contact tasks,” *Rob Auton Syst*, vol. 56, no. 4, pp. 306–316, 2008, 10.1016/j.robot.2007.09.001.

[64] D. M. Wolpert and Z. Ghahramani, “Computational principles of movement neuroscience,” *Nat Neurosci.*, vol. 3, no. 11s, pp. 1212–1217, Nov. 2000. 10.1038/81497

[65] H. Kimpara, K. C. Mbanisi, J. Fu, Z. Li, D. Prokhorov, and M. A. Gennert, “Human Model-Based Active Driving System in Vehicular Dynamic Simulation,” *IEEE trans Intell Transp Syst*, vol. 21, no. 5, pp. 1903–1914, Apr. 2020,

10.1109/TITS.2019.2906294

[66] N. Rhodes and K. Pivik, “Age and gender differences in risky driving: The roles of positive affect and risk perception,” *Accid Anal Prev,* vol. 43, no. 3, pp. 923–931, May 2011, 10.1016/j.aap.2010.11.015.

[67] C. Turner and R. McClure, “Age and gender differences in risk-taking behaviour as an explanation for high incidence of motor vehicle crashes as a driver in young males,” *Int J Inj Contr Saf Promot*, vol. 10, no. 3, pp. 123–130, Sep. 2003, doi.org/10.1076/icsp.10.3.123.14560

[68] E. C. Andrews and S. J. Westerman, “Age differences in simulated driving performance: Compensatory processes,” *Accid Anal Prev*, vol. 45, pp. 660–668, Mar. 2012, 10.1016/j.aap.2011.09.047

[69] Y. Okamoto, T. Sasaoka, T. Yoshida, K. Takemura, S. Zu, T. Nouzawa, S. Yamawaki, and T. Tsuji, “Development of fMRI-compatible steering reaction force generation unit,” *IEEE/ASME T. Mech*., vol. 24, no. 2, pp. 549–560, Jan. 2019, 10.1109/TMECH.2019.2895456.

[70] Y. Okamoto, T. Sasaoka, T. Yoshida, K. Takemura, S. Zu, T. Nouzawa, S. Yamawaki, and T. Tsuji, “Brain activity while waiting to steer a car: an fMRI study,” *Proceedings of the 2018 5th International Conference on Biomedical and Bioinformatics*, pp. 52–57, Nov. 2018, 10.1145/3301879.3301896.

[71] Y. Okamoto, T. Sasaoka, N. Sadato, M. Fukunaga, T. Yamamoto, S. Zu, T. Nouzawa, S. Yamawaki, and T. Tsuji, “Is human brain activity during driving operations modulated by the viscoelastic characteristics of a steering wheel?: an fMRI study,” *IEEE ACCESS*, vol. 8, pp. 215073-215090, Nov. 2020,

10.1109/ACCESS.2020.3040231.

Acknowledgments

I would like to express my deepest gratitude to my supervisor, Professor Toshio Tsuji, for his elaborate guidance, considerable encouragement, and the individual discussions that made my life as an adult graduate student unforgettable, helping me realize great research achievements. His perpetual energy and enthusiasm for research were extremely motivational to me during my studies.

I am also grateful to the committee members Professor Idaku Ishii and Professor Toru Yamamoto for their invaluable suggestions and opinions on this dissertation.

I would especially like to express my sincere appreciation to my adviser, Dr. Takafumi Sasaoka, Research Leader of the Center of Innovation, KANSEI Research Project with the Center for Brain, Mind and KANSEI Sciences Research, Hiroshima University, for his advice, suggestions, encouragement, and patience. His scientific expertise helped me immensely in many aspects, right from planning the studies to the final revision of the paper.

I am deeply appreciative of Professor Norihiro Sadato, Dr. Masaki Fukunaga, Dr. Tetsuya Yamamoto, and Dr. Yukiko Honda of the National Institute for Physiological Sciences for the elaborate guidance on neuroscience, collaborative work of fMRI denoising, regular discussions, and their considerable encouragement.

I would also like to show my greatest appreciation to the former Project Leader of the Center of Innovation, KANSEI Research Project and former director of Mazda Motor Corporation Technical Research Center, Professor (Special Appointment) Takahide Nouzawa of Hiroshima University Office of Academic Research and Industry-Academia-

Government and Community Collaboration, for encouraging me to pursue a doctoral course and supervising my study consistently.

I would like to express my gratitude to the former Research Leader of the Center of Innovation, KANSEI Research Project, Professor (Special Appointment) Shigeto Yamawaki of the Center for Brain, Mind and KANSEI Sciences Research, Hiroshima University for supportive supervision.

I would particularly like to thank Dr. Zu Soh of Hiroshima University Graduate School of Advanced Science and Engineering for supportive supervision in reviewing the written thesis and in the implementation of the experiment.

I am deeply grateful to Dr. Tsuneko Harada and Dr. Rodrigues Alan de Souza of Brain, Mind and KANSEI Sciences Research Center for their efforts and guidance on fMRI data analysis and presentations at international conferences.

I express my deepest gratitude to Ms. Noriko Miura, Dr. Shoichi Shiota, Mr. Ryohei Mizuochi, Ms. Yukari Kanayama, Ms. Chikako Arashi, Ms. Tamami Tomita, and Dr. Hironori Matsuura of the Center for Brain, Mind and KANSEI Sciences Research for their efforts in implementing the experiment.

Special thanks are also due to Mr. Takayasu Itou of Assist Technology Co. Ltd., Mr. Shinsuke Kawahara of Office Limelight, Mr. Hiroshi Kido and Mr. Hidenori Kido of EM Development Co. Ltd., Mr. Yu Yamamoto of ROBOTEC Inc., and Mr. Wataru Yasuda of the Leading-Edge Research and Development Accelerator Inc. for their efforts to develop the fMRI-compatible steering reaction force generation unit.

I would also like to show my greatest appreciation to Mr. Kazuo Sakamoto, Dr. Kazuo Nishikawa, Mr. Atsuhide Kishi, Mr. Toshihiro Hara, Dr. Nanae Michida, and Mr.

Nobuhiro Yonezawa of Mazda Motor Corporation Technical Research Center for their valuable guidance and management support.

I owe a very important debt of gratitude to Mr. Toshihiro Yoshida, Dr. Kazuhiro Takemura, Mr. Naoki Yamada and Mr. Daichi Sato of Mazda Motor Corporation Technical Research Center for their efforts in the design and implementation of the experiment and in data analysis.

Finally, I am forever indebted to my wife, children, father, and late mother for their endless love, understanding, support, encouragement, and sacrifice throughout my academic pursuits after crossing the age of fifty.

This work was supported by the Center of Innovation Program of the Japan Science and Technology Agency under Grant JPMJCE1311.